ADVANCED FUNCTIONAL MATERIALS
www.afm-journal.de

Modulating Bond Interactions and Interface Microenvironments between Polysulfide and Catalysts toward Advanced Metal–Sulfur Batteries

Ran Zhu, Weiqiong Zheng, Rui Yan, Min Wu, Hongju Zhou, Chao He, Xikui Liu, Chong Cheng, Shuang Li,* and Changsheng Zhao**

Advanced metal–sulfur batteries (MSBs) are regarded as promising next-generation energy storage devices. Recently, engineering polysulfide redox catalysts (PSRCs) to stabilize and catalytically convert polysulfide intermediates is proposed as an effective strategy to address the grand challenge of "shuttle effects" in the cathode. Therefore, modulating the bond interactions and interface microenvironments and disclosing the structure–performance correlations between polysulfide and catalysts are essential to guide the future cathode design in MSBs. Herein, from a multidisciplinary view, the most recent process in the reaction principles, in situ characterizations, bond interaction modulation, and interface microenvironment optimization of polysulfide redox catalysts, is comprehensively summarized. Especially, unique insights are provided into the strategies for tailoring the bond interactions of PSRCs, such as heteroatom doping, vacancy engineering, heterostructure, coordination structure arrangements, and crystal phase modulation. Furthermore, the importance of interface microenvironments and substrate effects in different PSRCs are exposed, and a detailed comparison is given to unveil the critical parameters for their future developments. Finally, the critical design principles on electrode microenvironments for advanced MSBs are also proposed to stimulate the practically widespread utilization of PSRCs-equipped cathodes in MSBs. Overall, this review provides cutting-edge guidance for future developments in high-energy-density and long-life MSBs.

1. Introduction

The constantly increasing demands for clean and renewable energy sources have motivated vigorous efforts to develop reliable, high-energy-density rechargeable batteries.[1] However, the market-mainstream lithium-ion batteries (LIBs), based on Li^+ intercalation mechanism, have approached their theoretical capacity limitation, which would hinder their pervasive satisfaction with ever-growing requirements.[2] Therefore, alternative new battery systems with higher energy density than LIBs have attracted unprecedented attention. Among various candidates, metal–sulfur batteries (MSBs) exhibit superb theoretical capacity and energy density owing to the multielectron electrochemical process; for instance, lithium–sulfur batteries (LSBs) can reach 1675 mAh g^{-1}. Moreover, considering the abundant reserves and environmental friendliness of sulfur, MSBs display competitive merits in widespread deployments.[3–6] Despite the attractive advantages, several intrinsic drawbacks of the sulfur cathode still hinder the commercialization process of MSBs:[7–11] 1) the electrical insulation of sulfur and M_2S results in the insufficient usage rate or passivation of active materials; 2) the possible volume expansion threatens the durability of the cathode; 3) the soluble polysulfides can cause severe "shuttle effects" and lead to irreversible capacity fading (**Scheme 1**a).

R. Zhu, W. Zheng, R. Yan, M. Wu, H. Zhou, C. He, X. Liu, C. Cheng, S. Li, C. Zhao
College of Polymer Science and Engineering
State Key Laboratory of Polymer Materials Engineering
Sichuan University
Chengdu 610065, China
E-mail: chong.cheng@scu.edu.cn; s.li@tu-berlin.de; zhaochsh70@scu.edu.cn

C. Cheng, C. Zhao
Med-X Center for Materials
Sichuan University
Chengdu 610041, China

S. Li
Department of Chemistry
Technische Universität Berlin
Hardenbergstraße 40 10623, Berlin, Germany

The ORCID identification number(s) for the author(s) of this article can be found under https://doi.org/10.1002/adfm.202207021.

DOI: 10.1002/adfm.202207021

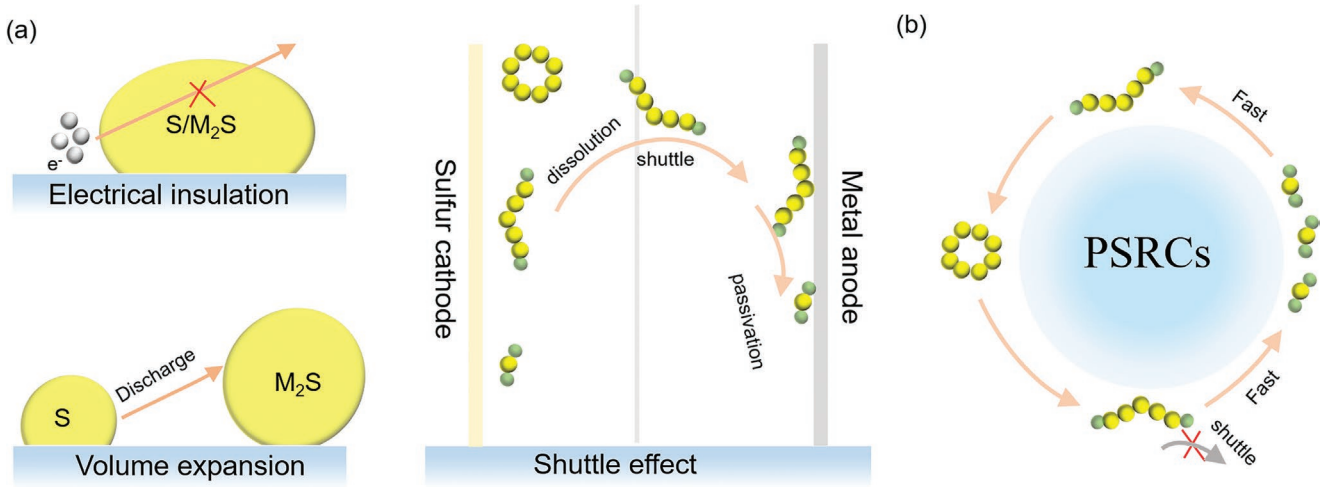

Scheme 1. a) The illusion of intrinsic drawbacks in the sulfur cathode. b) The illustration for the alleviating effect of PSRCs on the "shuttle effect" in MSBs.

In the past years, enormous endeavors have been invested in conquering the foregoing limitation; for instance, the combination of sulfur and porous carbon-based hosts made some achievements in facilitating the electron transfer and physical adsorption of soluble polysulfides.[10,12–15] However, the interactions between polar polysulfide intermediates and nonpolar carbon surface rely on the weak van der Waals force, which displays insufficient capability to suppress the "shuttle effects" during long-term cycling.[16] Recently, engineering polysulfide redox catalysts (PSRCs) to stabilize and catalytically convert polysulfide intermediates has been proposed as an effective strategy to address the grand challenge of "shuttle effects" in the cathode(Scheme 1b).[17] Based on the substrates, the currently developed PSRCs mainly include the metal compounds,[18–20] carbon-supported single-atom materials,[21,22] metal–organic frameworks (MOFs),[23–26] etc. Current researches have disclosed that modulating the bond interactions and interface microenvironments of PSRCs will bring significant impacts on the electronic structure and d-band center of metal atoms, thus tuning the intrinsic catalytic properties, reaction pathways, and long-term stabilities in boosting the electrochemical redox kinetics of polysulfides.

The design and evaluation key points on PSRCs include: i) the bond interactions of polysulfide intermediates on different active centers/adsorption sites; ii) the fast catalytic conversion of polysulfide intermediates; iii) the balanced adsorption–desorption ability to achieve reversible catalytic conversion; iv) synergetic effects between active sites and the interfacial microenvironments of support materials (Scheme 1b). Modulating and understanding the bond interactions and interface microenvironments between polysulfide and catalysts are unfading topics in the field of PSRCs toward high-performance and stable MSBs.[3,6] However, accompanying the promising potential of PSRCs, there are still essential challenges in the synthesis, characterization, analysis, and commercial applications of PSRCs in MSBs since the huge diversity of catalytic sites and support materials. Currently, engineering and analyzing the complex bond interactions and interface microenvironments of PSRCs with defined coordination configurations and spatial structures are extremely challenging,[27–29] which is indispensable for guiding the future design and performance optimization of PSRCs in MSBs.[30]

To guide the future design of PSRCs in the cathode, this review aims to provide a multidisciplinary view on modulating the bond interactions and interface microenvironments and disclosing the structure–performance correlations between polysulfide and catalysts in MSBs. First, we comprehensively summarized the most recent process in the reaction principles and in situ characterizations of PSRCs. Then, we provide unique insights into the strategies on tailoring the bond interactions of PSRCs, such as heteroatom doping, vacancy engineering, heterostructure, coordination structure arrangements, and crystal phase modulation. Thereafter, we expose the importance of interface microenvironments and substrate effects in different PSRCs, and give a detailed comparison to disclose the important indexes for their future developments. Finally, the critical design principles on electrode microenvironments for advanced MSBs have also been proposed to stimulate the practical utilization of PSRCs-equipped cathodes in MSBs. We anticipate that this review will provide timely and cutting-edge guidance for future prosperity in achieving high-energy-density and long-life MSBs.

2. Reaction Principles and Characterizations of PSRCs

It is investigated that the catalytic process of PSRCs in the cathodes contains two major steps: first, the adsorption/bonding of polysulfide intermediates on the catalytic sites and the conversion and then reversible conversion of polysulfide intermediates during the discharging/charging process. Modulating bond interactions and interface microenvironments between polysulfide and catalysts can efficiently affect electrochemical redox kinetics.

2.1. Design Principles on Optimal Adsorption Sites for Polysulfide Intermediates

The migration of long-chain soluble polysulfide from cathode to anode, which leads to the loss of active mass, has been regarded as the main obstacle to realizing long-term cycle MSBs. Over the past few years, numerous endeavors to fix polysulfide have

been developed to conquer the "shuttle effects." Physical confinement based on van der Waals force has been confirmed to have an inferior effect due to the weak affinity toward polysulfide, while the strong chemical bond interaction is regarded as the more promising strategy. Moreover, such effective chemical adsorption toward polysulfide could enhance the subsequent redox kinetics, which inspired us to investigate the anchoring mechanism of mediators. As a representative example, the binding energies of different PSRCs for polysulfide in LSBs and corresponding cycling performance are summarized in **Table 1**.

Although chemical adsorption plays an important role in anchoring polysulfide intermediates, it is worth noting that only appropriate binding affinity could alleviate their shuttle effects, whereas the strong binding energy would impede the continuous or reversible catalytic conversion process.[51] Typically, for the PSRCs with inferior intrinsic conductivities (e.g., metal oxides), the adsorbed polysulfide intermediates need to migrate to the interface between the conductive components and PSRCs to undergo the charge transfer. In this respect, the metal oxides with excessive binding interaction with polysulfide intermediates would inhibit the nucleation and growth of M_2S in the interface microenvironments between metal oxides and conductive components (**Figure 1**a,b). For instance, the relationship between the electrochemical redox performance and the polysulfide binding energy of different metal oxides (MgO, Al_2O_3, CeO_2, La_2O_3, and CaO) has been systematically investigated. Although Al_2O_3 possessed the highest binding ability to Li_2S_8 and Li_2S, the cycling performance was worse than MgO. Figure 1c shows that the MgO displays medium binding energy to polysulfide intermediates.[32] On the other hand, according to the Sabatier principle, excessive bonding of the catalyst toward the reaction intermediates would block the surface reaction sites and impede the reaction kinetics, which leads to the loss of active substances due to its insufficient catalytic conversion during the charging process.[52] Based on this, the diffusion energy barrier of Li_2S on the surface of a series of Co-based compounds and their electrochemical performance are investigated.[53] As shown in Figure 1d, the CoP surface proceeds with the lowest energy barrier, therefore resulting in the lowest overpotential for polysulfide transformation. Even at the charge/discharge rate of 40.0 C, the battery still delivers a high capacity of 417.3 mAh g^{-1} and an ultrahigh power density of 137.3 kW kg^{-1}. The catalytic conversion performance of CoP could be attributed to the moderate adsorption ability and superior diffusion dynamics of polysulfide intermediates (Figure 1e).

Table 1. Binding energies toward polysulfides of different PSRCs and corresponding battery performances.

Catalytic centers	Li_2S_8 [eV]	Li_2S_6 [eV]	Li_2S_4 [eV]	Li_2S_2 [eV]	Li_2S [eV]	Capacity decay [%, per cycle]	Cycle number	C rate	Sulfur loading [mg cm^{-2}]	Refs.
TiO_2	0.81	0.92	1.24	1.57	1.96	0.075%	300	1.0	≈2.0	[31]
Al_2O_3	7.12	–	–	–	–	0.171%	100	0.5	≈1.0	[32]
MgO	5.71					0.016%	100	0.5	≈1.0	[32]
Co_9S_8	6.08	4.03	2.97	4.52	5.51	0.041%	1000	2.0	≈2.0	[33]
CoS_2	–	–	1.97	–	–	0.034%	2000	2.0	≈0.4	[34]
MoS_2	0.98	0.87	0.68	0.89	0.82	0.080%	500	1.0	≈10.0	[35]
$MoSe_2$	0.19	0.18	0.31	0.54	0.81	0.137%	100	0.2	≈1.1	[36]
Co_3Se_4	1.03	0.81	1.41	–	–	0.067%	800	0.2	≈3.1	[37]
WSe_2	2.65	1.13	1.15	1.87	2.35	0.037%	500	1.0	≈1.0	[38]
W_2C	–	2.57	–	–	–	0.066%	200	0.2	≈2.0	[39]
Mo_2C	–	2.71	–	–	–	0.136%	200	0.2	≈2.0	[39]
TiC	–	2.32	–	–	–	0.142%	200	0.2	≈2.0	[39]
MoC	–	1.51	2.77	1.77	1.91	0.060%	300	1.0	≈3.0	[40]
TiN	3.73	3.24	3.02	3.34	2.26	0.160%	100	1.0	≈3.0	[41]
MoN	2.74	2.22	1.73	1.89	2.04	0.059%	200	0.5	≈6.5	[42]
VN	3.46	3.01	3.27	3.14	3.86	0.024%	1000	1.0	≈1.2	[18]
TiB	0.89	0.88	0.89	0.67	1.82	0.058%	500	1.0	≈1.2	[43]
CoB	11.60	9.32	7.24	6.34	5.56	0.013%	1500	5.0	≈1.5	[44]
CoP	–	5.00	1.46	3.30	5.41	0.077%	300	0.2	≈0.7	[45]
FeP	2.83	3.18	2.80	2.42	1.98	0.040%	400	1.0	≈1.0	[46]
V–N–C	–	3.38	–	–	–	0.073%	400	0.5	≈2.0	[47]
Co–N–C	–	1.67	–	–	–	0.079%	400	0.5	≈2.0	[47]
Fe–N–C	–	1.35	–	–	–	0.094%	500	1.0	≈1.5	[48]
Ni-ZIF-8	3.35	3.81	3.54	–	–	0.050%	500	1.0	≈1.5	[49]
Ce-MOF-2	–	2.48	2.78	2.35	–	0.022%	800	1.0	≈2.5	[50]

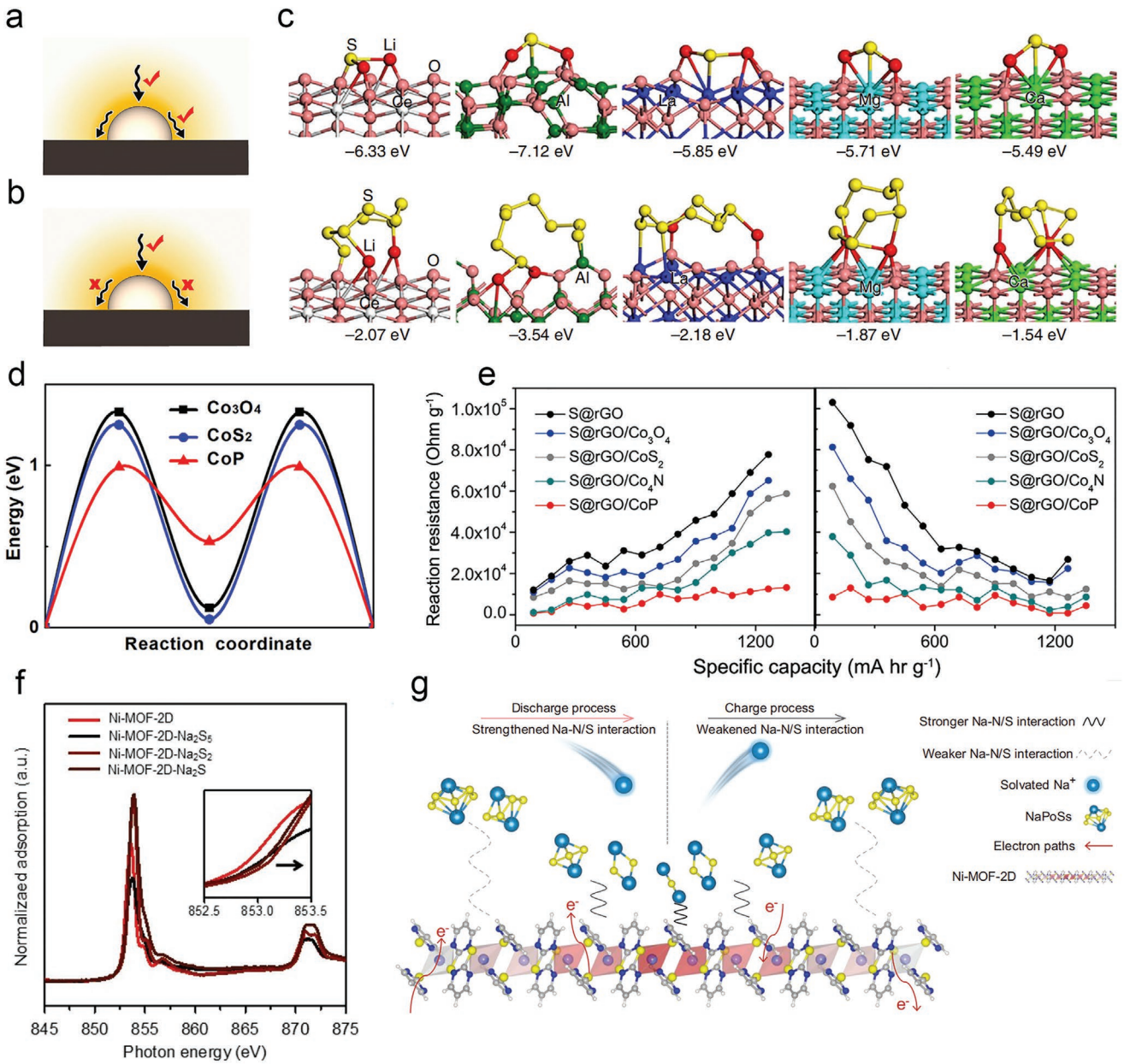

Figure 1. a,b) The schematic image of polysulfide diffusion on the surface of metal oxides with a different diffusion barrier. c) The binding energy of different metal oxides with polysulfide intermediates. Reproduced with permission.[32] Copyright 2015, Nature Publishing Group. d) The diffusion energy barrier of Li_2S on the surface of different Co-based compounds. e) The electrochemical performance of a series of Co-based compounds. Reproduced with permission.[53] Copyright 2018, Elsevier. f,g) The variable bond interaction between Ni-MOF-2D and polysulfide along with the charge/discharge process. Reproduced with permission.[54] Copyright 2020, Wiley-VCH.

Recently, a more desirable adsorption model for polysulfides with adjustable adsorption energy has been proposed by Qiao's group. A 2D Ni-MOF has been designed to enhance the adsorption and conversion of polysulfide intermediates in Na–S batteries, which delivers the dynamic interactions between sodium polysulfides and N sites. During the discharge process, the adsorption energy increased from Na_2S_5 to Na_2S, correlating with the electron transfer from Ni to N, which could be verified by the results of the Ni *L*-edge (Figure 1f). This strengthened Na–N/S interaction could facilitate the sodiation process from Na_2S_5 to Na_2S during discharge. In turn, during charge, the weakened Na–N/S interactions also facilitate the dissociation process of Na_2S to Na_2S_5. These gradually changing interactions can effectively promote the bidirectional conversion of polysulfide during the charge/discharge process and provide new design principles in related research (Figure 1g).[54]

2.2. Catalytic Conversion of Polysulfide Intermediates

Although preventing the dissolution of polysulfide intermediates by an effective anchoring mechanism could reduce the

loss of active sulfur to some extent, the "shuttle effects" could not be completely avoided due to the limited adsorption sites. On the contrary, promoting the sluggish catalytic conversion of polysulfide to decrease the retention time of soluble polysulfides could block the shuttle fundamentally. Moreover, the enhanced redox kinetics was expected to improve the performance of MSBs under high current density. In this section, the intrinsic mechanism of electrocatalysts in accelerating the polysulfide catalytic conversion will be concluded from two aspects.

It is well-known that sufficient interfacial electron transfer between the catalyst and polysulfide plays an important role in the rapid conversion of polysulfide. It has been found that the terminal S and Li atoms of polysulfide can bind to adjacent catalytic sites, which triggers strong bond interaction and sufficient charge transfer between sulfur species and catalysts. For example, such binding can be found on the CoS_2 materials to accelerate the polysulfide conversion kinetics (**Figure 2**a,b). The symmetrical Li_2S_6–Li_2S_6 cells with CoS_2 electrodes exhibit decreased impedance, indicating the optimized interfacial charge transfer between polysulfides and CoS_2 (Figure 2c).[34] The location of the d-band center of metal and the p-band center of nonmetal are usually regarded as the descriptor of electron transfer capacity of active sites. A close Fermi level facilitates electron transfer from the catalytic site to lithium polysulfides (LiPSs), thereby facilitating S—S breaking and accelerating LiPSs conversion. Based on this, a systematic investigation of the catalytic ability of Co-based compounds (CoP, CoS_2, Co_3O_4, and Co_4N) was first reported, where CoP exhibited the smallest energy gap between the Co 3d and P 2p band center (Figure 2d,e). Therefore, bringing the enhanced interfacial electron transfer dynamics for promoting S_6^{2-}/S^{2-} conversion and the CoP cathodes displayed the most desirable rate performance (Figure 2f).[53] Similarly, a systematic study was also performed on the Fe-based compounds, where this mechanism is also well-fitted.[51,55]

The lithiation-catalytic mechanism is identified in some special 2D layered mediators, which exhibit a Li^+ intercalation/deintercalation process with the cycling proceeding. The Chevrel-phase Mo_6S_8, which is a typical 2D material with polysulfide catalytic properties, has performed a fast lithiation reaction under the same redox potential window as sulfur: $4Li^+ + 4e^- + Mo_6S_8 \leftrightarrow Li_4Mo_6S_8$. Thus, it provides a fast lithium-ion transport mechanism for polysulfide conversion.[56] Very recently, the VS_2 has also been explored to show the same mechanism when used as a polysulfide regulator.[57] In addition to metal sulfides, some pseudocapacitive metal oxides also show similar properties. For example, orthorhombic Nb_2O_5 and birnessite MnO_2 were applied as desirable electron/ion sources during the chemical redox reactions of sulfur. During the discharge process, Li^+ was first reserved in Nb_2O_5 and spontaneously transferred to polysulfide with a reversible reaction of Nb_2O_5–$LiNb_2O_5$–Nb_2O_5 (Figure 2g). To be specific, such electron/ion reservoirs can ensure additional electrons and Li^+ supply to the sulfur species and facilitate the effective conversion of LiPSs during discharge, which can be proved by a much higher exchange current according to the linear voltammetry (Figure 2h). The same role is found for the MnO_2 during the charging process (Figure 2i).[58]

2.3. Reversible Electrodeposition of Metal Sulfide (M_2S)

The electrodeposition of M_2S from soluble polysulfide intermediates has been reported to be the rate-determining step in the cathode of MSBs, which involves the sluggish catalytic conversion of soluble polysulfides into insoluble M_2S. Meanwhile, the fundamental understanding of metal sulfides electrodepositions and reaction mechanisms remains ambiguous. In the past few years, numerous PSRCs have been introduced to reduce the energy barriers to the deposition of M_2S. For instance, it has been confirmed that the conversion between Li_2S_2 and Li_2S with sluggish kinetics accounted for about half of the theoretical capacity of LSBs.[59] According to previous research, the precipitation of Li_2S presents a 2D lateral growth at the triple-phase interfaces containing sulfur species, electrolytes, and conductive additives.[60] However, the uncontrollable growth of Li_2S would passivate the catalysts surface, inhibit the electron/ion transfers, and restrain the subsequent process, which eventually leads to "dead S." Hence, it is crucial to realize the reversible electrodeposition of Li_2S to avoid the passivation of catalytic centers for continuous polysulfide regulation capability.

Adjusting the deposition morphology of M_2S at the interface microenvironments has been considered an effective strategy to improve electrochemical redox performance. Based on this, a unique triple-phase interface that synergizes chemisorption, electronic supply, and catalytic activity has been constructed to regulate the catalytic behaviors of polysulfide intermediates and ensure the uniform and controllable growth of solid Li_2S.[61] The 3D growth model of Li_2S rather than 2D lateral growth seems to be a promising approach to realizing the reversible electrodeposition (**Figure 3**a,b). Very recently, a Mo_2N–SnO_2 heterostructure (denoted as SND-Mo_2N) was designed to guide the Li_2S nuclear in a 3D growth model, which could avoid the passivation that occurred on the catalytic interface.[62] The compact Li_2S particles could be observed on the surface of Mo_2N, indicating a weak deposition capacity and severe surface passivation. While the SND-Mo_2N surface was covered by a rough Li_2S layer, indicating a different Li_2S growth behavior (Figure 3c,d). Furthermore, a stronger ability to promote the dissolution of Li_2S could be easily observed on the interface (Figure 3e–g), indicating the merit of the 3D growth model (Figure 3h,i). More recently, the catalytic decomposition mechanism of Li_2S has been systematically investigated on the surface of a series of metal sulfides (e.g., Ni_3S_2, FeS, CoS_2, VS_2, SnS_2, and TiS_2).[63] It was found that the energy barrier of decomposition was positively correlated with the initial peak voltage in the charging process and dominated by the interaction between the Li^+ and S in sulfides (Figure 3j,k). Therefore, a desirable Li^+ diffusion in the sulfur host is also vital to the reversible deposition of Li_2S.

2.4. In Situ Characterization of Reaction Processes

The fast advancements of PSRCs require to design of novel target-oriented characterization techniques for the complex catalytic conversion chemistry of polysulfide intermediates and the uncovering of bond interactions between intermediates and catalytic sites in MSBs, especially the in situ methods. So far, the electrochemical measurements (e.g., cycle voltammetry

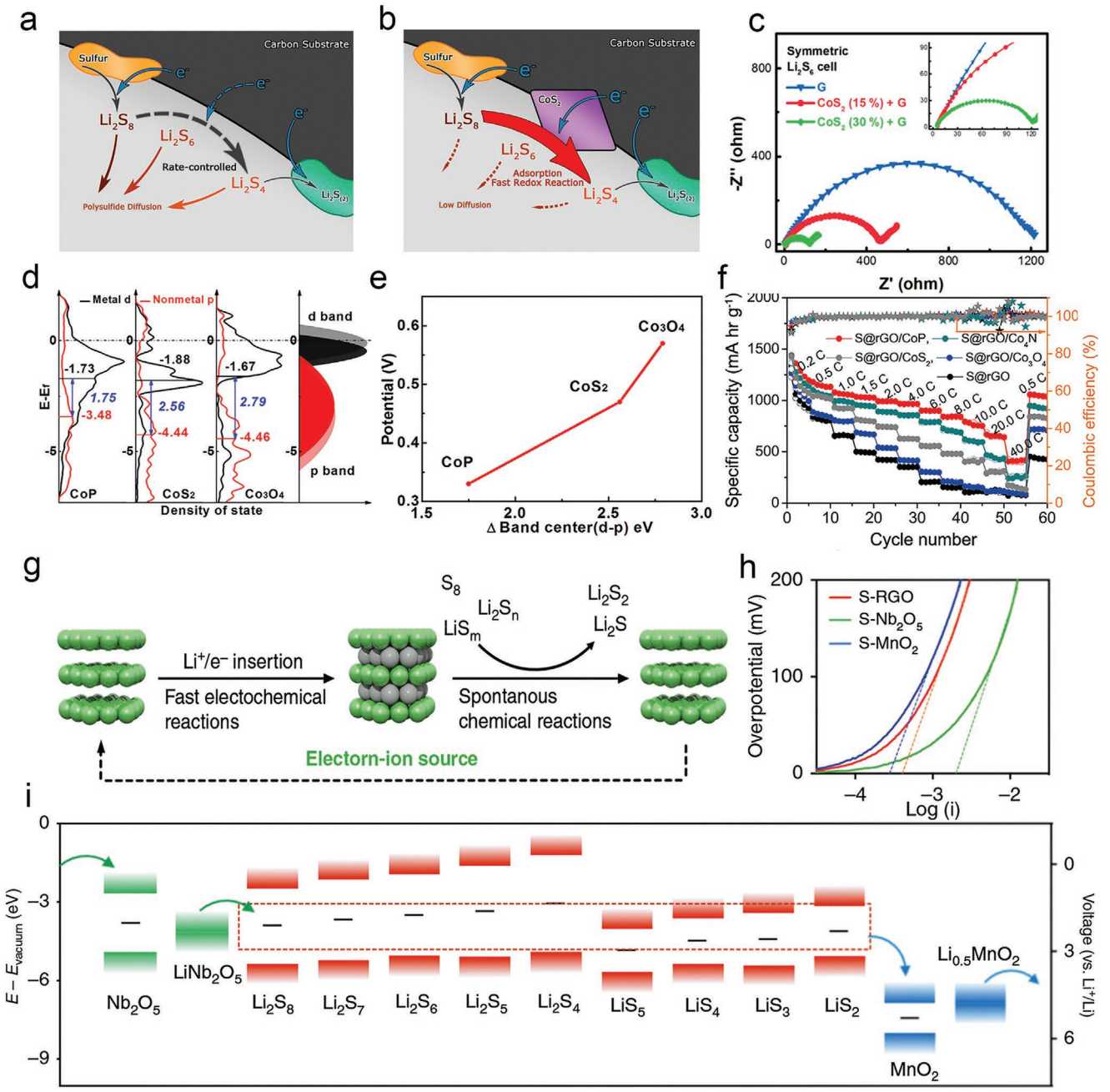

Figure 2. a,b) The schematic image of enhanced electron transfer between LiPSs and mediator by the CoS_2. c) Nyquist plots of the symmetric Li_2S_6 cells with different cathodes. Reproduced with permission.[34] Copyright 2016, American Chemical Society. d) The density of states (DOS) analysis of different Co-based compounds about the distance of the d–p bands center. e) The relation between redox potentials of Li_2S_6 and Δ band (d–p) center. f) The rate performance of cells assembled with different Co-based compounds. Reproduced with permission.[53] Copyright 2018, Elsevier. g) Schematic illustration of the electron/ion source mechanism during the charging process and h) corresponding evidence supported by the Tafel plot. i) The whole lithiation-catalytic mechanism during the charge–discharge process. Reproduced with permission.[58] Copyright 2020, Nature Publishing Group.

(CV), linear sweep voltammetry (LSV), electrochemical impedance spectroscopy (EIS)) and ex situ normal characterization (e.g., scanning electron microscope (SEM), transmission electron microscope (TEM), X-ray diffraction (XRD), X-ray absorption spectroscopy (XAS)) are still the mainstream methods to establish the relationship between the optimized performance and catalytic action of materials. However, the electrochemical measurements are usually limited by the capacity to combine the microscopic behavior of catalysts with the macroscopic electrochemical performances. Moreover, considering the air sensitivity of alkali metal and polysulfides, aerial oxidation of electrode materials may occur during the sample transfer and characterization process for the ex situ measurement. By contrast, in situ characterization techniques (**Figure 4**a),[64] such as in situ XRD, in situ XAS, and in situ Raman, are emerging as advanced methods to monitor real-time information on

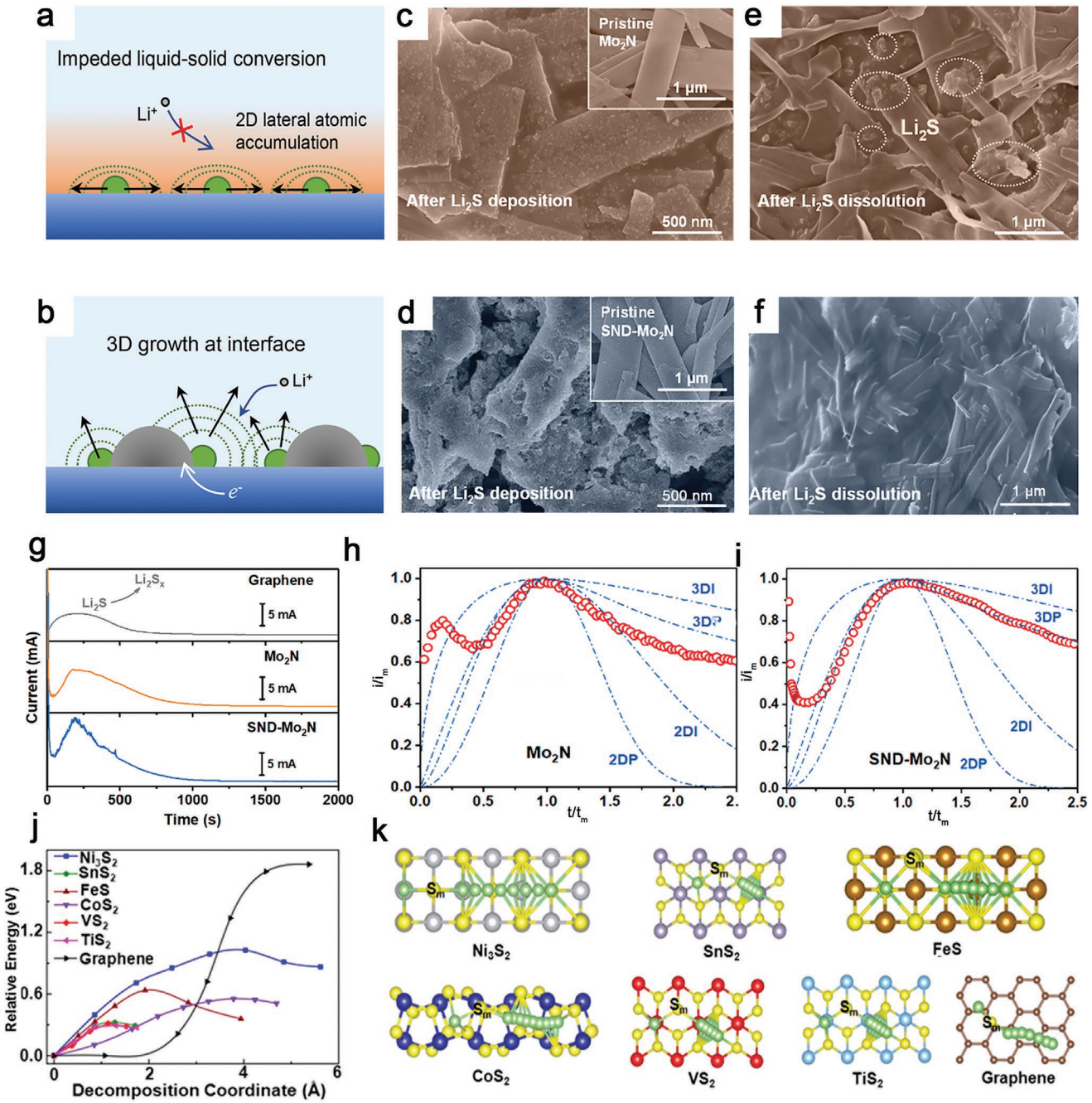

Figure 3. a,b) The growth model of Li_2S on the surface of Mo_2N and SND-Mo_2N. c,d) The electrodeposition morphology of Li_2S on the surface of Mo_2N and SND-Mo_2N. The surface image of e) Mo_2N and f) SND-Mo_2N after Li_2S dissolution. g) The kinetics evaluation of the Li_2S decomposition process. Dimensionless transient profiles of h) Mo_2N and i) SND-Mo_2N. Reproduced with permission.[62] Copyright 2021, American Chemical Society. j) Energy barrier of the Li_2S dissolution on different matrices. k) The schematic models of the Li_2S decomposition pathways on different substrates. Reproduced with permission.[63] Copyright 2017, National Academy of Sciences.

reaction kinetics for understanding the catalytic mechanisms of polysulfide intermediates and guide the future design of PSRCs.[65,66]

In situ XRD is based on the characteristic diffraction patterns derived from the X-ray scattering by the regular arrangement of atoms, which has been widely applied to detect the real-time phase transition of crystalline structured components. When it comes to MSBs, the application of in situ XRD can identify the phase transformation of insoluble sulfur species and also monitor the timing and account of their presences to evaluate the reaction dynamics, thus reflecting the catalytic performance of PSRCs. For example, Manthiram and co-workers probed the substantially improved conversion kinetics for polysulfide intermediates on the hydrophilic MoB nanoparticles via the in situ XRD analysis.[67] As shown in Figure 4b, accompanied by the disappearance of the α-S_8 signal ($2\theta = 23°$), the distinct

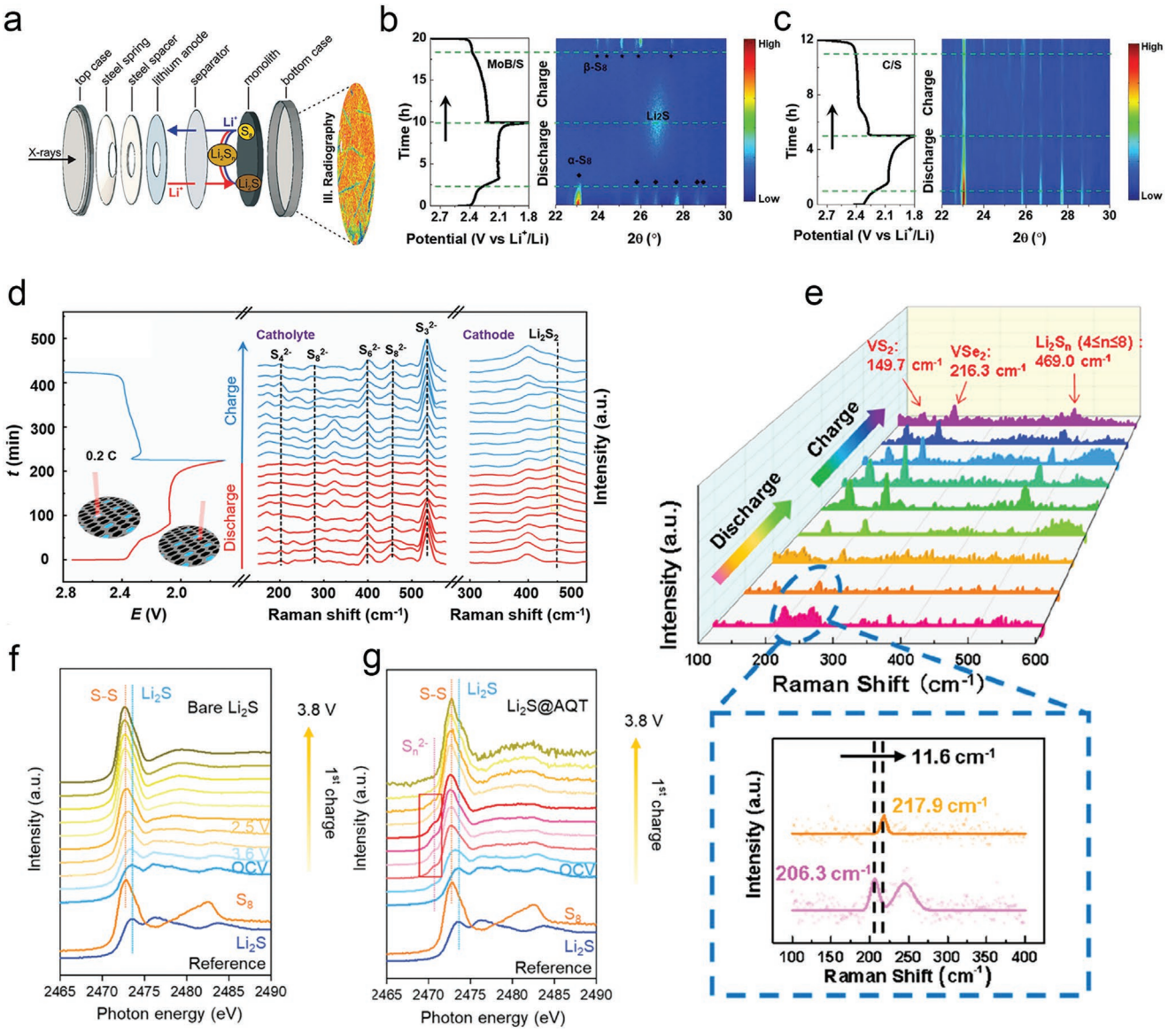

Figure 4. a) The schematic image of the cell used for in situ X-ray radiography. Reproduced with permission.[64] Copyright 2016, Royal Society of Chemistry. In situ XRD patterns of LSBs b) with MoB and c) without MoB as the catalytic cathode. Reproduced with permission.[67] Copyright 2020, Wiley-VCH. d) In situ Raman spectral of the cells assembled with V–N–C active sites. Reproduced with permission.[69] Copyright 2021, Elsevier. e) In situ Raman spectral of the cells assembled with VSe_2. Reproduced with permission.[70] Copyright 2020, American Chemical Society. The in situ sulfur *K*-edge XAS spectra of all-solid-state LSBs with f) bear Li_2S and g) Li_2S@AQT cathode. Reproduced with permission.[71] Copyright 2021, American Chemical Society.

signals located at ≈27° could be observed, which is attributed to the deposition of solid Li_2S. By contrast, there is no obvious Li_2S that can be detected in the C/S cathode without a catalyst (Figure 4c). Such in situ XRD measurement could clearly reveal the successful catalytic transformation of soluble intermediates into the solid Li_2S, which helps to resolve the questions regarding when solid Li_2S is present during cycling. Most current research on in situ XRD is applied for investigating the intermediate transformation in MSBs, however, rarely used in probing the real-time phase transition of the catalysts to interpret the mechanism better. Nevertheless, limited by the working principles, the in situ XRD is generally difficult to detect soluble polysulfide intermediates directly; therefore, integrated in situ techniques are required.

In situ Raman spectra is a powerful optical technique to detect the vibrational or rotational modes of functional groups in the molecular structure, which can be used to observe the soluble polysulfide intermediates in the electrolyte during cycling.[68] The Raman spectra of the catholyte region can clearly show the high-order soluble sulfur species involving S_8^{2-}, S_6^{2-}, and S_4^{2-}, and the spectra on the cathode can present the signal of low-order insoluble Li_2S_2 and Li_2S. As for the S/V–N–C cell in the work of Zhang and co-workers, the intensities of Raman signals for soluble polysulfide intermediates decrease gradually

during the discharging process, and it can be strengthened reversibly during the charging process.[69] Moreover, significant changes in the Li_2S signal can also be observed during one charging-discharging cycle when the focus was switched to the cathode part (Figure 4d). All these results demonstrate that the V–N–C PSRCs can accelerate the reaction kinetics of polysulfide to realize the reversible solid–liquid–solid conversion of sulfur species.

In addition to reaction kinetics, in situ Raman spectra can also be utilized to identify the bond interactions between PSRCs and polysulfide intermediates by detecting the signal change of PSRCs. For example, Sun and co-workers investigated the interface microenvironments between VSe_2-vertical graphene catalysts and polysulfide intermediates by in situ Raman spectra.[70] As shown in Figure 4e, the strong bond interactions between polysulfide intermediates and VSe_2 during the discharging process can be revealed by the obvious peak shift from 206.3 to 217.9 cm^{-1} (attributed to compression stress for VSe_2) in the Raman signals. Despite the versatility of this technology, it is still difficult to monitor soluble polysulfide intermediates under high spatial and temporal resolution because of their intrinsically weak signal response.

In situ XAS is a technique based on measuring electronic transitions to reflect the chemical composition and atomic environments, including the X-ray absorption near edge structure (XANES) and extended X-ray absorption fine structure. Because the *K*-edge and pre-edge resonances of XANES of sulfur are highly relevant to the oxidation state and bond environment, the relative content of each sulfur species can be determined precisely by a linear combination from the known XANES spectra, which will deepen our understanding of the mechanism of multistep conversion in MSBs. Moreover, by analyzing the dynamic transformation of the oxidation state and bonding environment, the catalytic mechanism of PSRCs in accelerating sulfur redox kinetics could be inferred. For example, Cui and co-workers have used operando sulfur *K*-edge to directly track the sulfur speciation in LSBs, and they have disclosed that the solid–polysulfide–solid reaction of cathodes with catalysts can facilitate the Li_2S oxidation.[71] As shown in Figure 4f, only the characteristic peaks of the Li_2S and S—S bond can be detected in the pristine Li_2S cathode, indicating the direct Li_2S—sulfur conversion in the LSBs. By contrast, the peak of S_n^2-species can be observed in the Li_2S@catalysts, indicating that the catalyst can induce the formation of polysulfide intermediates to reduce the activation energy barrier of Li_2S in all-solid-state LSBs. In general, researchers have gained much insight into the reaction mechanism of MSBs and the role of PSRCs using the in situ XAS. However, the in situ XAS usually has a relatively high test threshold due to the dependence on the synchrotron radiation sources.

In summary, in situ characterization has provided profound insights into the reaction process of MSBs and the catalytic mechanism of PSRCs, which is crucial for the rational design of PSRCs and the vigorous development of high-performance MSBs. Apart from the representative in situ XRD, in situ Raman spectra, and in situ XAS, many other advanced in situ techniques, such as SEM, TEM, Fourier transform infrared spectroscopy (FTIR), ultraviolet-visible spectroscopy (UV–vis), atomic force microscope (AFM) and nuclear magenetic resonance spectroscopy (NMR) have also possessed great potential in promoting the development of MSBs (the specific functions and limitations of such techniques have been summarized in **Table 2**). Generally, the in situ techniques regarding the disclosure of the reaction process and the role of PSRCs could be mainly divided into five aspects (**Scheme 2**): 1) polysulfide intermediates, 2) "shuttle effects" and corresponding reaction kinetics, 3) the bond interactions between polysulfide and catalytic sites, 4) the interface microenvironments and substrate effects, and 5) catalytic mechanism.

Table 2. Summary of the specific functions and limitations of each in situ characterization technique.

In situ techniques	Specific functions	Limitations	Refs.
XRD	Identify the voltage at which metal sulfides appeared to verify the catalytic kinetics	Limited to the detection of solid phases, it cannot detect the soluble polysulfides	[72,73]
Raman	Identify the polysulfide intermediates at the interface of PSRCs to verify the bond interactions	The signal is weak for most polysulfide intermediates	[70,74]
XAS	Can quantitatively detect the polysulfide intermediates and monitor the electronic states of catalytic sites	It can only be used under low sulfur loading; a high test threshold on devices	[75,76]
FTIR	Detect the polysulfide intermediates at the molecular level via the S–S vibration mode	Susceptible to interference from other components, it may be difficult to distinguish the spectra from electrolytes and catalysts' interfaces	[77,78]
UV–vis	Detect the soluble polysulfide intermediates qualitatively and quantitatively	Limited to detect the soluble phases, it cannot be used to detect solid metal sulfides	[79,80]
NMR	Detect the soluble polysulfide intermediates and distinguish the types	Susceptible to expensive setup and long sample preparing time	[81,82]
SEM	Monitor the nuclear and dissolution of solid metal sulfides	Complicated cells are needed and consume a lot of electrolytes.	[83,84]
TEM	Detect the size and morphology of solid metal sulfides	Electron beam damage to the intermediates can affect the results	[85,86]
AFM	Detect the real-time nucleation, growth, and dissolution of solid polysulfide	The signal is limited to the volume of solid-phase and also shows limited information on mechanisms	[87]

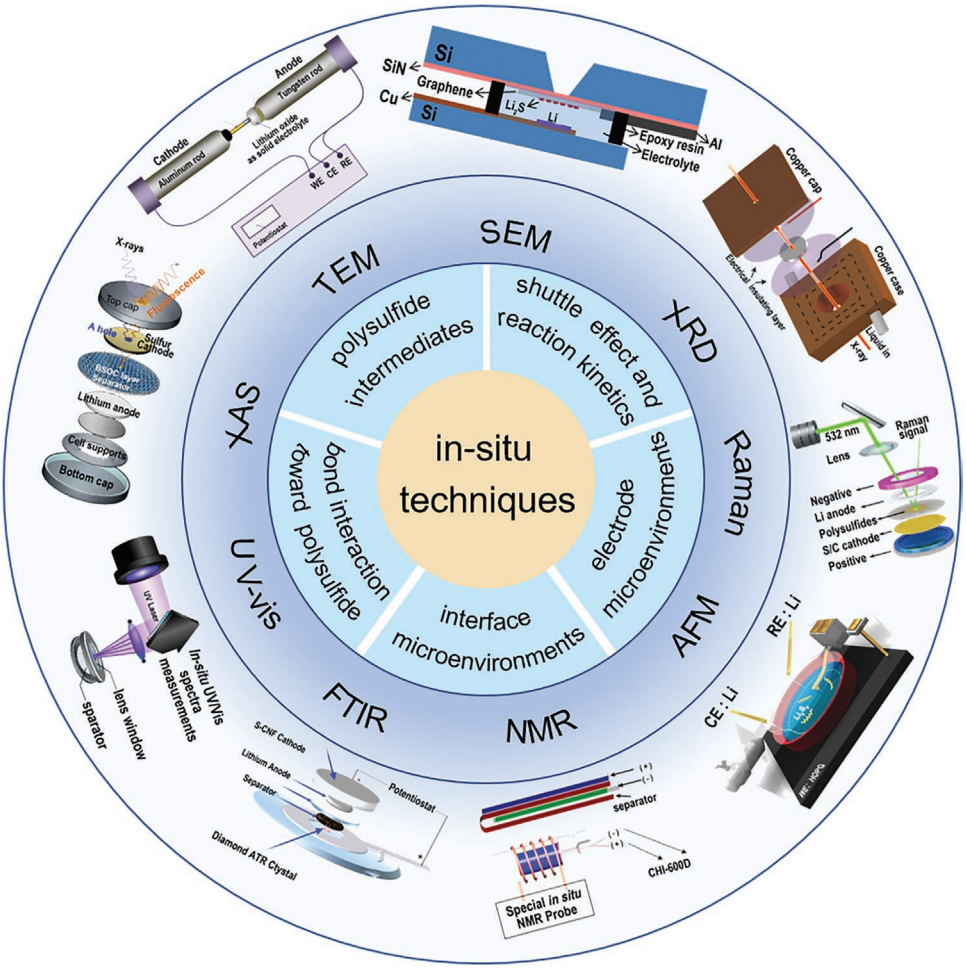

Scheme 2. The in situ techniques for understanding the catalytic mechanisms and corresponding reaction processes of PSRCs. AFM: Reproduced with permission.[88] Copyright 2016, Wiley-VCH. Raman: Reproduced with permission.[89] Copyright 2018, Wiley-VCH. SEM: Reproduced with permission.[83] Copyright 2015, Wiley-VCH. XAS: Reproduced with permission.[90] Copyright 2021, Wiley-VCH. XRD: Reproduced with permission.[91] Copyright 2018, Royal Society of Chemistry. NMR, Reproduced with permission.[92] Copyright 2015, American Chemical Society. FTIR: Reproduced with permission.[78] Copyright 2018, American Chemical Society. UV–vis: Reproduced with permission.[93] Copyright 2017, American Chemical Society. TEM: Reproduced with permission.[94] Copyright 2015, Wiley-VCH.

3. Modulating Bond Interactions of PSRCs for Advanced MSBs

Although tremendous efforts have been invested in designing desirable sulfur hosts for efficient polysulfide regulation, there is still huge space for improving the adsorption and catalytic sites of PSRCs. According to the previous interpretation of the reaction mechanisms of PSRCs, the appropriate structure/configuration of catalytic sites and moderate bond interactions with polysulfide intermediates play key roles in regulating the "shuttle effects." Therefore, to achieve optimal catalytic conversion efficiency, it is necessary to adopt different engineering strategies to modulate the catalytic sites and corresponding bond interactions with intermediates. The following sections will depict the detailed design methods and corresponding merits/defects that have been established recently for PSRCs, such as heteroatom doping,[95–97] vacancy engineering,[98] heterostructure construction,[16,99,100] coordination structure arrangements,[101–103] and crystal phase modulation.[104–106]

The bond interactions between PSRSs and polysulfide intermediates, such as binding resistance, binding energies, and electron transfer capacity, are crucial in optimizing the electrocatalytic polysulfide intermediates conversion. Therefore, it is highly essential to construct more satisfactorily while avoiding the introduction of extra inactive materials. The core objectives of bong interactions modulation can be summarized as the following three aspects: 1) the moderate binding energies can ensure sufficient chemical anchoring without hindering the migration of polysulfide intermediates and the re-exposure of the catalytic sites; 2) the desirable band structure of PSRCs for sufficient electron; 3) the integration of adsorption–catalytic platforms. In this review, we mainly focus on tailoring the bond interactions and interface between PSCRs and polysulfide intermediates, which could be categorized into five strategies: heteroatom doping, vacancy engineering, heterostructure construction, coordination structure arrangements, and crystal phase modulation (**Scheme 3**). Correspondingly, **Table 3** summarizes the state-of-the-art advancements regarding enhanced

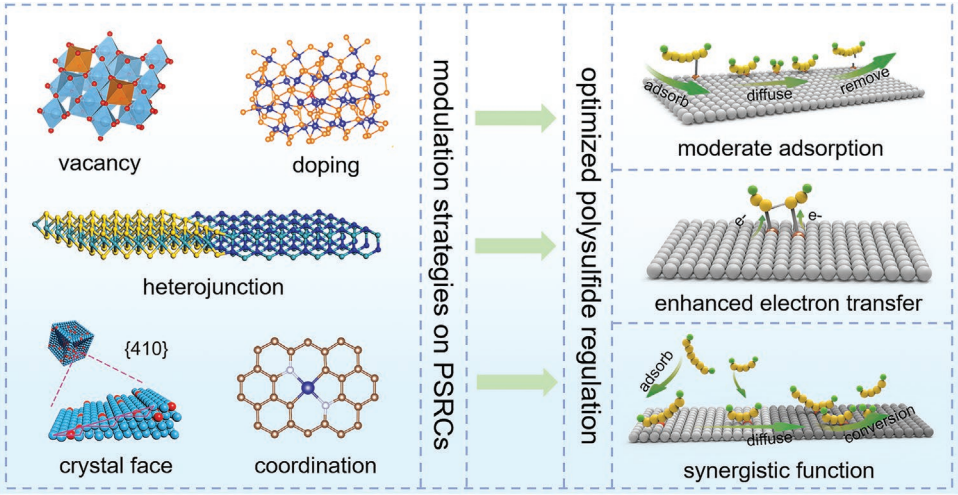

Scheme 3. The illustration of five modulation strategies for bond interactions and interface of PSRCs, as well as the thus-derived results. The crystal face model: Reproduced with permission.[107] Copyright 2022, Wiley-VCH.

electrochemical performance with the aid of these promising modulation strategies.

3.1. Heteroatom Doping

As an imperative strategy to modify the electronic structure and surface property of broad catalysts, heteroatom doping plays a pivotal role in enhancing the performances of catalysts in diverse application fields. For the recent study of MSBs, heteroatom doping engineering has been widely performed due to its promising potential in adjusting the adsorption ability of polysulfide intermediates and realizing rapid catalytic conversion kinetics.[98]

To obtain ideal MSBs performance, heteroatoms-doped carbon materials have been widely developed and reported during the last five years, including the N/S elements and transition metal doped porous carbon.[58,65,96] One of the most representative N/S elements doping has been carried out by Duan's group; they introduced the N and S atoms in the graphene substrate to further improve the synergistic catalytic regulation ability of carbon sheets for LiPSs.[108] The activation energy of N or/and S doped multihole graphene frameworks (N-HGF, S-HGF, and N, S-HGF) was investigated, wherein the N, S-HGF exhibited the smallest value of activation energy (**Figure 5**a). The N, S-HGF with the mediate p-band center of the volcano diagram when combining the overpotential of Li_2S deposition step with the binding energy toward LiS^* intermediate (Figure 5b,c). Compared with carbon, the exploration of heteroatom doping on metal compounds is still in its early stage. Liu and co-workers reported the synthesis of N-doped Co_9S_8 nanoparticles (N-Co_9S_8), which possessed stronger binding energy toward polysulfide than undoped Co_9S_8.[124] The inherent factor for the desired catalytic activity of N-doping is the changes in polysulfide bond length. Similarly, the N-$CoSe_2$ has been designed to compare with that of $CoSe_2$; as exhibited in Figure 5d, the S—S bond of Li_2S_4 was stretched when anchored on N-$CoSe_2$, thereby causing lower breaking energy and giving rise to the electrodeposition of Li_2S. Similarly, the Li—S bond of Li_2S was also longer on the N-$CoSe_2$ than on the pristine $CoSe_2$, implying a more efficient dissolution of Li_2S (Figure 5e). As a result, the dual-directional catalytic action toward the polysulfide intermediates could be realized with N doping in a pristine $CoSe_2$ (Figure 5f).[97]

Owning to the diversification of cations, cation-doping metal compounds have also shown abundant opportunities and gave rise to favorable impacts on polysulfide modulation.[95,109,110,125] For example, the Sn-doped ultrathin-layered α-MoO_3 nanoribbons show improved electrical conductivity and stronger binding energy toward S_8, Li_2S_4, and Li_2S as compared to those of MoO_3.[110] This intensified chemical adsorption of Sn-MoO_3 toward polysulfide intermediates could generate more competent mitigation for the "shuttle effects." Another important study has shown that the 3d-band center of Ni-based PSRCs can be obviously elevated by Co doping in Co-Ni_2P (Figure 5g), which will not only strengthen the affinity toward LiPSs but also lower the activation energy of Li_2S deposition, in turn effectively accelerating the polysulfide redox reaction process (Figure 5h,i).[109] In a word, the strategy of heteroatom doping has exhibited great potential in tailoring the conductivity and electronic configuration of the PSRCs, which is crucial to modulating the adsorption and desorption of polysulfide intermediates, thus optimizing their catalytic performances. Nevertheless, it should be noted that the precise control of the number and location of heteroatom via advanced synthetic methods would provide new opportunities for designing efficient and affordable PSRCs.

3.2. Vacancy Engineering

The introduction of vacancies was also considered a significant engineering strategy to modify the geometrical and chemical configuration of PSRCs. On the one hand, profiting from the unique localized electrons, the vacancy could serve as the adsorption or catalytic sites for the catalytic conversion

Table 3. Performances comparison of PSRCs-based cathodes via different modulation strategies.

Modulation strategy	Materials	S loading [mg cm^{-2}]	Initial capacity [mAh g^{-1}]	Rate [C]	Cycles/capacity retention [%]	Refs.
Heteroatom doping	N, S-HGF	≈4.0	840.0	1.0	500/87.5	[108]
	Co-Ni_2P	≈5.0	1223.0	0.1	100/90.8	[109]
	Sn-MoO_3	≈1.5	905.7	1.0	500/79.6	[110]
	N-$CoSe_2$	≈2.0	926.0	2.0	250/90.75	[97]
	B-MoS_2	≈1.5	711.0	5.0	1300/74.0	[111]
Vacancy engineering	DHPCs	≈1.5	746.0	2.0	500/70.0	[112]
	$Ni_3N_{0.85}$	≈1.5	1097.4	2.0	1000/61.0	[113]
	Nb_2O_{5-x}	≈1.0	1056.6	0.2	100/81.8	[114]
	Ta_2O_{5-x}	≈1.0	913.7	1.0	1000/71.0	[115]
	$Fe_{3-x}C$	–	834.0	1.0	1000/60.0	[116]
Heterostructure construction	ZnS–SnS_2	≈2.0	843.8	4.0	2000/74.9	[117]
	VO_2–VN	≈1.6	1425.0	0.2	100/77.9	[118]
	MoO_2–Mo_2N	≈3.1	790.0	0.1	100/74.0	[119]
	WS_2–WO_3	–	998.0	0.5	500/70.0	[113]
Coordination structure arrangements	Fe–N_2	≈1.5	1103.4	1.0	500/72.5	[48]
	Fe–N_5	≈1.0	906.8	1.0	500/73.0	[101]
	Ni–N_5	≈1.3	1086.0	0.5	500/73.5	[102]
	W–O_2N_2	≈1.1	1100.0	2.0	1000/55.0	[120]
Crystal phase modulation	SnO_2 (332)	≈1.2	941.1	0.5	500/73.0	[104]
	VO_2 (110)	≈2.4	543.0	5.0	1000/87.0	[121]
	Ni–Pt (410)	≈1.3	591.9	1.0	1000/75.0	[107]
	c-Fe_2O_3	≈1.0	1007.6	0.5	300/79.3	[122]
	a-CoO	≈2.0	1248.2	1.0	500/83.1	[123]

of polysulfide intermediates. On the other hand, the appearance of vacancies is inevitably accompanied by corresponding changes in the inherent electronic property and band structure, which would contribute to a deeper understanding of the polysulfide catalytic conversion mechanism.[98]

Owning to their high electrical conductivity and good structural tailor-ability, the carbon-based scaffold has been recognized as an optimal candidate for engineering vacancy-based catalytic materials.[126,127] Previous work has demonstrated that the edge sites of carbon vacancy present higher oxygen reduction reaction activity.[128] The introduction of intrinsic vacancy into carbon to expose more marginal sites is expected to increase the reaction kinetics of polysulfide redox catalysis, which has already been widely reported for the oxygen reduction reaction. For instance, abundant vacancy sites have been introduced into the porous carbon nanotube (CNT)-based microspheres (PCNTMs) via a critical "sauna" process to obtain reversible and fast redox conversions of polysulfide intermediates (**Figure 6**a,b).[129] Meanwhile, the occurrence of inherent defects in the graphitic structure of ePCNTM shows a much higher deposition capacity of Li_2S and stronger current rising, indicating the competitive reduction of polysulfide and deposition/decomposition of Li_2S compared to pristine CNT and PCNTM (Figure 6c).

Vacancy in metal compounds has also shown outstanding performance for optimizing the electrochemical redox activity of polysulfide. Thermal treatment for the metal compound in a reducing atmosphere (NH_3/H_2) has been identified as a productive method to generate vacancy. A simple thermal treatment of N-$MoSe_2$/C can be used to generate numerous Se vacancies. Accordingly, as-synthesized N-$MoSe_{2-x}$/C with an active site of Se vacancy could catalyze Li_2S nucleation and dissociation, respectively.[130] Moreover, a polysulfide etching-induction mechanism was also proposed as a newly emerged strategy to generate vacancy. For example, the Fe atom in the corner site of Ni_3FeN was etched by LiPSs during the charge and discharge process, forming the defect-rich $Ni_3Fe_{1-\delta}N$ (Figure 6d). The highest current response could be observed in the symmetric cell with Ni_3FeN/G (Figure 6e), indicating the fast polysulfide conversion accelerated by introducing defects. When assembled for working LSBs, the Ni_3FeN/G-based cells showed more obvious redox peaks than the pristine Ni_3N/G, further confirming excellent synergetic activity with high rate performance (Figure 6f,g).[131]

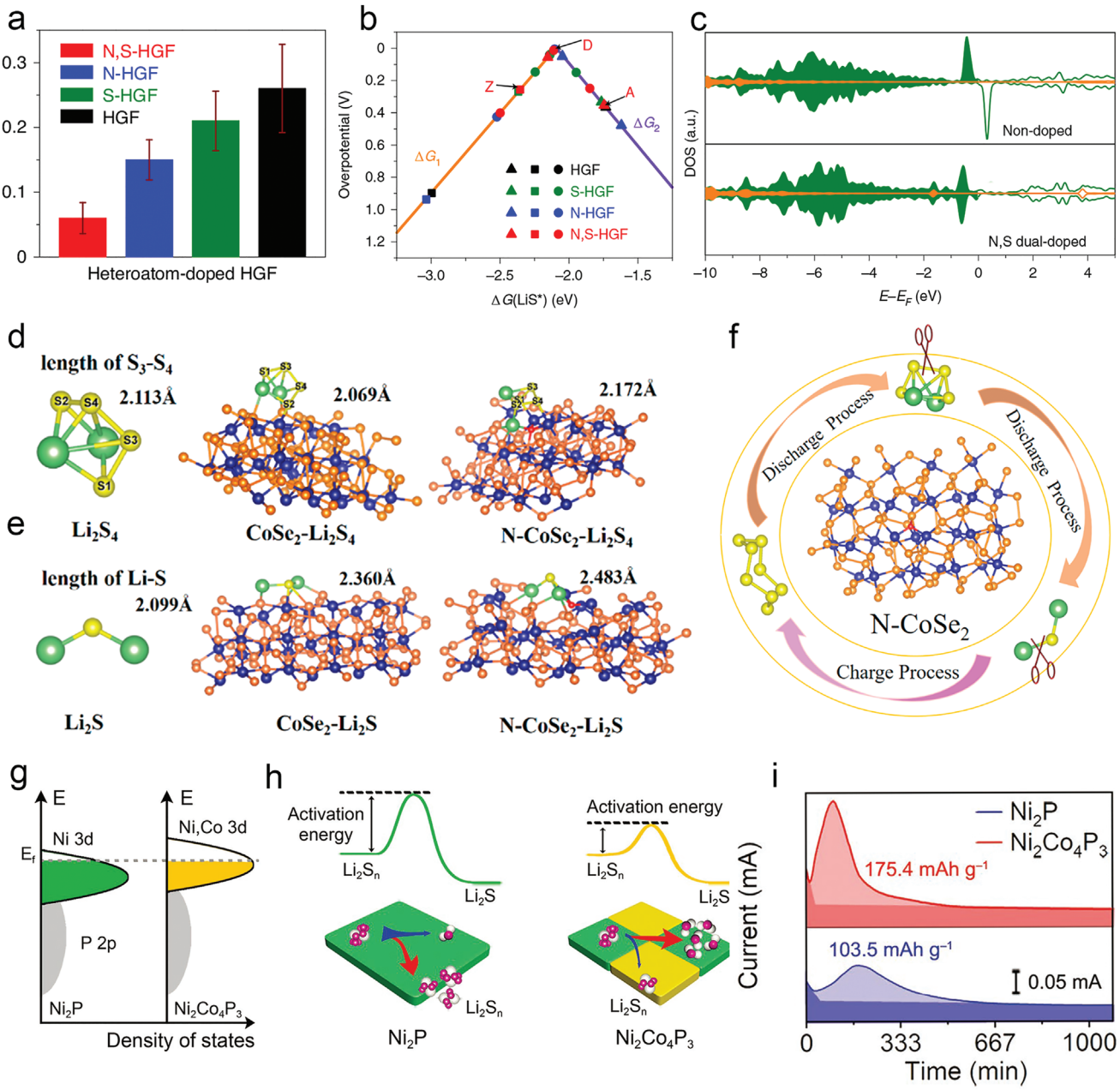

Figure 5. a) The activation energy and b) the volcano plot of the rate-determining step for polysulfide redox reaction. c) The p-band center shift after dual-doping. Reproduced with permission.[108] Copyright 2020, Nature Publishing Group. d) The S—S bond lengths of Li_2S_4 and e) Li—S bond lengths of Li_2S when anchored on $CoSe_2$ and N-$CoSe_2$. f) The mechanism of the dual-directional catalytic action of N-$CoSe_2$. Reproduced with permission.[97] Copyright 2020, American Chemical Society. g) The inherent cause and h) the action mechanism of optimized catalytic performance for polysulfide redox reaction. i) The Li_2S deposition experiment before and after Co doping. Reproduced with permission.[109] Copyright 2020, Wiley-VCH.

Similar to heteroatom doping engineering, the d-band theory has also been frequently employed to reveal the origin of the optimized electrocatalytic property of vacancy strategy. By introducing the N vacancy (Figure 6h), the d-band of Ni_3N was adjusted, in turn enhancing the catalytic capacity of inert Ni_3N and improving the redox kinetics for LSBs.[113] Combined with theoretical calculations, it could be identified that the existence of N vacancies endowed the $Ni_3N_{0.85}$ with a raised 3d-band center, which has been thought beneficial in decreasing the conversion energy barrier of polysulfide (Figure 6i). In addition, $Ni_3N_{0.85}$ possesses a higher electron filling in the antibonding states of the S—S bonds than Ni_3N. In this respect, the binding energy of S—S in Li_2S_4 was weakened when anchored on the surface of $Ni_3N_{0.85}$, which indicated that less energy was required to break the S—S bond and promoted the subsequent process (Figure 6j).

Although vacancy engineering has been recognized as an effective route to optimize the electronic structure and promote

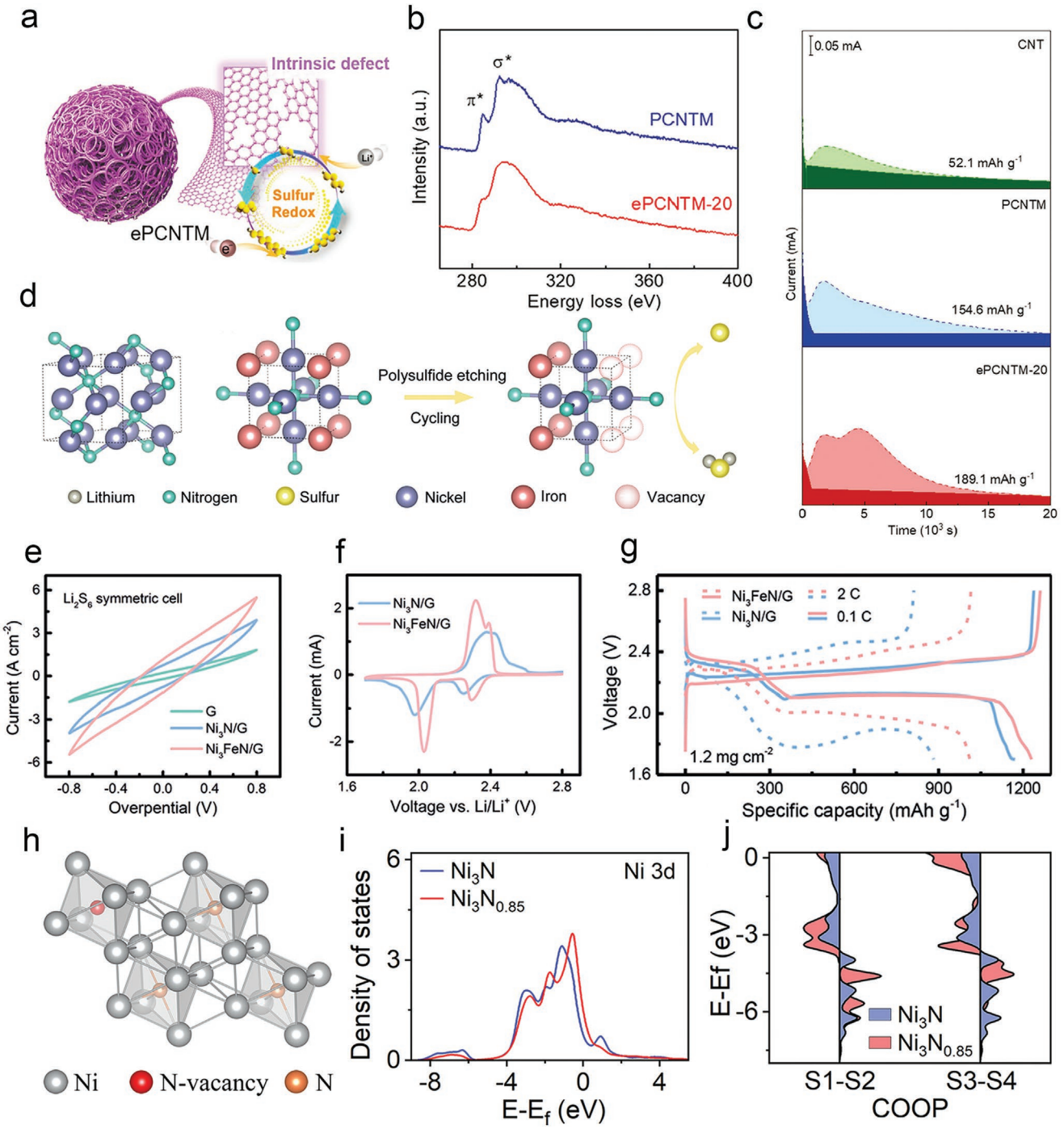

Figure 6. a) Schematic image of ePCNTM with defects for fast polysulfide conversion. b) Electron energy loss spectroscopy of PCNTM and ePCNTM. c) The deposition profiles of Li_2S on CNT, PCNTM, and ePCNTM. Reproduced with permission.[129] Copyright 2021, Wiley-VCH. d) The illustration of polysulfides etching-induction process toward defective $Ni_3Fe_{1-\delta}N$. CV curves of e) Li_2S_6 symmetric cells and f) working cells with modified separators, and g) corresponding rate performance. Reproduced with permission.[131] Copyright 2018, Wiley-VCH. h) Schematic image of N vacancy in Ni_3N. i) Density of States of Ni 3d orbitals before and after inducing N vacancy. j) Crystal orbital overlap population of S—S bonds of Li_2S_4 when anchored on the surface of $Ni_3N_{0.85}$ and prostate Ni_3N. Reproduced with permission.[113] Copyright 2020, American Chemical Society.

the catalytic activity of PSRCs, there are obstacles needed to be conquered to realize the further applications of vacancies strategy. For example, in addition to modulating the intrinsic catalytic activity of PSRCs, the vacancies themselves would also evolve accompanied by the conversion of polysulfide, which should be interpreted via more advanced characterization, and further investigations are needed. Moreover, it has been identified that excessive vacancies may generate a negative impact on

the adsorption or conversion of polysulfide intermediates.[132] In this regard, the vacancy concentration needs to be properly optimized for achieving desirable catalytic performances.

3.3. Heterostructure Construction

To ensure rapid and durable electrochemical redox conversion of polysulfide intermediates, the heterostructures combining the merits of different components have been investigated and received constant attention. It is worth noticing that an unhindered "anchoring–diffusion–conversion" of polysulfide could be conducted by the synergy of unique functional components. Furthermore, the optimized electronic structure exhibited desirable catalytic conversion ability due to the mutual adjustment of different components.[133,134]

Metal oxide exhibits outstanding chemisorption capacity toward polysulfide but is limited by unsatisfactory catalytic conversion performance.[135] From this perspective, incorporating metal oxides with active components to endow composites synergizing both polysulfide anchoring and rapid conversion capabilities was an effective strategy to inhibit the "shuttle effects" and achieve cycling performances. Therefore, a series of metal oxide-based heterostructures, such as WS_2–WO_3,[113] TiO_2–Ni_3S_2,[99] etc., were fabricated to achieve the adsorption–conversion of polysulfide intermediates. Nitride has been considered a conductive and catalytic active component for heterostructures. Therefore, the VO_2–VN heterostructure that combines the characteristic of ultrastrong anchoring (VO_2) and effective catalytic (VN) was reported. Hence constructing a smooth "anchoring–diffusion–conversion" pathway of polysulfide (**Figure 7**a–c).[118] The VO_2–VN heterostructure has obtained the highest Li_2S precipitation mass compared with the individual VO_2 and VN, thus offering intensified redox kinetics (Figure 7d–f). With such an effective synergy strategy, the assembled LSBs deliver desirable rate performance and cycling stability.

Another advantage of the heterostructure is the optimized electronic properties at the interface, which provide reversible electrochemical redox ability due to the mutual adjustment of both components. For example, atoms at the interface of $CoSe_2/Co_3O_4$ heterostructure show higher electron density than individual $CoSe_2$ and Co_3O_4 at the Fermi level (Figure 7g–i). The binding energy of the $CoSe_2/Co_3O_4$ interface toward Li_2S_6 species (–4.94 eV) is much higher than individual $CoSe_2$ and Co_3O_4, which further confirms this conclusion (Figure 7k). Meanwhile, the $CoSe_2/Co_3O_4$ heterostructure could effectively promote the reversed decomposition of Li_2S, thus alleviating the "shuttle effects" at the heterostructure interface.[136]

In summary, heterostructure catalysts composed of binary materials with different functions, like metal/semiconductors and p-/n-type semiconductors, would manifest charge migration and built-in electric field formation in the structure, which enables synergetic functions between different components. These extraordinary structure advantages of the heterogeneous interfaces would promote the combination of adsorption–conversion–desorption abilities on polysulfide intermediates, thus creating more interfaces in heterostructures will offer new direction for further performance optimization.

3.4. Coordination Structure Arrangements

Regulating the coordination environments around the active sites of PSRCs is considered an effective strategy to modulate the bond interactions and interface microenvironments for enhancing the electrochemical redox performance, especially for the single-atom catalysts (SACs) and MOFs-based PSRCs.[137,138] As for the MSBs, the optimized coordination structure of active sites could endow suitable bond strength and accelerated reversible catalytic conversion for polysulfide intermediates. In this section, the modulation of the coordination structures in SACs, and MOFs-based PSRCs will be discussed in detail.

The carbon materials supported M–N_4 structure is considered the dominant form of SACs-based PSRCs. Recently, the influence of Co-SAC with different N coordination numbers on the polysulfide conversion kinetics has been investigated systematically by combining theoretical calculation and electrochemical performances.[139] While this highly symmetrical local electron distribution may also lead to inferior catalytic performance. The coordination-defect Co–N_2 with asymmetric electron distribution exhibited greater advantages in anchoring polysulfide intermediates as well as accelerating catalytic conversion ability due to the stronger bond interaction than Co–N_4. The same conclusion can be extended to the Fe-SAC on carbon, where unsaturated Fe–N_2 coordination was synthesized using a "polymerization–pyrolysis" process (**Figure 8**a).[48] According to the DOS, the d-band center of Fe in FeN_2 (–0.74 eV) is approaching the Femi level than that of FeN_4 (–0.92 eV). After anchoring the Li_2S_6, a more pronounced charge can be observed on the Li_2S_6–FeN_2 interaction, which means a stronger electron transfer (Figure 8b,c). As a result, the Fe–N_2 electrode assembled cell exhibit a reversible areal capacity of 4.5 mAh cm^{-2} even under a high sulfur loading of 5.0 mg cm^{-2}.

On the contrary, the M–N_5 structure with oversaturated coordination environments is also thought of as a superior catalytic structure to the general M–N_4 structure. A novel oversaturated Fe–N_5 site was precisely synthesized by the absorption–pyrolysis strategy for the effective sulfur host (Figure 8d). The results exhibited that the sulfur composite cathode built on the Fe–N_5 structure could not only strengthen the binding energy and reduce the Li_2S decomposition barrier but also accelerate the Li^+ migration (Figure 8e,f).[101] After 500 cycles at 1 C, the battery cells assembled with Fe–N_5 electrodes exhibited higher capacity retention of 662 mAh g^{-1} than those assembled with Fe–N_4 electrodes (560 mAh g^{-1}). This strategy was also applicable to the Ni SACs. The Ni–N_5 sites were fabricated using a self-templating route, which was used as an ideal sulfur cathode for LSBs. Electrochemical analysis and theoretical calculations demonstrated that the oversaturated Ni–N_5 not only anchored polysulfide effectively but also accelerated their conversion. As a result, the cells exhibited desirable rate performance and long-term cycling stability when assembled at Ni–N_5 sites.[102]

The saturated ligands around the active metal centers in a well-crystallized MOF structure also hinder their bond interaction with polysulfide intermediates, thereby decreasing the catalytic ability toward polysulfide conversion. Therefore, regulating the coordinate ligands around metal ions in MOFs to obtain more open metal sites is an effective strategy

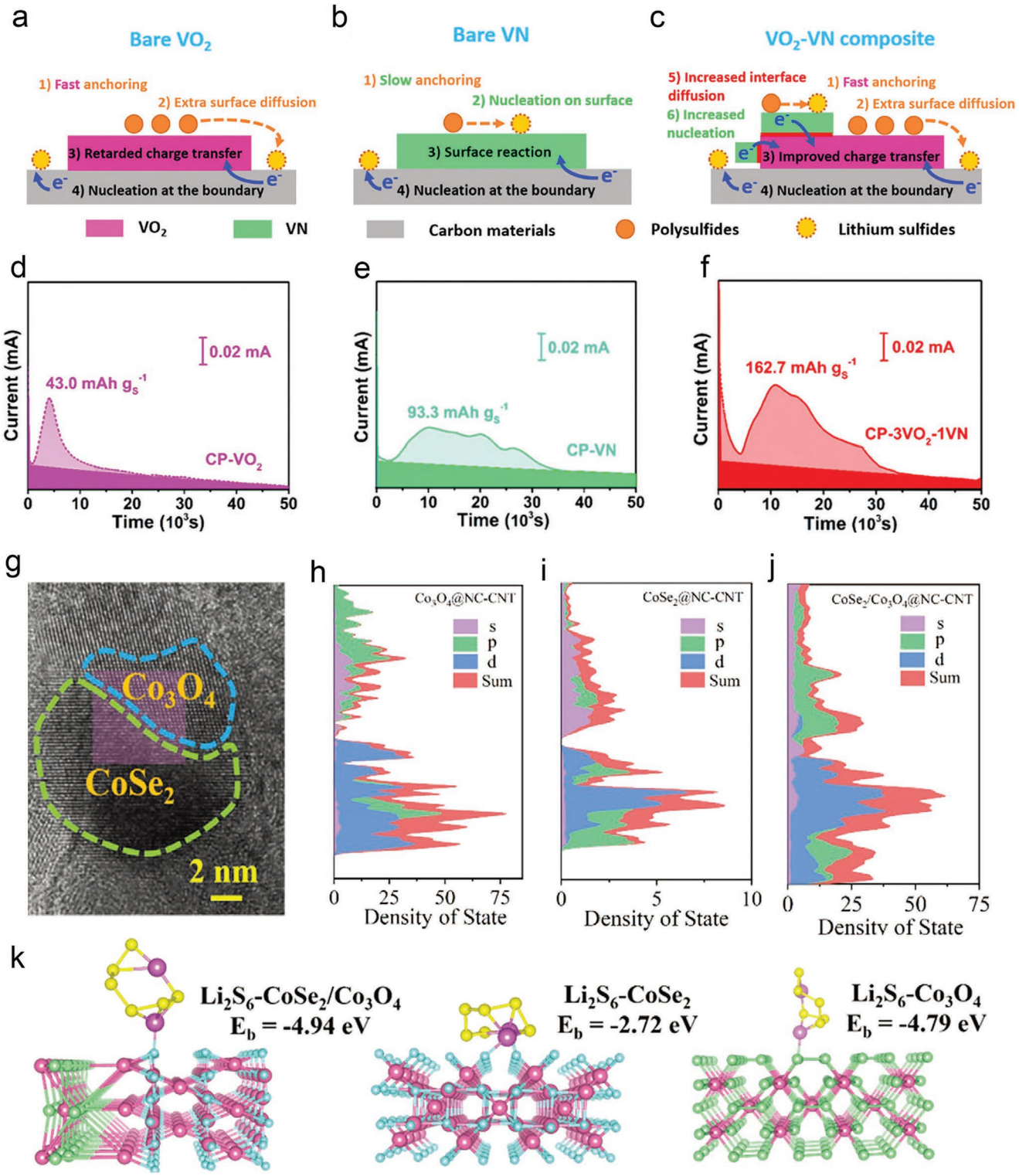

Figure 7. a–c) Schematic illustration of the cooperative effect between VN and VO_2 for effective polysulfide regulation. d–f) The facilitation toward Li_2S nucleation of VN–VO_2 composite. Reproduced with permission.[118] Copyright 2018, Royal Society of Chemistry. g) TEM image of $CoSe_2$–Co_3O_4 heterostructure. DOS of h) Co_3O_4, i) $CoSe_2$, and j) $CoSe_2$–Co_3O_4 heterostructure. k) The Li_2S_6 binding energy on different surfaces. Reproduced with permission.[136] Copyright 2022, Wiley-VCH.

for improving adsorption/catalytic performance.[50,103] For instance, Ce-MOF with different ligands amounts were designed, of which the Ce-MOF-2 with fewer ligands and more open metal sites exhibited stronger bond interaction toward

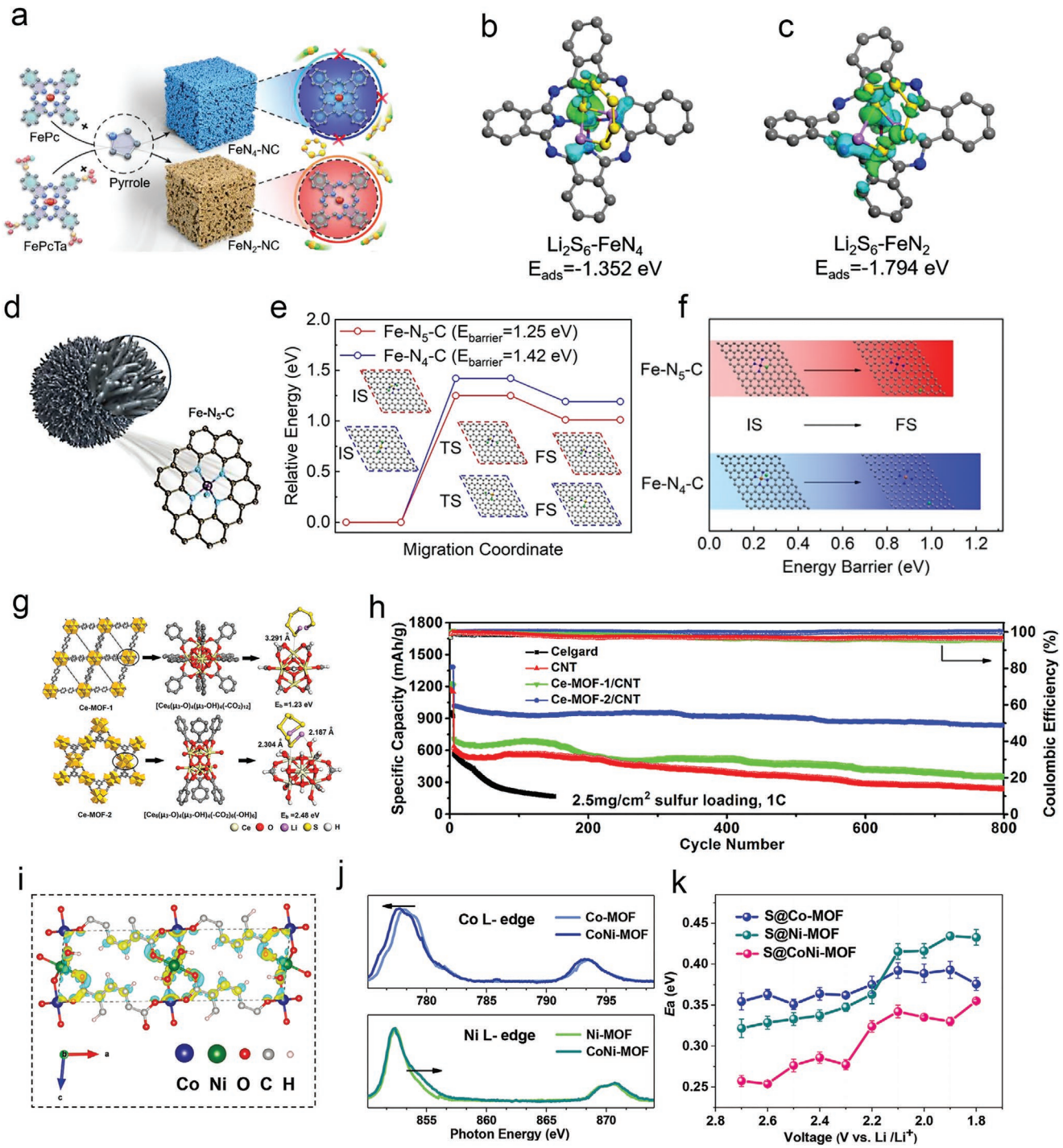

Figure 8. a) Fabrication of FeN_2-NC and FeN_4-NC. The optimized configuration after anchoring Li_2S_6 of b) FeN_4 and c) FeN_2. Reproduced with permission.[48] Copyright 2022, Elsevier. d) The Schematic illustration of FeN_5–C. The DFT calculation of e) the Li_2S decomposition and f) Li^+ diffusion energy barrier on Fe–N_4–C and Fe–N_5–C. Reproduced with permission.[101] Copyright 2021, Wiley-VCH. g) The bond interaction between Ce-MOF and polysulfides. h) The long-term cycling stability of LSBs assembled with Ce-MOF. Reproduced with permission.[50] Copyright 2019, American Chemical Society. i–k) The electron transfer between Ni and Co in the CoNi-MOF and corresponding influence on the activation energy barrier for polysulfide catalytic conversion. Reproduced with permission.[140] Copyright 2021, Wiley-VCH.

polysulfide for the unsaturated coordination of hexanuclear clusters (Figure 8g).[50] As a result, the cell assembled with a Ce-MOF-2 decorated separator displayed a capacity retention of 838.8 mAh g^{-1} after 800 cycles at 1 C, which is higher than that with Ce-MOF-1 (622.9 mAh g^{-1}) (Figure 8h). In addition to ligands, modulating the adjacent metal sites is considered to be another effective coordination engineer to improve the catalytic performance of MOFs. For instance, the 2D integrated

bimetal CoNi-MOF, where the Ni and Co sites were connected via an O bridge (Figure 8i).[140] The photon energy of Co and Ni in CoNi-MOF was changed compared to that in single-metal MOFs, confirming the charge transfer between the Ni–O–Co bridge (Figure 8j). This electron redistribution endowed the unoccupied 3d e_g state of Ni or Co, which would enhance the electrocatalytic activities for polysulfide conversion. As a result, the S@CoNi-MOF electrode exhibited the smallest activation energy barrier compared with single metal Co-MOF and Ni-MOF, indicating superior catalytic performance (Figure 8k).

Modulating the coordination structures of metal centers in SACs and MOFs, including changing the coordination atoms, adjusting the coordination numbers, introducing dual-atom centers, and further altering the coordination environments in the second coordination sphere, will provide further opportunities to improve the catalytic performances. However, there are still challenges that need to be overcome for both SACs and MOFs. For example, for SACs, the guarantee of the proportion of active sites with specific coordination environments appears to be in a dilemma due to the uncertain structural evolution during pyrolysis. For MOFs, the insufficient conductivity and stability still hinder its large-scale applications in batteries.

3.5. Crystal Phase Modulation

Since the arrangement of atoms on the interface of PSRCs has a significant influence on its catalytic properties, the modification of the crystal phase of PSRCs will lead to unique bond interactions and interface microenvironments of the catalytic sites. Especially, the high-index facets of PSRCs with high-density unsaturated coordinated sites in the steps or ledges have been believed to deliver superior catalytic performance than low-index facets, which exhibit great potential for optimized polysulfide regulation.[105,106,141] For example, the SnO_2 with different crystal facets were decorated on the reduced graphene oxide (rGO) to investigate their catalytic properties for polysulfide conversion.[104] As investigated, the SnO_2 (332) with high-index facets exhibited higher bonding energy with polysulfide than that of SnO_2 (111), indicating the stronger polysulfide anchoring capacity (**Figure 9**a). The stronger adsorption of SnO_2 (332) toward polysulfide can be predicted according to the orbital hybridization analyses; therefore, superior catalytic ability in both Li_2S precipitation and decomposition process was obtained (Figure 9b–d). A similar result was then extended to the high-index Fe_2O_3 with a high density of unsaturated coordinated Fe sites.[122] Such high-index Fe_2O_3 possessed both strong bond interaction and superior catalytic activity to the polysulfide catalytic conversion, thus resulting in a low capacity decay of 0.025% per cycle for 1600 cycles at 2 C when working as the cathode in the battery.

Amorphous materials have also provided a new opportunity for modulating the electronic properties of PSRCs toward satisfactory electrochemical intermediates adsorption, therefore attracting significant attention to the electrochemical redox reaction of polysulfides.[142] Very recently, the amorphization-induced strategy was proposed to enhance the polysulfide affinity of CoO (Figure 9e).[123] The enhanced bond interaction with polysulfide is caused by the redistribution of d-orbitals of Co atom in amorphous CoO (Figure 9f,g). As a result, the battery cells with amorphous CoO cathode exhibit smaller overpotential than that with crystalline CoO, and excellent capacity retention (1037.3 mAh g^{-1} after 500 cycles at 1 C) has been obtained (Figure 9h,i). In addition to CoO, amorphous FeP also displays stronger polysulfide management ability than the corresponding crystalline state.[143] Overall, crystal structure regulation and amorphization control have exhibited great potential in enhancing the intrinsic activity of catalysts for MSBs. Notably, amorphous structures usually display high catalytic activity due to their disordered surface atoms. However, this atomic uncertainty makes it difficult to investigate the detailed reaction mechanisms. The merits of amorphous structure on the PSRCs are still ambiguous, and more efforts should be devoted to this area.

4. Interface Microenvironments and Substrate Effects on PSRCs

The fatal polysulfide shuttle can result in the continuous loss of active sulfur of the cathode and the passivation of the anode, which lead to inferior electrochemical performances of MSBs. Benefitting from van der Waals force and physical confinement, various porous carbon materials, such as carbon fibers,[144] carbon nanotube,[145] and graphene,[146] have been used as the sulfur host in MSBs systems to trap polysulfide during the past few years. However, such strategies are still unsatisfactory in completely inhibiting the "shuttle effects" due to the weak physical interaction between the carbon interface and polysulfide intermediates. To conquer the inherent shortage of carbons, polar components with the chemical interactions with polysulfide are considered more efficient hosts to hinder the shuttle effects. Moreover, considering that the migration of polysulfide driven by concentration gradient is mainly caused by the sluggish conversion kinetics between soluble polysulfide species and insoluble polysulfide species (for example, from Li_2S_4 to Li_2S_2 in LSBs), the design of sulfur hosts with suitable interface microenvironments combined with physical interactions and catalytic conversion toward polysulfide is promised to overcome the "shuttle effects" from the root.[147,148] Up to now, there are enormous progress on developing PSRCs with tunable microenvironments and substrate effects to block polysulfide shuttle, including diverse metal compounds,[18–20] carbon-supported SACs,[21,22] metal–organic frameworks,[23–26] etc. In this section, we give a deep discussion on the interface microenvironments and substrate effects of different types of PSRCs on the battery performance.[149,150]

4.1. Metal Oxides

Metal oxides have emerged as promising candidates for high-performance cathodes in MSBs, due to the effective chemical affinity to the polysulfides due to their strong electronegativity oxygen anions. This substrate effect is attributed to the strong polarity of metal oxides;[7] however, the poor electron conductivity and low specific surface area of most metal oxides make them not suitable to direct use as a sulfur host. Consequently,

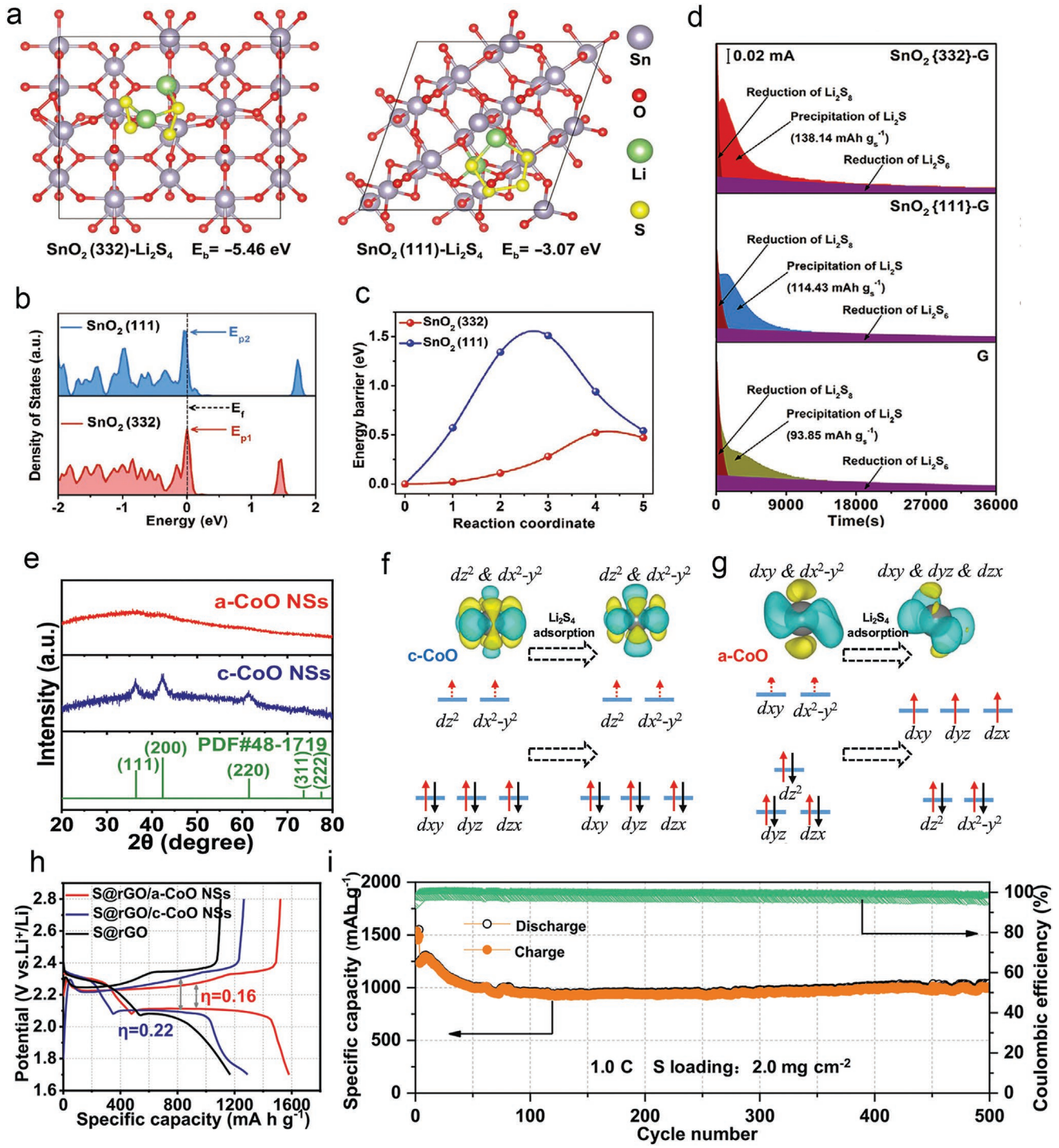

Figure 9. a) The binding energies of Li_2S_4 on the different facets of SnO_2. b) The DOS of Sn on different crystal facets. c,d) Comparison of Li_2S nucleation/decomposition energy barriers on different crystal facets. Reproduced with permission.[104] Copyright 2021, Wiley-VCH. e) The XRD of a-CoO and c-CoO, NSs indicate nanosheets. The binding mechanism toward Li_2S_4 by f) c-CoO and g) a-CoO. h,i) The priority of a-CoO in overpotential and cycling stability for LSBs. Reproduced with permission.[123] Copyright 2021, Nature Publishing Group.

most of the metal oxides are loaded on highly conductive and porous materials to modulate the interface microenvironments to satisfy their usage in the cathode of MSBs, such as the porous carbon or construction of heterojunctions.[151–153]

The Fe-based metal oxides (e.g., Fe_2O_3,[154] Fe_3O_4,[155] etc.) with a strong affinity toward polysulfides and electrochemical catalytic activities have been widely used in the MSB systems. For instance, the γ-Fe_2O_3 nanoparticles have been anchored in

a conductive CNT substrate for cathodes in LSB, where γ-Fe_2O_3 acts as active sites and the CNT increases the conductivity of cathode microenvironments for fast polysulfide conversion.[156] The corresponding LSB shows high rate capability (over 340 mAh g^{-1} at 7 C) and stable cycle performance (500 cycles at 1 C, 545 mAh g^{-1}). Subsequently, an in situ formed N-doped microporous carbon-supported superfine Fe_2O_3 nanocrystals (Fe_2O_3/N-MC) were reported as sulfur hosts, where the sulfiphilic Fe_2O_3 nanocrystals and the lithiophilic N-doped carbon are considered as dual active sites (**Figure 10**a).[157] The hybrid Fe_2O_3/N-MC cathode delivers an ultrahigh specific capacity of 730 mAh g^{-1} and excellent cycling stability at 5.0 C (Figure 10b). The excellent performance of these materials can be attributed to the increased interface conductivity and the formed dual active sites by forming "Fe—S, Li—O, or Li—N" bonds. Beside Fe-based oxides, titanium oxide (TiO_2) is also one of the most frequently studied sulfur hosts due to its natural abundancy and versatile structures.[158,159] For instance, a C@TiO_2@C sandwich-type composite was fabricated with the TiO_2 layer protected between both sides of carbon, which can efficiently retain the polysulfides with the assistance of physical confinement of interface via sandwich carbon structure.[160] Consequently, a battery with high specific capacity retention of 74% over 300 cycles was obtained at 0.5 C.

Instead of relying on conductive carbon to ensure electron transport, the Ti_4O_7 Magnéli phase with inherent metallic conductivity has been reported recently, which was then widely investigated as a sulfur host in MSBs.[161–164] The Ti_4O_7 Magnéli phase not only provides high conductivity but also can mitigate polysulfide intermediates dissolution by forming an excellent interface with polysulfide (Figure 10c).[161] The evidence for interface redox chemistry by strong polysulfide binding with the "sulphiphilic" host is proven by complementary physical and electrochemical probes. After that, the morphology and synthesis method of the Ti_4O_7 Magnéli phase were further optimized. For example, mesoporous Magnéli phase Ti_4O_7 microspheres were synthesized by in situ carbothermal reductions with resol,[162] polydopamine,[163] or Ti.[163] With the increased pore volume and surface area of the Ti_4O_7 Magnéli phase (Figure 10d),[162] the corresponding LSBs exhibited superior capacity retention of 78% after 400 cycles at 0.2 C (Figure 10e). Strong Ti–S interactions between Ti_4O_7 and polysulfide, as well as efficient physical trapping in the mesopores, are considered responsible for the improved electrochemical redox performance.

In addition to the well-known polar–polar interactions at the interface, a novel anchoring mechanism by redox interaction with polysulfide has been proposed, which happens when the redox potential window of the meal oxides is appropriate.[165,166] Nazar and co-workers have investigated the chemical reactivity of different metal oxides with polysulfide as a function of redox potential versus Li/Li^+, which indicates that VO_2, CuO, and MnO_2 with suitable redox potential are more efficient in blocking the emigration of the polysulfide from cathodes (Figure 10f).[166] Take MnO_2 as an example; the polysulfide produced in the beginning could react with MnO_2 to form thiosulfate groups (Figure 10g,h), then continues binding soluble polysulfides and convert them to insoluble polysulfides via disproportionation.[165] As a result, the sulfur/MnO_2 composite exhibited a reversible capacity of 1300 mAh g^{-1} at 2 C and a fade rate over 2000 cycles of 0.036%/cycle(Figure 10i). In general, as a strong polar host, the metal oxides play an important role in anchoring polysulfide intermediates in MSBs. However, the unsatisfactory electron transport capacity and too strong binding energy to the reaction intermediates largely hinder the subsequent catalytic conversion of polysulfide. Therefore, further optimization and surface functionalization of metal oxide by various engineering strategies are usually required, such as doping and vacancy, heterostructure construction, and crystal phase modulation.

4.2. Metal Chalcogenides

Compared with metal oxides, metal chalcogenides, which consist of metal elements and chalcogens (S,[167] Se,[168] or Te[169]), usually possess unique advantages, such as appropriate redox potentials, strong binding ability to polysulfides, and high stabilities when working in MSBs. These advantages can be attributed to the following characteristics of metal chalcogenides: 1) the softer bass of chalcogens anions will lead to a weakness of the ionic nature, which renders a higher electrical conductivity than metal oxides; 2) the higher valence electron density of the chalcogens–metal bond at the interface can accelerate electron transfer between substrate and polysulfide.[170,171] Up to now, various metal chalcogenides, such as MoS_2,[172,173] CoS_2,[174,175] Co_9S_8,[33,176] FeS,[177,178] etc., have been employed as sulfur hosts for polysulfide regulation. Among them, the MoS_2, as a typical 2D material, has great advantages in electron/ion conduction and high specific surface area.[170,179,180] In terms of accelerating polysulfide conversion, the coordination of unsaturated Mo atoms can form a strong Mo—S bond at its interface, thus facilitating the catalytic conversion of polysulfide intermediates. Under the theoretical calculation and experimental results, it is also confirmed that the active sites mainly occurred on the edge part of the substrates (**Figure 11**a).[181] It has been realized that 1T-MoS_2 shows higher conductivity and more active sites than 2H-MoS_2, which is a favorite for polysulfide catalytic conversion.[182] For example, a freestanding, 3D graphene/1T-MoS_2 (3DG/TM) constructed by graphene nanosheets sandwiched by hydrophilic, metallic, and few-layered 1T-MoS_2 nanosheets with abundant active sites was reported as efficient polysulfides redox catalysis (Figure 11b). The resulted 3DG/TM battery exhibits a high reversible discharge capacity of 1181 mAh g^{-1} and capacity retention of 96.3% after 200 cycles (Figure 11c).[35] Co_8S_9, which is considered to provide stronger bond interaction with polysulfide, was reported as a promising sulfiphilic cathode.[183] The synergistic strong dual-interactions (Co–S and Li–S) between polysulfide and Co_8S_9 resulted in a stable cycling behavior (ultralow capacity decay rate of less than 0.045% per cycle at 0.5 C) (Figure 10d,e).[184]

Since Se shows similar electronegativity and radius to S, metal selenides also possess desirable interface electronic and catalytic properties to metal sulfides.[185] Moreover, the higher tap density of metal selenide exhibits more promising in high volume energy density MSBs.[186] Similar to MoS_2, $MoSe_2$ is also considered to perform an enhanced catalytic activity at the edge.[187] In addition to Li—Se bonds, the Mo—S bond is also

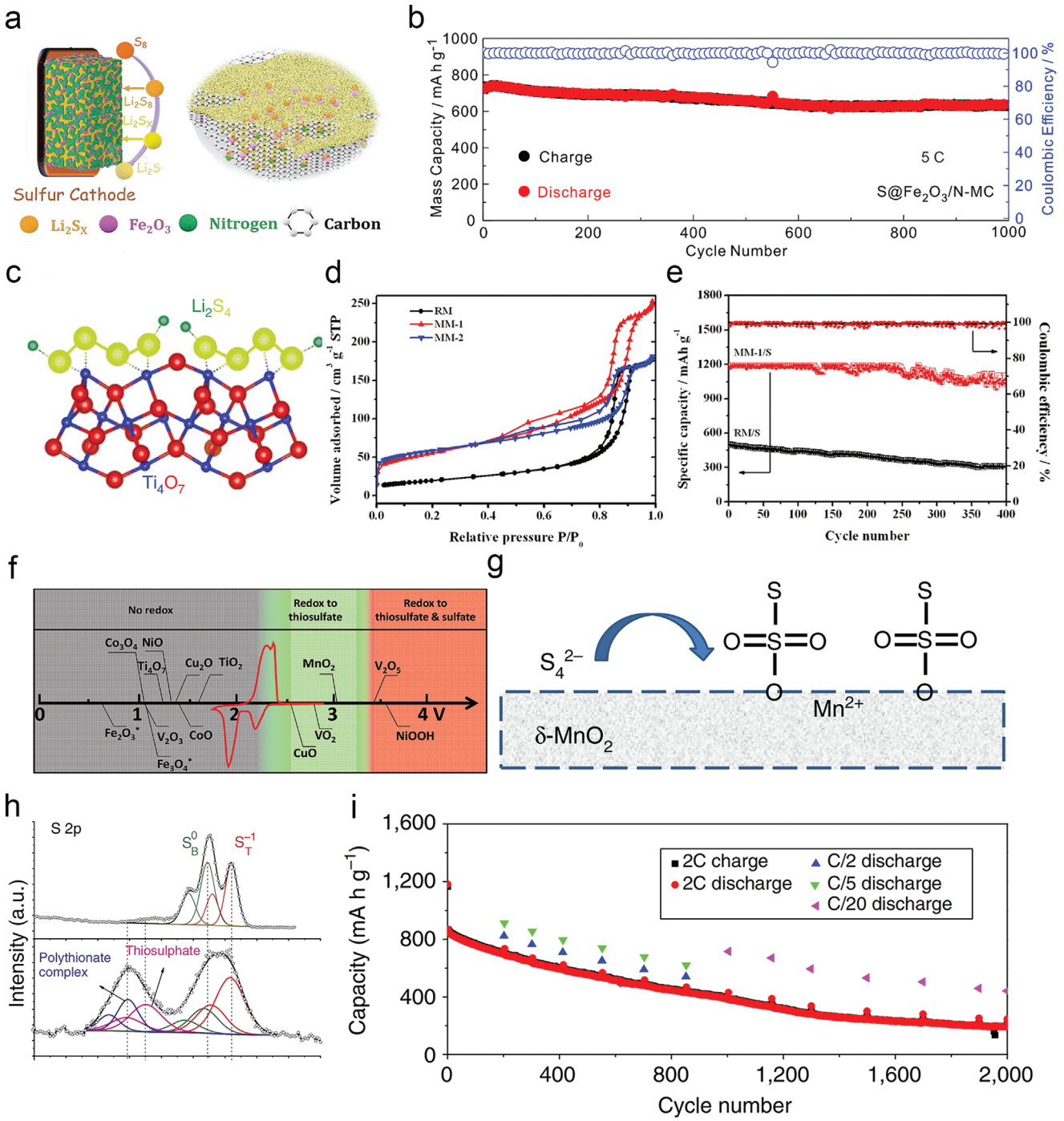

Figure 10. a) The catalytic mechanism of Fe_2O_3/N-MC for fast polysulfide conversion and b) corresponding cycling stability under a high current rate. Reproduced with permission.[157] Copyright 2021, Wiley-VCH. c) The bond interaction between Ti_4O_7 Magnéli phase and polysulfide. Reproduced with permission.[161] Copyright 2014, Nature Publishing Group. d) The nitrogen adsorption isotherms of mesoporous Ti_4O_7 with different carbon contents and e) corresponding cycling performance. Reproduced with permission.[162] Copyright 2017, Wiley-VCH. f) The classification of metal oxides according to the "goldilocks principle." Reproduced with permission.[166] Copyright 2016, Wiley-VCH. g) The bond interactions illustration between MnO_2 and polysulfide and h) corresponding X-ray photoelectron spectroscopy results. i) The electrochemical performance of MnO_2/S electrode when assembled for LSBs. Reproduced with permission.[165] Copyright 2015, Nature Publishing Group.

discovered at the edge, contributing to the strong chemical interaction with polysulfides. Recently, the ultrathin $MoSe_2$ nanosheet was decorated on the surface of rGO vertically and exposed with abundant edge sites to regulate the polysulfide conversion kinetics (Figure 11f). When modified on the separator, the battery cells performed impressive capacity retention of 546.8 mAh g^{-1} after 1000 cycles at 0.5 C (Figure 11g). The excellent electrochemical redox performance could be attributed

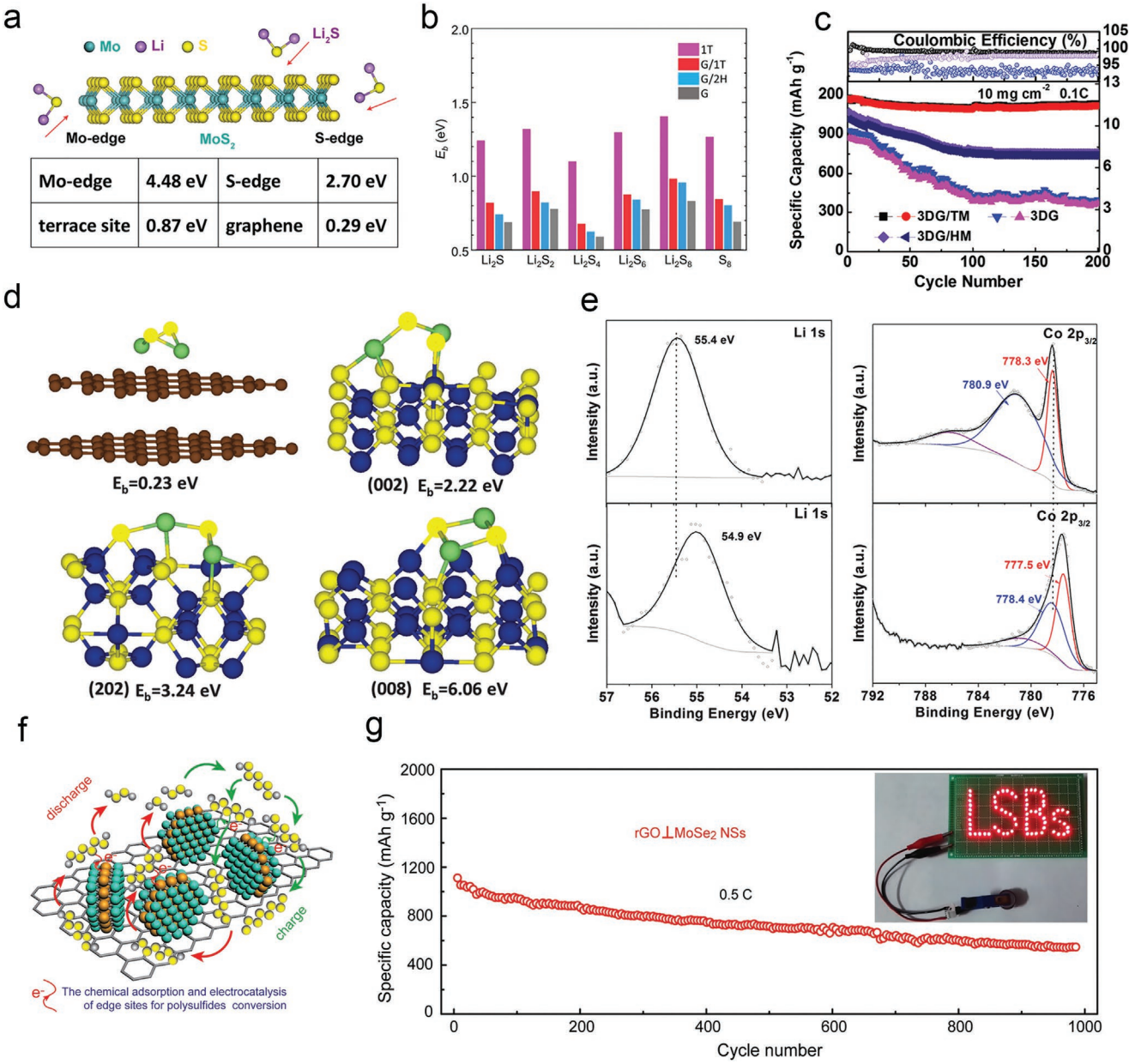

Figure 11. a) The interface anchoring of Li_2S on different MoS_2 sites. Reproduced with permission.[181] Copyright 2014, American Chemical Society. b) The bond free energy and c) the cycling performance of 1T-MoS_2 compared with 2H-MoS_2. Reproduced with permission.[35] Copyright 2019, Royal Society of Chemistry. d) The dual-interactions between Co_9S_8 and Li_2S_2 and e) corresponding XPS results. Reproduced with permission.[184] Copyright 2016, Royal Society of Chemistry. f,g) The scheme of $MoSe_2$ for polysulfide conversion and corresponding long-term cycling stability when assembled as sulfur host. Reproduced with permission.[188] Copyright 2018, Wiley-VCH.

to the fast interface anchoring and electron transfer of polysulfides.[188] To date, the mechanism of the metal chalcogenides in polysulfide conversion has not been fully comprehended. Diverse types of metal chalcogenides have been reported in terms of composition, shape, and morphology, which render a magnificent prospect in polysulfide redox chemistry. It has been revealed that the interactions between polysulfide and the preferred edge sites contribute most of the catalytic activity. In the future, to make the basal plane possess a similar high adsorption–catalytic capacity to the edge sites, new methods should be introduced to optimize the electronic structures and adsorption/desorption abilities of the basal plane in metal chalcogenides.

4.3. Metal Carbides, Nitrides, Borides, and Phosphides

Besides the extensively investigated metal oxides and chalcogenides, metal carbides,[189,190] nitrides,[129,191] borides,[43,67] and phosphides[45,192] have also emerged as superior candidates in inhibiting the polysulfide "shuttle effects." On the one hand, they generally exhibit high conductivity close to that of metals,

which is important to the interfacial electrochemical redox reaction. On the other hand, these emerged metal compounds also display satisfactory bond interactions with polysulfide intermediates, which imply the enhanced adsorption/catalytic properties at the interface.

Recent studies have discovered that the WC materials show Pt-like catalytic properties partially due to their unique d-band electronic density states, such as W_2C,[193] Ti_3C_2,[194] and Mo_2C,[195] which has riveted immense attention in the field of catalysis due to their catalytic activity, unique structure, and desirable electrical conductivity similar to noble metals. As for MSBs, metal carbides could effectively adsorb the soluble polysulfide via a chemical route and accelerate the redox reaction.[39,194,196] For example, the Mo_2C nanoclusters were decorated on the hollow carbon spheres (Mo_2C/CHS) as sulfur hosts for high-performance LSBs (**Figure 12**a–c). The theoretical calculation reveals that the d-band of Mo_2C is near the Fermi level, indicating a metallic nature electrical conductivity, which is a benefit for enhancing catalytic performance (Figure 12d). Therefore, the battery with Mo_2C/CHS cathode exhibits outstanding capacity retention of 85% after 100 cycles at 0.3 C, even at a high area loading of 3 mg cm^{-2} (Figure 12e).[40] Similarly, the highly dispersed Mo_2C in carbon matrix shows great promise in sodium–sulfur batteries.[190] Moreover, W_2C was considered to possess a more efficient polysulfide catalytic activity than Mo_2C due to its moderate and reversible interfacial binding energy toward polysulfide intermediates. As explored, the LSBs based on W_2C electrodes exhibited higher capacity retention (650 mAh g^{-1}) than Mo_2C electrodes (406 mAh g^{-1}) after 500 cycles at 1 C.[39]

Metal nitrides, which exhibit similar interface properties to metal carbides, have also been widely investigated as the cathode in MSBs. TiN is considered one of the most promising candidates for regulating polysulfide intermediates, especially when compared with the corresponding metal oxide for the higher conductivity (46 S cm^{-1} for TiN and 1.69×10^{-5} S cm^{-1} TiO_2).[197] Representatively, the TiN nanocrystal decorated on N-doped graphene (TiN@NG) composite was reported for LSBs with enhanced electrochemical performances. The TiN nanoparticles could efficiently bind with polysulfide at both Ti site and N site, thereby accelerating the reaction kinetics (Figure 12f). As a result, the TiN@NG/S cathode delivers a remarkable reversible capacity of 1390 mAh g^{-1} at 0.1 C and excellent cycling performance (730 mAh g^{-1} after 300 cycles) (Figure 12g,h).[198] In addition to TiN, VN also exhibited a strong affinity toward polysulfide through the formation of the V—S bonds as well as Li—N bonds.[199] The porous VN/NG was reported for sulfur host and exhibited a high initial capacity of 1471 mAh g^{-1} and a capacity retention rate of 85% after 100 cycles at 0.2 C even under a high sulfur loading of 3 mg cm^{-2}. The excellent battery performance could be attributed to the high conductivity and strong interfacial affinity of VN with polysulfides.[200]

The emerging metal borides also exhibit excellent conductivity and electrocatalytic effects for polysulfide conversion. Moreover, the boron atoms at the interface with empty 2p orbital endow metal borides strong anchoring ability to polysulfide via both M—S bonds and B—S bonds.[44,201] In this aspect, the polar TiB_2 was synthesized as a sulfur host and PSRC for LSBs without combining with conductive carbon pioneeringly.[43] The prolonged cycling performances at 1 C with a capacity decline rate of 0.058% per cycle over 500 cycles were obtained. The effect of nonmetal elements on the binding capability with polysulfide was further revealed by taking titanium-based composite (TiX) as model compounds (**Figure 13**a). The binding strength toward LiPSs enhances with the decrease of electronegativity of the nonmetal element (X) gradually with an order of TiB_2 > TiC > TiO_2 (Figure 13b), which is in the same order as the catalytic ability (Figure 13c). As a result, it could be inferred that the bond interactions between TiX and polysulfide increase with the decrease of electronegativity of nonmetallic elements (X), which demonstrates the advantages of borides in the regulation of polysulfide.[202] Moreover, a higher electronegativity metal element than Ti, for example, Cu and Co, was predicted to be satisfactory candidates for polysulfide reduction reactions. Therefore, the CoB composites as the sulfur host exhibited superior cycle stability in ultralong 1500 cycles at 5 C (Figure 13d,e).[44]

Metal phosphides, where the phosphors element exhibits high electronegativity, are also considered a promising PSRC to regulate polysulfide.[143,203] Furthermore, the convenient and low-cost synthetic process endows the metal phosphides with enormous potential as the cathode material applied in MSBs.[204] One of the first examples is synthesizing CoP nanoparticles with surface oxidation layers to enhance the interfacial polysulfide affinity. As shown in Figure 13f, the surface oxidized Co–O–P groups endowed the Co sites with high valence, creating strong bond interaction with polysulfide via Co—S bonding. With the anchoring capacity of polysulfide and desirable electrons conduction, the battery exhibited superior capacity retention after 200 cycles under a high loading of 7 mg cm^{-2}.[205] This phenomenon was also verified by the surface chemistry modulation on the FeP to enhance its electrochemical redox activity.[51]

With the advantages of promising electrical conductivity and excellent catalytic capability, emerging metal carbides, nitrides, borides, and phosphides have rendered a magnificent prospect for the PSRCs to realize high-performance MSBs. Despite that, the current synthetic processes usually involve high temperature or polluting atmosphere (such as NH_3 and PH_3), which prevent their large-scale preparation. Moreover, there are also barriers to regulating morphology and porosity of these materials. Thus, new researches into the facile, gentle, and controllable preparation of such materials are imperative to realize their future wide applications.

4.4. Metal Alloys

Benefiting from the high electrical conductivity and affinity with the S atom, metal nanoparticles have possessed a certain potential in regulating the polysulfide intermediates. However, their catalytic performance is usually restricted by the relatively fixed band structure and charge distribution. In comparison, by alloying with different metal species, the metal alloys have attracted great interests in catalyzing polysulfide intermediates owning to their tunable electronic structures.[74] For example, a Fe–Ni alloy has been prepared as a desirable PSRCs to realize the accelerated conversion kinetics of sulfur species in LSBs

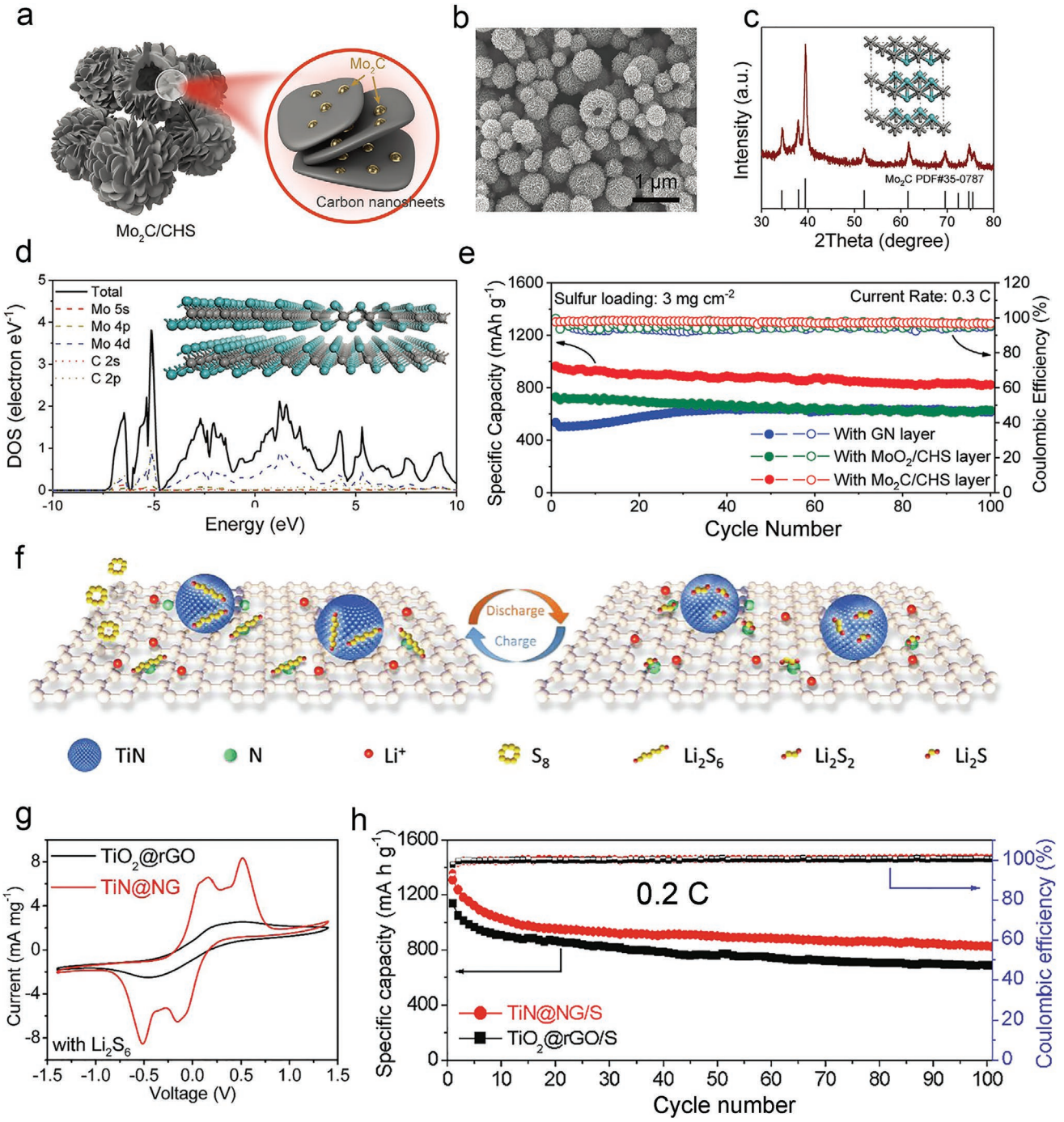

Figure 12. a) Schematic structure image, b) SEM, and c) XRD of Mo_2C/CHS. d) DOS of Mo_2C. e) Cycle stability of the battery with GN, MoO_2/CHS, and Mo_2C/CHS layers. Reproduced with permission.[40] Copyright 2021, Wiley-VCH. f) Scheme of chemical trap and electrocatalysis for LiPSs of TiN. g) Symmetrical CV curves and h) cycling performances of TiN@NG and TiO_2@rGO cathodes. Reproduced with permission.[198] Copyright 2021, Elsevier.

(**Figure 14**a–e).[206] As shown in Figure 14b, reversible disappearance and reappearance of S_8 peaks, and the obvious peaks of Li_2S have been detected in the cells assembled by Fe–Ni alloy-based PSRCs by in situ XRD. The well-designed Fe–Ni/S cathode showed excellent catalytic performance and desirable cycling stability compared to the Ni/S and C/S cathodes (Figure 14d). More impressively, the pouch cells assembled with Fe–Ni/S cathodes possessed a high capacity retention of about 400 mAh g^{-1} after 66 cycles even under pouch cell conditions, which indicates a promising application possibility (Figure 14e).

Considering the synergistic effects of diverse metals, emerging high entropy alloy (HEA) containing more than four metal elements has been designed and investigated for

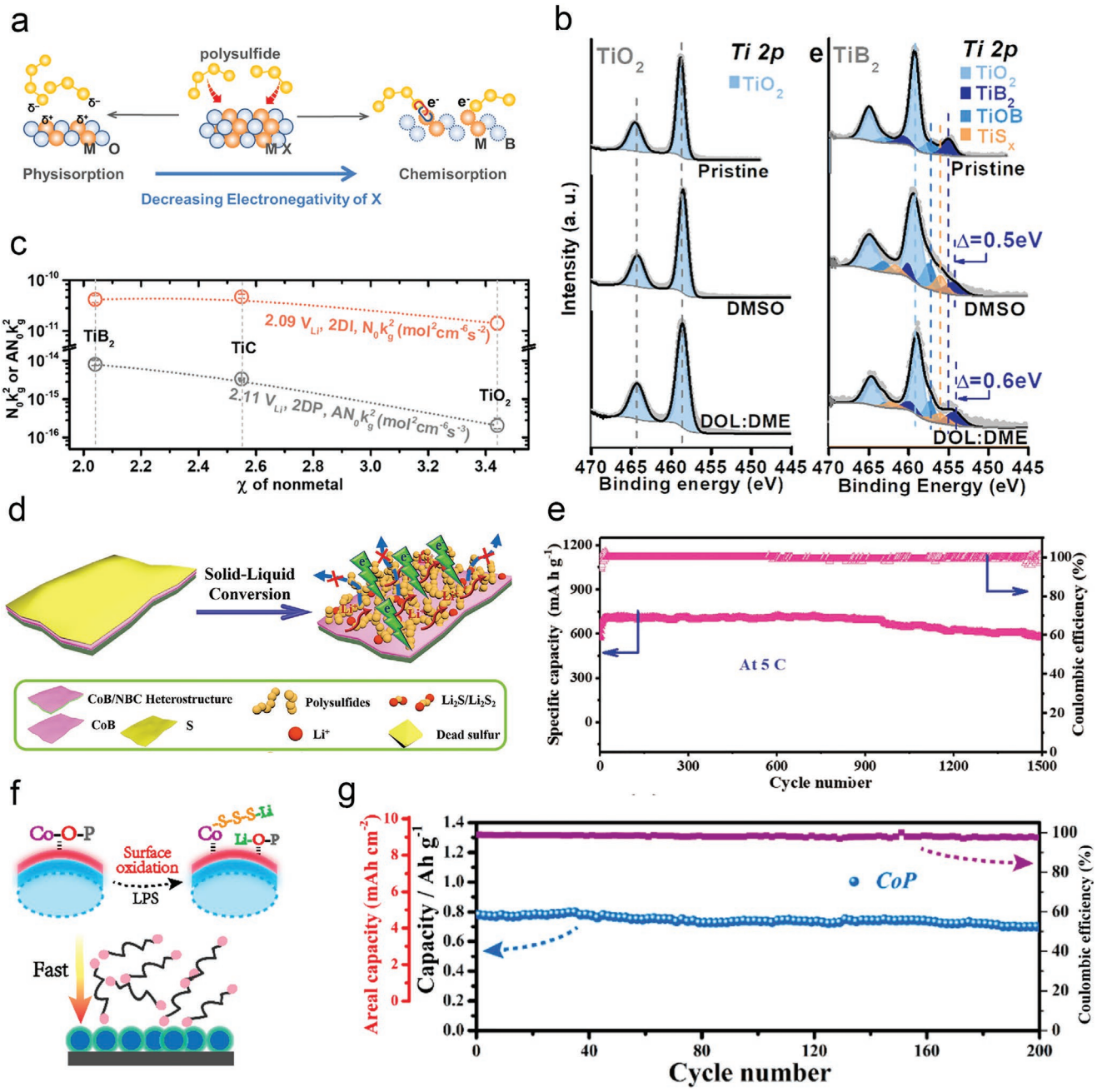

Figure 13. a) The influence of nonmetal element electronegativity on anchoring ability to polysulfides of MX. b) Ti 2p XPS of TiO_2 and TiB_2 before and after adsorbing Li_2S_8 in different solvents. c) The kinetics parameters of TiB_2, TiC, and TiO_2 for LSBs. Reproduced with permission.[202] Copyright 2019, American Chemical Society. d) The scheme of optimized polysulfide evolution in the surface of CoB/NBC heterostructure and e) corresponding cycling performance under a high current rate. Reproduced with permission.[44] Copyright 2021, Wiley-VCH. f) The scheme of the strong binding interaction between polysulfide and surface modulated CoP. g) The cycling performance of the CoP electrode under a high sulfur loading of 7 mg cm^{-2}. Reproduced with permission.[205] Copyright 2018, American Chemical Society.

PSRCs in MSBs. For example, Li and co-workers have developed a single-phase nano HEA containing Fe, Co, Ni, Mn, and Zn elements via a fast thermal reduction process, which exhibits excellent catalytic activity in multiple electrochemical reactions (Figure 14f,g).[207] Compared with the pristine Zn and FeCoNi alloy, the d-band center of FeCoNiMnZn HEA is closer to the Fermi level, indicating stronger bond interactions with polysulfide intermediates, thus ensuring the rapid kinetics of multielectron conversion of sulfur (Figure 14h). As a result, the cells assembled with FeCoNiMnZn HEA exhibit much lower overpotential than that of pristine Zn and FeCoNi alloy (Figure 14i). The rational regulation of HEA components opens a new avenue for the precise design of high-performance PSRCs via alloying method.

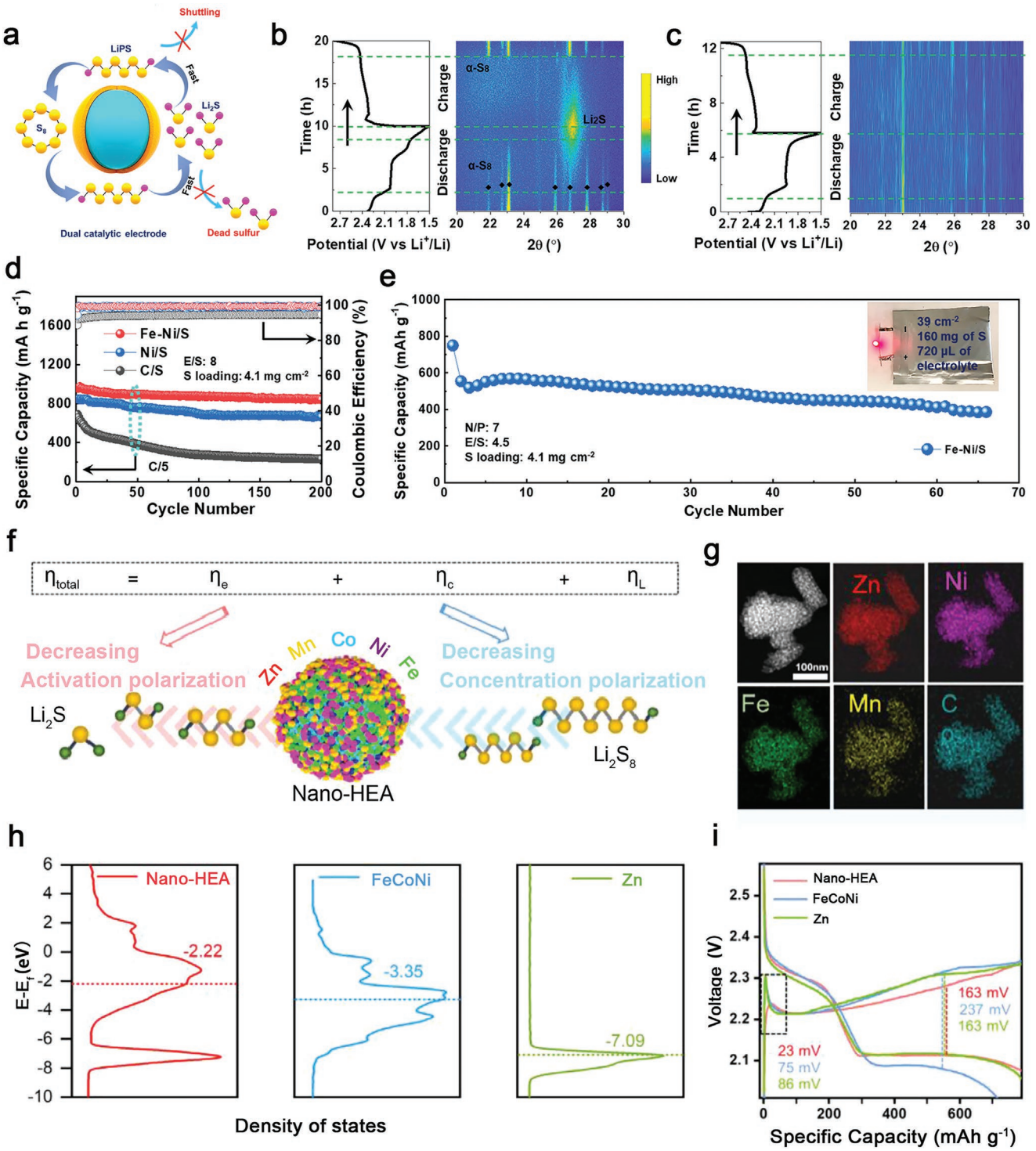

Figure 14. a) The schematic image of Fe–Ni alloy in regulating polysulfide intermediates. The in situ XRD pattern of cells b) with and c) without Fe–Ni alloy as the PSRCs. d)The cycling performance of LSBs assembled with Fe–Ni/S, Ni/S, and C/S cathodes. e) The practical potential of Fe–Ni/S cathode under the pouch cell. Reproduced with permission.[206] Copyright 2021, American Chemical Society. f) The catalytic mechanism of ZnMnCoNiFe HEA for polysulfide conversion and g) corresponding HAADF image and elemental mappings. h) The density of states of pristine Zn, FeCoNi, and nano-HEA. i) The charge/discharge profiles of the cells assembled with different PSRCs. Reproduced with permission.[207] Copyright 2021, Elsevier.

4.5. Carbon-Supported Single-Atom Materials

SACs supported on carbon with isolated metal sites have been a fascinating research direction in catalysis because of the superior interface microenvironments with unique electronegativity, catalytic properties, and maximized atom-utilization efficiency.[208] As for MSBs, the large aggregates of traditional metal-based inorganics severely hinder the prospect of high

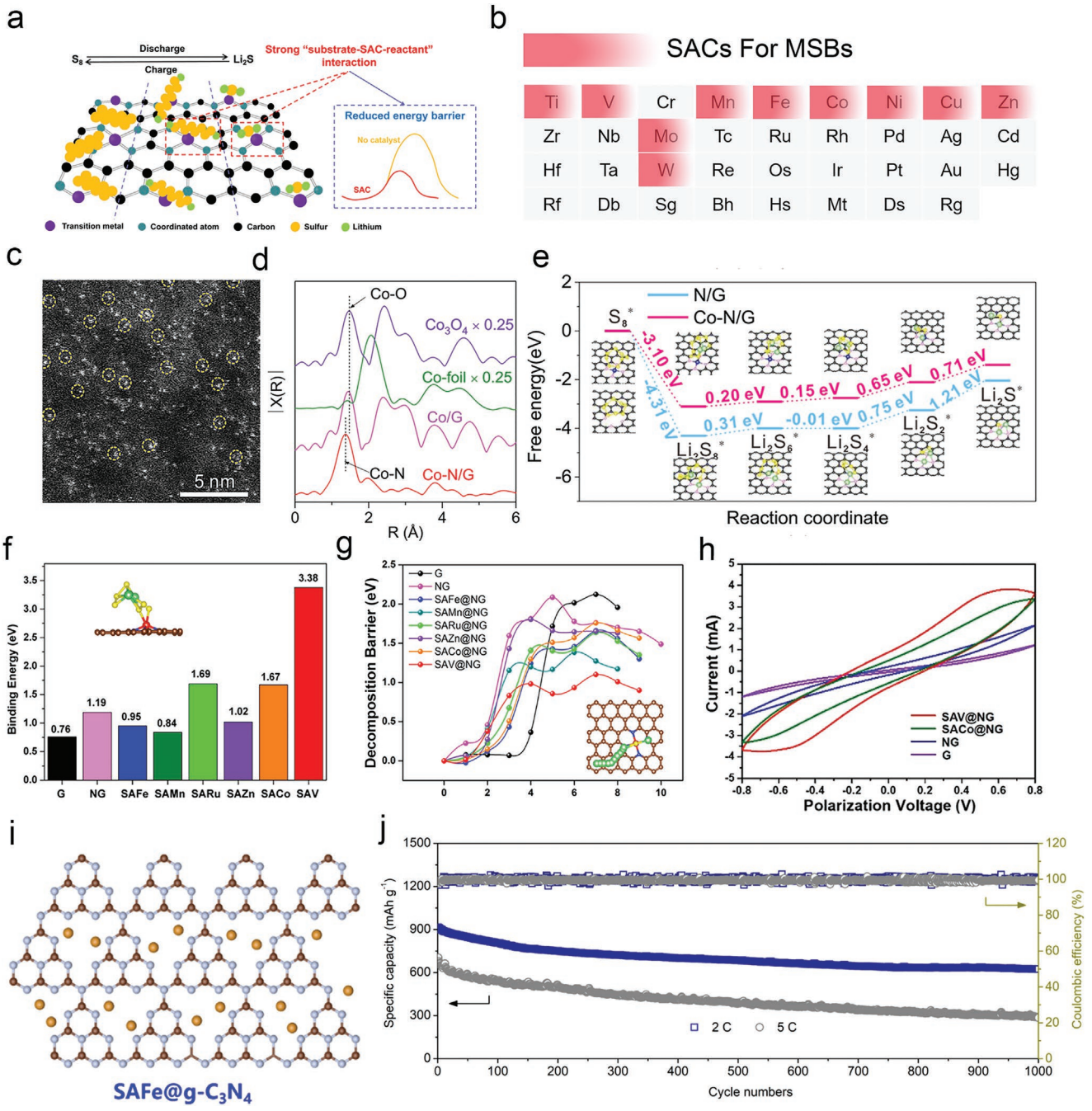

Figure 15. a) Catalytic mechanism of SACs toward polysulfide. Reproduced with permission.[21] Copyright 2021, Elsevier. b) Summary of different metal centers used in MSBs. c) High-angle annular dark field STEM image and d) X-ray absorption fine structure spectra of Co-N/G. e) Gibbs free energy of the polysulfide conversion on Co-N/G and N/G. Reproduced with permission.[210] Copyright 2019, American Chemical Society. f) The Li_2S_6 binding energy, g) Li_2S decomposition barrier, and h) symmetry CV on the surface of SAV@NG, SACo@NG, NG, and G. Reproduced with permission.[47] Copyright 2020, American Chemical Society. i) Illustration of SAFe@g-C_3N_4 and j) corresponding long-term cycling stability of LSBs in a bear electrolyte addition. Reproduced with permission.[216] Copyright 2020, American Chemical Society.

energy density batteries. Therefore, applying SACs to serve as PSRCs could effectively anchor and accelerate the catalytic conversion of polysulfide intermediates without sacrificing the proportion of active substances in the cathode, thereby increasing the energy density of MSBs (**Figure 15**a).[21] The Fe SACs on carbon support were first introduced to MSBs by Yang and co-workers in 2018. The results indicate that single Fe atoms function as adsorption sites for polysulfide and promote the uniform nucleation of Li_2S, thereby enhancing the cycling stability of the batteries.[209] This pioneering work provided a new method for efficient polysulfide regulation. Afterward, the Co-SACs with Co–N_4 coordination (Co–N/G) were then

reported as the sulfur host, which can trigger the surface-mediated reaction of polysulfides (Figure 15c,d).[115,210] The S@Co–N/G composite cathode delivers a high specific capacity of 1210 mAh g^{-1} with a low capacity fading rate, which could be attributed to the bifunctional electrocatalytic activities (revealed by the first-principles calculation result in Figure 15e of Co-SACs to facilitate both the formation and the decomposition of Li_2S in discharge and charge processes, respectively. Single Ni atoms on nitrogen-doped graphene (Ni@NG) were reported to modify the separators of LSBs, in which the oxidized Ni sites in the Ni–N_4 structure can trap polysulfide and show efficient accommodation of polysulfide ion electrons by forming a strong bond between S_x^{2-} and Ni–N. Therefore, the LSBs with Ni@NG modified separator exhibit stable cycling life with a low-capacity decay rate of 0.06% per cycle.[211] Until now, various metal atoms have been reported to mitigate the "shuttle effects," including the Co, Fe, Ni, etc., which are summarized in Figure 15b.[120,211–214] This pioneering research affords fresh insights for developing SACs to accelerate the conversion kinetics of polysulfides in MSBs.

To avoid the randomness in center metals selected, the V-NG catalysts have been designed for efficient LSBs under the supervision of theoretical simulations.[47] Various SAC@NG were evaluated from binding energy, Li_2S decomposition energy barrier, and other aspects. It was found that SAV@NG showed the largest adsorption energy toward Li_2S_6 (3.38 eV, Figure 15f) and the decomposition barrier of Li_2S (Figure 15g), indicating the best potential to inhibit polysulfide dissolution as well as promote the nucleation of Li_2S in LSBs. When assembled as the symmetry cells, the SAV@NG electrode exhibited the highest current response, indicating a more rapid polysulfide redox conversion than the others (Figure 15h). Very recently, various 3d metal centers (Sc to Cu) from the d–p orbital hybridization theory have been assessed to serve as PSRCs.[215] The result revealed that Ti-SAC exhibited a stronger d–p orbital hybridization degree with sulfur species, which was not only beneficial for effective polysulfide binding but also weakened the Li—S bonds, thus decreasing the associated dissociation energy barriers. As a result, the battery cells with Ti-SAC cathode delivered an excellent electrochemical performance.

The high content of single-atom sites in the interface microenvironments is crucial for maximizing polysulfide catalytic conversion activity during the cycling process, thereby improving the energy densities of LSBs. Under this consideration, high-content Fe-SACs decorated on C_3N_4 (SAFe@g-C_3N_4) with desirable catalytic capacity were fabricated to alleviate the "shuttle effects" in LSBs (Figure 15i).[216] Thanks to the abundant N sites in the support for strong coordination, as much as 8.5 wt% Fe content was reached, far more than previously reported Fe-SACs. Moreover, the inherent high charge polarity allows for enriched binding interactions of polysulfide intermediates. The reduced energy barrier for Li_2S delithiation on SAFe@g-C_3N_4 resulted in desirable rate and cycling performances in a rare electrolyte addition (Figure 15j).

In summary, carbon-supported SACs have exhibited fascinating performances in catalyzing the catalytic conversion of polysulfide intermediates. However, due to the complexity of the polysulfide intermediates ranging from soluble to insoluble species, the current polysulfide redox catalysis ability of carbon-supported SACs still needs to be further improved. First, designing carbon-supported SACs with an ultrahigh density of active sites is needed to promote the in situ contact of intermediates with the metal center for fast redox reactions. Second, the reported carbon-based SACs in MSBs are limited to single metal sites, and the synergistic effects of multimetal species deserve in-depth exploration. Third, the combination of theoretical and experimental analysis has offered the certain potential to reveal the catalytic mechanisms of PSRCs, while the discrepancy between theoretical and experimental results still exists, such as the possible changes in chemical structures and electronic structures of SACs. Therefore, more in situ characterization methods should be explored to offer reliable input for the theoretical analysis and reaction activity, such as the in situ Raman, XAS, and XPS tests.

4.6. Metal–Organic Frameworks

Recently, MOFs have attracted tremendous research interest in the energy storage and conversion fields because of their large porosities, high surface areas, and tunable chemical compositions and catalytic sites.[217,218] When applied in MSBs, it has been identified that the abundant coordination of metal ions with unoccupied orbitals in the MOFs can interact readily with electron-rich polysulfide anions via Lewis acid–base interactions.[23,24,219] Because of the strong chemical bond interactions (**Figure 16**a), MOFs-based PSRCs delivered desirable capacity in anchoring and catalyzing polysulfide intermediates. For example, the defect Zr-based MOFs (D-UiO-66) was confirmed to endow superior electrocatalytic capacity to promote the bidirectional conversion of polysulfides. When decorated on the membrane, the battery cells exhibited ultrahigh capacity-retention after 600 cycles at 3 C (Figure 16b).[220] To date, various metal ions and organic ligands have been widely combined to construct MOFs-based PSRCs for MSBs.[221,222]

The $Ni_3(HITP)_2$ MOF, which formed by linking the highly conjugated triphenylene-2,3,6,7,10,11-hexamine (HITP) with Ni (II) ion, exhibited superior electroconductivity due to the tight π-stacking facilitating effective linker orbital overlap (Figure 16c).[223] With ordered microporous structure, large specific surface area, good sulphiphilicity, and excellent conductivity, the $Ni_3(HITP)_2$ MOF was used to modify the commercial separator for suppressing the polysulfide shuttling. Taking the advantages of this $Ni_3(HITP)_2$ MOF, the battery with ultrahigh-sulfur-loading (8.0 mg cm^{-2}) delivers a high area capacity of 7.24 mAh cm^{-2} after 200 cycles (Figure 16d,e). Another approach to constructing conductive MOFs depends on a "π–d bond" form, which is constructed by hybridizing the frontier π orbital of the conjugated ligand and the d-orbital of a transition metal (Figure 16f). When presented as a sulfur host, a remarkable binding interaction for trapping soluble polysulfides was realized by Ni-MOF-1D (Figure 16g–i). As a result, impressive cycling stability with over 82% capacity retention over 1000 cycles at 3 C, superior rate performance of 575 mAh g^{-1} at 8 C, and a high areal capacity of 6.63 mAh cm^{-2} under raised sulfur loading of 6.7 mg cm^{-2} were obtained.[224]

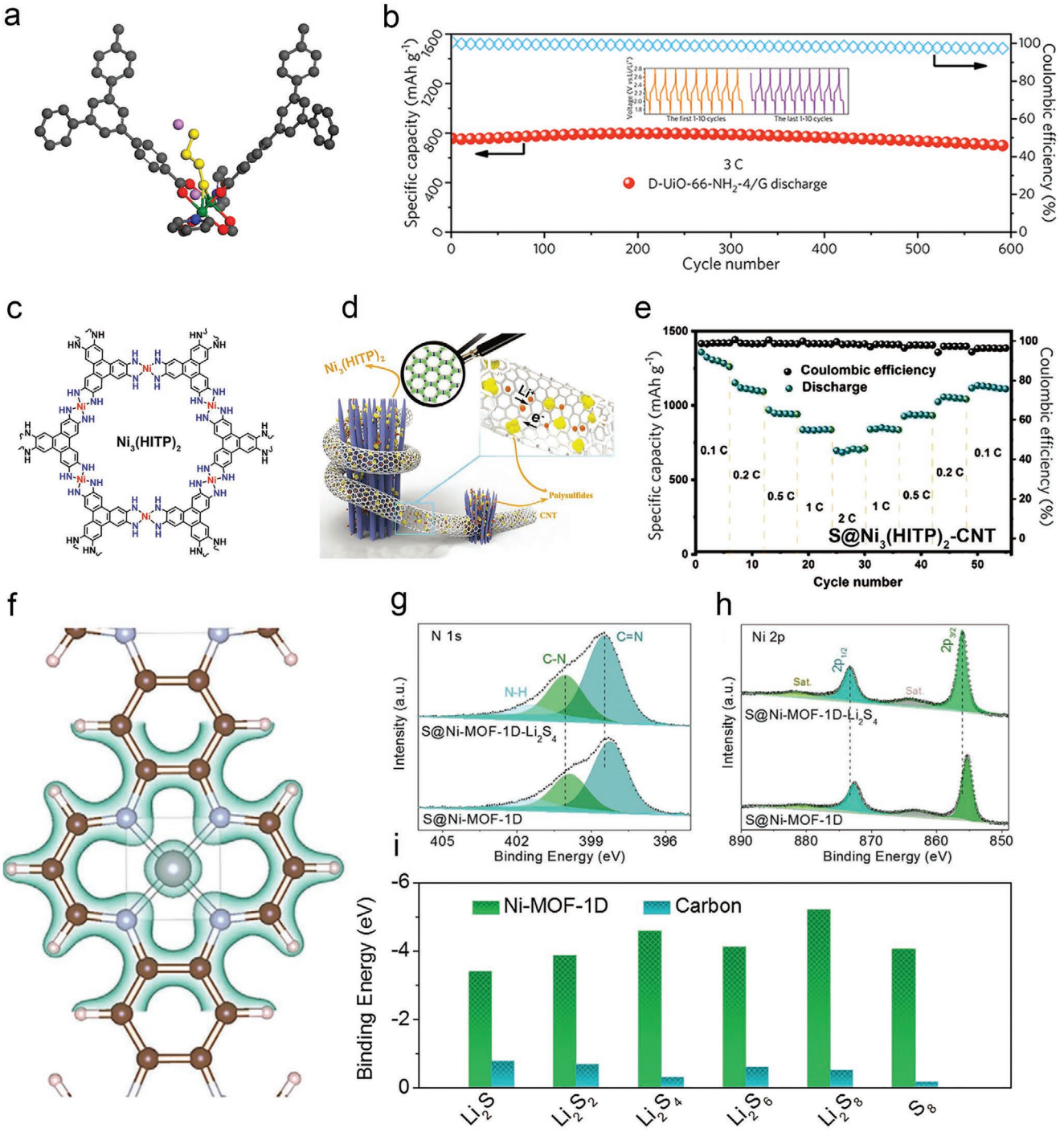

Figure 16. a) The schematic diagram of Lewis acid–base interaction between LiPSs and MOFs. Reproduced with permission.[219] Copyright 2014, American Chemical Society. b) The long-term cycling performance of LSBs when assembled with Zr-MOFs-decorated membranes under 3 C. Reproduced with permission.[220] Copyright 2021, American Chemical Society. c) The π–π conjugation structure of $Ni_3(HITP)_2$. d) The synergistic effect of $Ni_3(HITP)_2$ and CNTs for the effective regulation of polysulfide and e) corresponding rate performance for LSBs. Reproduced with permission.[223] Copyright 2019, Wiley-VCH. f) The high conductivity of Ni-MOF-1D is confirmed by DFT. g–i) The strong bond interaction between Ni-MOF-1D and polysulfide from the XPS and DFT results. Reproduced with permission.[224] Copyright 2022, Wiley-VCH.

Generally, MOFs possess unquestionably great promise as PSRCs due to their well-defined structure and controllable morphology. However, the insufficient conductivity and stability of pristine MOFs have always been a problem when serve as electrode materials; thus, the highly conductive and stable MOFs structures with large in-plane π-conjugation, such

as phthalocyanine-contained and metalloporphyrin-contained MOFs, should be carefully considered in the future design of MOFs-based PSRCs.

5. Design Principles of Electrode Microenvironments for Advanced MSBs

Due to the severe "shuttle effects," huge volume expansion, and low conductivity of sulfur, desirable cathode materials usually need to meet the following requirements: 1) abundant active sites for anchoring and fast conversion of polysulfides, 2) rapid electron/ionic conductivity, and 3) high surface area and pore volume to accommodate sulfur and sustain the volume expansion. In particular, as most host materials do not participate in capacity contribution, it is of great significance to realize maximum utilization of the host materials for high energy density batteries. Therefore, it is necessary to build elaborate architecture to realize full exposure of active sites, thereby minimizing the introduction of inactive substances as far as possible.[225] Combining the advantages of a variety of low-dimensional units (1D nanofiber and 2D nanosheets), 3D materials with a complicated hierarchical structure have displayed unique advantages for loading sulfur and catalyzing polysulfide intermediates.[215,226,227] In this section, the 3D structures for high energy density MSBs cathodes will be introduced from the view of nanostructure design (hollow structure and pore structure) and freestanding electrodes.

5.1. Hollow Structure Design

Hollow-structure-based materials stick out for abundant void spaces to accommodate sulfur species and increase the density of catalytic sites.[228] In the initial stage, a variety of carbon-based hollow structures derived from hard or soft templates provided enormous opportunities for enhancing the sulfur loading amount in cathodes.[47,229–231] A hollow carbon sphere (HCS) prepared by the sacrificial template method was first used as the sulfur host, and a high sulfur loading of 70 wt% could be achieved when exposed to sulfur vapor three times. Moreover, the battery cells with HCS/S cathodes showed desirable sulfur utilization and cyclic stability (capacity retention of 850 mA g^{-1} for 100 cycles at 0.5 C).[229] With an emphasis on providing enough space to buffer the volume changes of S during the cycle, a unique sulfur–TiO_2 yolk–shell nanoarchitecture has been constructed by dissolving part of the sulfur inside.[232] Compared with pristine sulfur–TiO_2 core–shell nanoparticles, the optimized nanoarchitecture exhibited more internal space to accommodate the large volume expansion of sulfur, thus avoiding structural damage and polysulfide dissolution (**Figure 17**a). As a result, the assembled LSBs could maintain a high coulombic efficiency of 98.4% over 1000 cycles.

In order to further improve the utilization rate of sulfur in the cavity, various more ingenious hollow structures are designed to increase the host/sulfur contact interface and provide additional bond interactions to anchor polysulfides. For example, a hollow carbon nanosphere with radially aligned carbon supporting ribs inside was reported (Figure 17b).[231] The unique internal structure endowed sufficient electron/ion transport paths as well as interface interaction, resulting in much higher performance with a capacity decay of 0.044% per cycle for 1000 cycles at 1 C (even under a high sulfur loading of 75%). A similar internal structure (multichambered carbon nanoboxes) is also designed by Yu and co-workers for high-performance room-temperature sodium–sulfur batteries (Figure 17c,d).[233] Moreover, a yolk–shell structure with the TiS_x placed inside the hollow carbon sphere (TiS_x@HCS) was designed to compensate for the imperfection of the original hollow one (Figure 17e).[234] Due to the anchoring and catalytic conversion ability of TiS_x toward polysulfide, the TiS_x@HCS/S cathode exhibited higher capacity retention (455.7 mAh g^{-1} was maintained after 400 cycles at 0.5 C) than the bare HCS/S cathode (only 229.1 mAh g^{-1} was maintained), indicating more efficient sulfur utilization. Similarly, the yolk–shelled Fe_2N@C nanoboxes were prepared as sulfur hosts for LSBs, which possessed long-term cycling stability over 600 cycles at 1 C.[235] Increasing the number of shells has also been considered an effective strategy to increase the interface interaction between catalysts and sulfur. From this perspective, the Lou's group has designed a double-shell $Co(OH)_2$ LDH hollow structure, which not only possesses the merit of hollow structures for loading a high content of sulfur (75 wt%) but also provides an enlarged polar surface for chemically bonding polysulfides (Figure 17f).[236] The assembled LSBs exhibited excellent high-rate performance under a high sulfur loading of 3 mg cm^{-2}. Moreover, the multishell structure was designed to demonstrate similar advantages further (Figure 17g,h).[237] Benefiting from the optimized spatial confinement and short electron/ion transfer path, the TiO_{2-x} with multishelled structure exhibited desirable coulombic efficiency of 97.5% over 1000 cycles at 0.5 C.

5.2. Pore Configuration Optimization

Although the PSRC with hollow structures has shown great advantages in improving both the sulfur loading and conversion in MSBs. The PSRCs with abundant micro-/mesopores are also considered to play an important role in the loading and catalytic conversion of polysulfides. According to the literature, the porous materials could be mainly classified into microporous (<2 nm), mesoporous (2–50 nm), and macroporous (>50 nm), in which mesoporous structures have been frequently introduced as sulfur hosts to optimize cathodes performance.[238,239] For example, Co_8S_9 with mesoporous carbon matrix has been reported by our group as a promising sulfur cathode, which shows strong interfacial affinity with polysulfides. The synergistic strong dual-interactions (Co–S and Li–S) toward polysulfide intermediates and advantages of mesoporous structure resulted in a stable cycling behavior (ultralow capacity decay rate of less than 0.028% per cycle at 0.2 C).[176] However, a comprehensive understanding of the effects of different pore sizes is still very important for the rational design of cathodes.

Macropores materials were generally considered to have an advantage in Li-ion transport capacity but were limited by inferior polysulfides fixation.[240] One effective strategy to address this problem was the introduction of additional sulfur

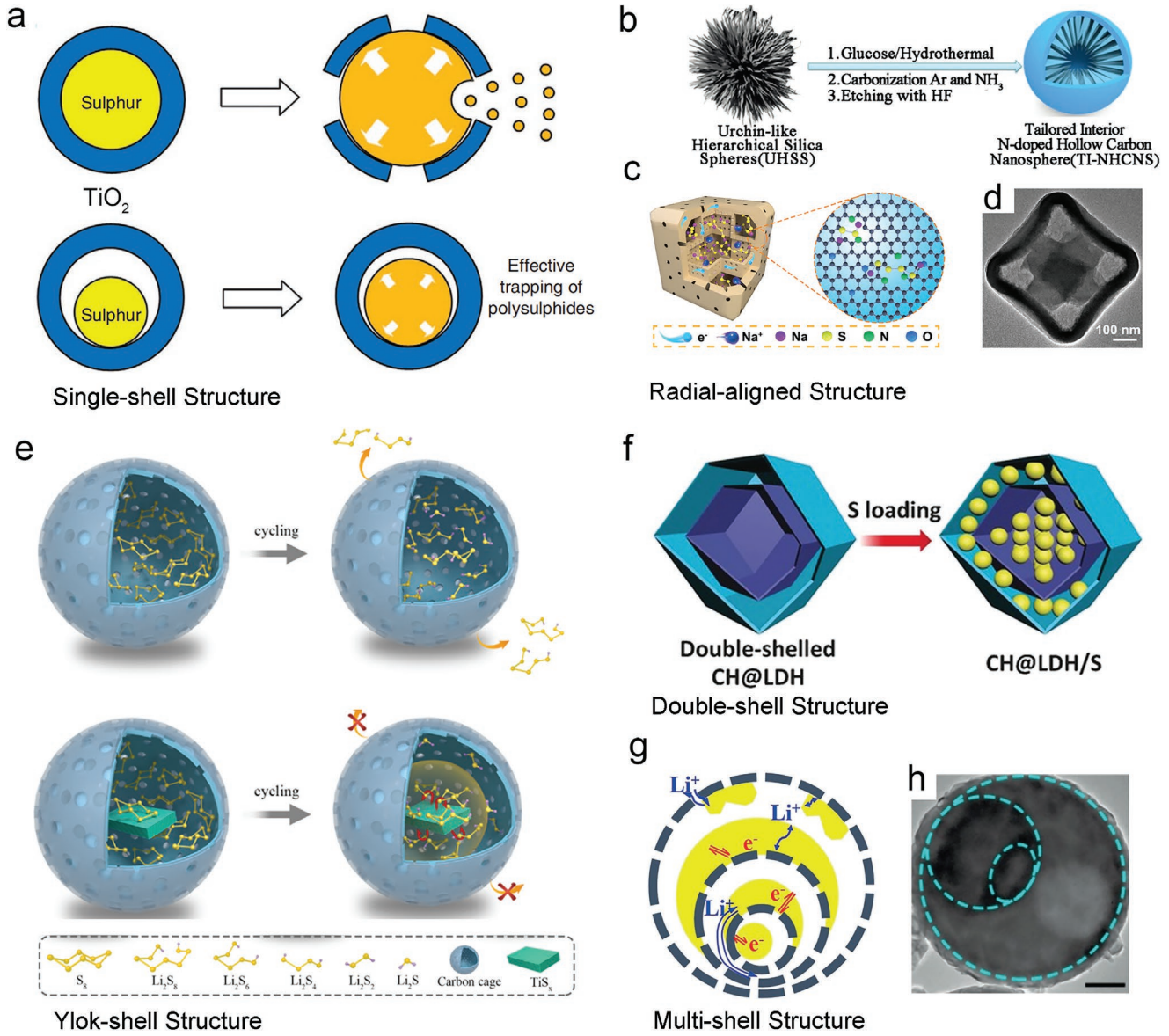

Figure 17. a) The merit of sulfur–TiO_2 yolk–shell nanoarchitecture compared with pristine sulfur–TiO_2 core–shell nanoparticles. Reproduced with permission.[232] Copyright 2013, Nature Publishing Group. b) The fabrication and images of N-doped carbon nanosphere with a radial aligned carbon supporting ribs inside. Reproduced with permission.[47] Copyright 2020, Wiley-VCH. c) The scheme of multichambered carbon nanoboxes as sulfur cathodes and d) corresponding TEM images. Reproduced with permission.[233] Copyright 2021, American Chemical Society. e) The optimized sulfur utilization caused by TiS_x@HCS yolk–shell structure. Reproduced with permission.[234] Copyright 2021, American Chemical Soceity. f) The schematic double-shell $Co(OH)_2$ LDH hollow structure. Reproduced with permission.[236] Copyright 2021, American Chemical Society. g,h) The schematic multi-shell structure. Reproduced with permission.[237] Copyright 2019, Wiley-VCH.

fixation mechanisms into the macropores. For example, polar ZnS nanoparticles and Co-SACs were decorated on a conductive macroporous carbon matrix as an outstanding sulfur host (**Figure 18**a). The macropore could effectively ensure the Li^+ transport kinetics while the ZnS and Co-SACs could provide the adsorption and conversion sites of polysulfide intermediates, thereby suppressing the repulsive "shuttle effects." As a result, the battery cells assembled with the desirable cathodes exhibited remarkable cycling stability (capacity retention of 700 mAh g^{-1} after 1000 cycles at 1.6 C).[80] In addition, the inherently polar units are also assembled as macroporous structures for a combination of efficient Li-ion transport and polysulfide anchoring. For example, a macroporous PSRCs based on 2-methylimidazole zinc salt has been synthesized via a self-templated coordination–replication strategy, which exhibits excellent performance as LSBs cathodes with long-term cycling stability at 2 C (0.028% capacity decay per cycle over 500 cycles) (Figure 18b).[226]

In general, limited by slow Li^+ ions diffusion dynamics, micropores were considered ineffective in mitigating the "shuttle effects," which rely solely on physical barriers. However, more recent research focused on ultra-micropores

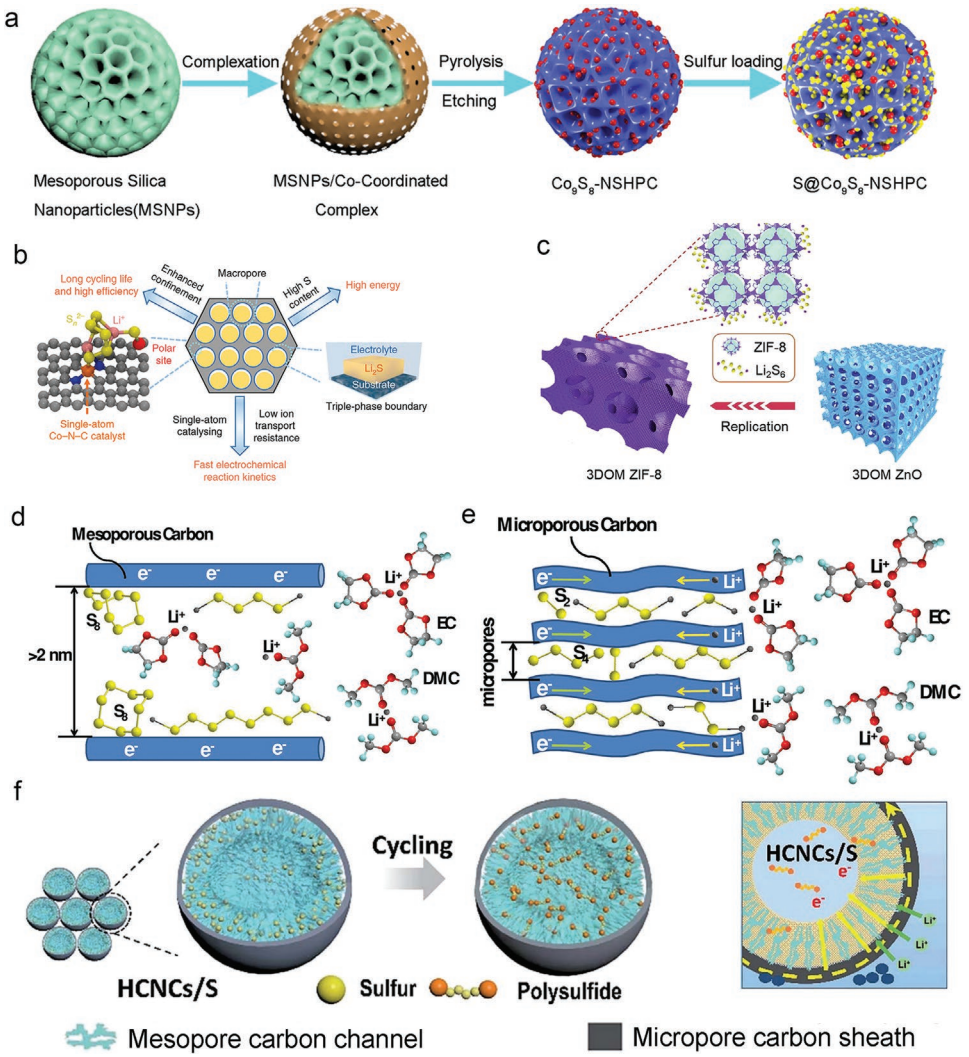

Figure 18. a) The synthesis process of the Co_8S_9 anchored on the mesoporous carbon matrix. Reproduced with permission.[176] Copyright 2021, American Chemical Society. b) The schematic macroporous carbon matrix decorated with ZnS and Co–N–C double sites to suppress "shuttle effects." Reproduced with permission.[80] Copyright 2021, Nature Publishing Group. c) The synthesis process of marco-ZIF-8. Reproduced with permission.[226] Copyright 2020, Elsevier. The lithiation process of sulfur is confined in d) microporous and e) mesoporous carbon. Reproduced with permission.[242] Copyright 2014, Wiley-VCH. f) The schematic image of HCNSs/S with multiscale porous structure. Reproduced with permission.[244] Copyright 2019, Royal Society of Chemistry.

(<0.7 nm), which revealed the unique electrochemical behavior of sulfur when confined in the ultrasmall pore. For example, the metastable S_{2-4} species were identified as the dominant form rather than cyclo-S_8 in a microporous carbon structure with a pore size of ≈0.5 nm. There were no soluble long-chain polysulfides appearing in the conversion of sulfur "shuttle effects" was resolved completely.[241] As a result, the obtained LSBs exhibited impressive capacity retention of 1149 mAh g^{-1} after 200 cycles. This phenomenon was further elucidated recently from a theoretical perspective,[242] the micropores could prevent the electrolyte infiltration through size limit, realizing a "solid–solid" conversion of sulfur. At the same time, for the mesopores, the solvent could easily infiltrate and cause the formation of soluble polysulfide (Figure 18c,d). Furthermore, combining multiscale porous structures was also considered a promising candidate to overcome the inherent limitation of single pore type and synergistic advantages of different pores.[243,244] For example, a pomegranate-like carbon sphere that integrates micropores and mesopores has been designed;[244] the microporous shell outside can prevent the polysulfide from escaping, and the mesoporous channels inside can ensure fast ion transport (Figure 18e).

5.3. Freestanding Electrodes

Constructing 3D freestanding electrodes through either introducing an active center into existing 3D skeletons or assembling various low-dimension blocks to foam or aerogel has been an outstanding strategy for fabricating high-loading cathodes with polysulfide redox activity.[200,215,245,246] For a traditional coating electrode, agent particles that facilitate the

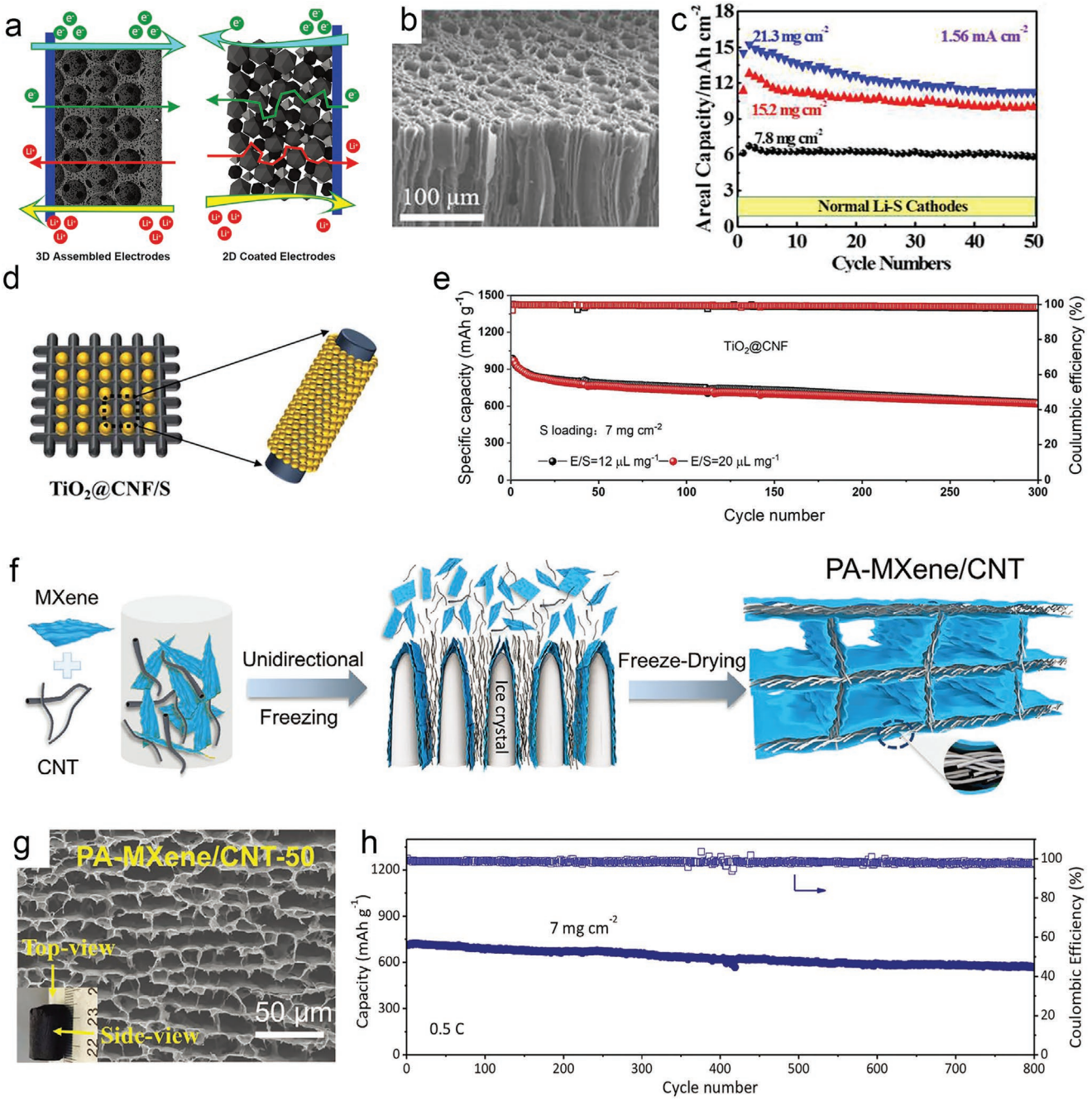

Figure 19. a) Schematic merits of 3D freestanding electrodes for electron/ion transport. Reproduced with permission.[247] Copyright 2022, Wiley-VCH. b,c) The 3D electrodes derived from woods and corresponding performance under high sulfur loading. Reproduced with permission.[248] Copyright 2017, American Chemical Society. d,e) The illustration of the sulfur loading in TiO_2/S and high-loading cycling performance at 0.2 C. Reproduced with permission.[251] Copyright 2022, Royal Society of Chemistry. f,g) The schematic design of CNT aerogels coassembled with MXene. h) The long-term cycling stability of MXene/CNT electrode with an area loading of 7 mg cm^{-2}. Reproduced with permission.[252] Copyright 2021, Wiley-VCH.

transfer of the electrons and ions are not closely connected, which causes a long distance of electron/ion transfer and increases the resistance.[5] While, for a 3D assembled electrode, the quick transfer of electrons and ions between the bottom and top sides of the electrode could be realized via the long-continuous channel (**Figure 19**a).[247] Furthermore, the binder-free feature also reduced the proportion of non-active components, which will benefit in achieving high energy density.

The 3D self-supporting matrix with a fast pathway for electronic transmission and abundant channels for sulfur accommodation was obtained by pyrolysis of wood. After being embedded with rGO, the freestanding 3D carbon electrode with aligned microchannels shows excellent polysulfide anchoring

capability (Figure 19b).[248] The area loading of sulfur can reach 21.3 mg cm^{-2}, and the assembled LSBs have achieved a remarkable areal capacity up to 15.2 mAh cm^{-2} (Figure 19c). Moreover, when the defective $LaNO_{3-x}$ nanoparticles were further introduced to catalyze the polysulfides conversion, the as-prepared LSBs exhibited a desirable areal-specific capacity (8.5 mAh cm^{-2} at 0.05 C) even under an ultrahigh areal loading of 11.6 mg cm^{-2}.[249]

The 3D freestanding N, O-codoped wood-like carbon was further decorated with carbon nanotubes forest (WLC-CNTs) and used as the sulfur host for enabling scalable high-performance LSBs. With such interconnected 3D structures, the ionic and charge-transfer resistance per unit of the electroactive surface area of the S@WLC-CNTs electrode does not change with the increase of thickness, resulting in a thickness-independent performance of LSBs. The electrode displays a capacity of up to 692 mAh g^{-1} after 100 cycles at 0.1 C, even with a thickness of 1200 µm (sulfur loading of 52.4 mg cm^{-2}).[250] In order to restrain polysulfide more effectively, various polar components were introduced to the 1D nanounits-based 3D electrodes. For example, TiO_2 was decorated on the carbon nanofiber network, which could anchor and catalyze polysulfides (Figure 19d).[251] When increased the areal loading to 7 mg cm^{-2}, the battery cells could still operate stably for over 300 cycles (Figure 19e). Very recently, MXene was introduced to the 3D CNT framework via a freeze-drying method as a freestanding electrode in LSBs (Figure 19f–h),[252] which provided sufficient space to accommodate sulfur, ensured the electron/ion transport, and promoted the catalytic conversion of polysulfide.

In addition to the intrinsic catalytic activities of PSRCs, the electrode structure design also exhibits a profound impact on the performance of MSBs, which can be divided into the following aspects: 1) for the pursuit of practical high-energy-density MSBs, sufficient space is necessary to accommodate volume changes of sulfur species in the PSRCs; 2) to ensure the contact area between sulfur species and PSRCs, it is important to design structures with high surface area; 3) multiscale porous structures that integrate the advantages of different pore sizes would be an optimal option for combining physical confinement and ion transport.

6. Conclusion and Outlook

In this review, we have comprehensively summarized the most recent process in the reaction principles, in situ characterizations, bond interaction modulation, and interface microenvironment optimization of PSRCs. Uniquely, we have provided detailed strategies for tailoring the bond interactions of PSRCs and offer a careful comparison on disclosing their critical parameters to promote future developments. Limited to some inherent shortages, particularly the persistent loss of active substances due to the "shuttle effects," the commercial application of MSBs still faces significant obstacles. Over the past few years, unprecedented efforts have demonstrated that introducing the PSRCs into the MSBs systems could significantly improve cathode performances. The PSRCs with efficient polysulfide adsorption or catalytic conversion activities are vital components to alleviate the "shuttle effects" in MSBs. Besides providing the critical design principles on electrode microenvironments, this review also offers cutting-edge guidance for the future developments of practically affordable PSRCs in MSBs. The main conclusion and outlook are summarized as follows.

1) Discovery of new materials: Most currently designed PSRCs are based on the trial-and-error synthetic approaches; it is suggested that the "ab initio" design concepts should be taken gradually in the future to fabricate desirable catalytic sites based on the targeted sulfur redox reactions. For example, constructing multiple or tandem catalytic centers offers special advantages in multistep and tandem polysulfide redox reactions where integration of diverse catalytic sites is necessary. However, it still remains an open question to disclose the origin of many types of PSRCs for the optimal polysulfide redox reactions. Besides the traditional synthetic methods, as discussed in this review, recent studies have indicated that the high-throughput methodologies and data mining will also provide new routes for constructing PSRCs.

2) Precisely active center design: The modulation of interface microenvironments between polysulfide and catalysts/cathodes plays an essential role in catalytic reactions. The preparation of PSRCs with defined structures and active centers provides enormous opportunities for precisely predicting their reaction pathways and mechanisms at the cathode interface. However, further optimization of the engineering strategies on catalysts, such as precise control of active site concentration or coordination environments, is still a challenge in sample synthesis. Exploiting advanced fabrication techniques, such as vapor-phase transportation and atomic layer deposition, many new PSRCs with high intrinsic performance would be appealed. The utilization of recently developed in situ electron microscopy with atomic structural images and spatial resolutions would also offer essential data to detect the corresponding interface microenvironments.

3) The structure design of PSRCs: The realization of MSBs with high areal capacity and high sulfur loading should be considered first and foremost. Because of the merits of accommodating high sulfur content, facilitating rapid ion migration, and physically confining polysulfides, the construction of 3D conductive frameworks with abundant space and larger surface area is worth to be explored in the future MSBs. Moreover, the 3D freestanding electrodes could decrease the mass proportion of inactive materials (i.e., conductive agent, current collector, and binder), which is of great significance for high gravimetric energy density batteries.

4) Operando techniques: The rapid advancements of state-of-the-art characterization tools with high spatial and temporal resolution provide new insights into decoupling the catalytic mechanism of PSRCs in accelerating the multistep polysulfide conversion at the atomic and molecular levels. In this respect, the in situ characterization, which can monitor the real-time evolution of polysulfide intermediates and PSRCs during the sulfur redox reaction, has exhibited great potential in revealing the catalytic mechanism of PSRCs. However, most current in situ characterization mainly focuses on the reaction process rather than the catalytic mechanism of PSRSs. For example, in situ X-ray radiography has been

used to observe the deposition of insoluble Li_2S in LSBs,[64] which means that the catalytic effects of PSRCs on reducing the deposition energy barrier of Li_2S can be investigated by this technology. As such, it is desirable to apply more in situ techniques to reveal the catalytic mechanism to guide the rational design of PSRCs. Considering the redistribution of insulation sulfur species accompanied by the cycling process, the surface of PSRCs may be passivated due to the coverage of the insulating components. However, the research on the structural evolution of PSRCs via in situ characterization is still limited to the first few cycles. In this regard, it is important to investigate the passivation of PSRCs in a long-cycle process, which is of great significance for achieving long-term stable MSBs.

5) The practical application of PSRCs: The ultimate purpose for the fabrication of desirable PSRCs involves achieving the commercialization of MSBs. However, there are still some obstacles for applying PSRCs under practical conditions, such as the pouch cells with high sulfur loading and low E/S ratio. First, the concentrated intermediates could react with the electrolyte to form a cluster under this strict condition, which would hinder the transformation of ionic conductivity and weak the catalytic effect of PSRCs. Second, such clusters could deposit on the surface of PSRCs, leading to the passivation of PSRCs. Third, the catalytic mechanism of PSRCs in pouch cells remains unclear due to the absence of specific in situ techniques. In this regard, the catalytic effects of PSRCs need to be evaluated comprehensively under the pouch cells, which is critical for the practical applications of PSRCs.

In summary, the deployment of catalytic materials, especially the regulation of bond interactions and interface microenvironments, has been regarded as one of the most promising strategies for developing high-performance MSBs. The exploitation and design of highly efficient PSRCs are still in the incubation stage, and the chemical interactions at the molecular level need to be further investigated, where we can draw lessons from other catalytic fields, for example, the electrocatalytic reduction/oxidation of O_2. With the gradual accumulation of the structure–property correlation of PSRCs, it is expected that it will soon become possible to achieve MSBs with superior activity, high stability, and low cost in the near future. The rapid development of PSRCs in MSBs is expected to provide substantial and multidisciplinary guidance for other related energy storage systems.

Acknowledgements

R.Z. and W.Q.Z. contributed equally to this work. This work was financially supported by the National Natural Science Foundation of China (Nos. 52173133, 52161145402, and 51803134), the Science and Technology Project of Sichuan Province (Nos. 2021YFH0180 and 2022YFH0088), the 1·3·5 Project for Disciplines of Excellence, West China Hospital, Sichuan University (No. ZYJC21047), the innovation project of Med-X Center for Materials, Sichuan University (No. MCM202102), the State Key Laboratory of Polymer Materials Engineering (Grant Nos. sklpme2022-3-07 and sklpme2021-4-02), and Fundamental Research Funds for the Central Universities.

Open access funding enabled and organized by Projekt DEAL.

Conflict of Interest

The authors declare no conflict of interest.

Keywords

catalytic materials, electrodes, electrocatalysts, metal–sulfur batteries, polysulfide redox catalyses, shuttle effects

Received: June 20, 2022
Revised: July 28, 2022
Published online: August 16, 2022

[1] A. Manthiram, X. Yu, S. Wang, *Nat. Rev. Mater.* **2017**, *2*, 16103.
[2] S. Evers, L. F. Nazar, *Acc. Chem. Res.* **2013**, *46*, 1135.
[3] P. Wang, B. Xi, M. Huang, W. Chen, J. Feng, S. Xiong, *Adv. Energy Mater.* **2021**, *11*, 2002893.
[4] H. Li, Y. Li, L. Zhang, *SusMat* **2022**, *2*, 34.
[5] H.-J. Peng, J.-Q. Huang, X.-B. Cheng, Q. Zhang, *Adv. Energy Mater.* **2017**, *7*, 1700260.
[6] X. Hong, J. Mei, L. Wen, Y. Tong, A. J. Vasileff, L. Wang, J. Liang, Z. Sun, S. X. Dou, *Adv. Mater.* **2019**, *31*, 1802822.
[7] S.-F. Ng, M. Y. L. Lau, W.-J. Ong, *Adv. Mater.* **2021**, *33*, 2008654.
[8] B. Liu, R. Fang, D. Xie, W. Zhang, H. Huang, Y. Xia, X. Wang, X. Xia, J. Tu, *Energy Environ. Mater.* **2018**, *1*, 196.
[9] S.-E. Cheon, K.-S. Ko, J.-H. Cho, S.-W. Kim, E.-Y. Chin, H.-T. Kim, *J. Electrochem. Soc.* **2003**, *150*, A796.
[10] L. Zhou, D. L. Danilov, R.-A. Eichel, P. H. L. Notten, *Adv. Energy Mater.* **2021**, *11*, 2001304.
[11] J. Mei, J. Wang, H. Gu, Y. Du, H. Wang, Y. Yamauchi, T. Liao, Z. Sun, Z. Yin, *Adv. Mater.* **2021**, *33*, 2004920.
[12] J. Liang, Z.-H. Sun, F. Li, H.-M. Cheng, *Energy Storage Mater.* **2016**, *2*, 76.
[13] Z. Li, Y. Huang, L. Yuan, Z. Hao, Y. Huang, *Carbon* **2015**, *92*, 41.
[14] X. Ji, K. T. Lee, L. F. Nazar, *Nat. Mater.* **2009**, *8*, 500.
[15] R. Fang, K. Chen, L. Yin, Z. Sun, F. Li, H.-M. Cheng, *Adv. Mater.* **2019**, *31*, 1800863.
[16] J. Lei, T. Liu, J. Chen, M. Zheng, Q. Zhang, B. Mao, Q. Dong, *Chem* **2020**, *6*, 2533.
[17] L. Kong, B.-Q. Li, H.-J. Peng, R. Zhang, J. Xie, J.-Q. Huang, Q. Zhang, *Adv. Energy Mater.* **2018**, *8*, 1800849.
[18] X. Liu, J.-Q. Huang, Q. Zhang, L. Mai, *Adv. Mater.* **2017**, *29*, 1601759.
[19] M. Zhang, W. Chen, L. Xue, Y. Jiao, T. Lei, J. Chu, J. Huang, C. Gong, C. Yan, Y. Yan, Y. Hu, X. Wang, J. Xiong, *Adv. Energy Mater.* **2020**, *10*, 1903008.
[20] X. L. Huang, S. X. Dou, Z. M. Wang, *Mater. Horiz.* **2021**, *8*, 2870.
[21] R. Xiao, K. Chen, X. Zhang, Z. Yang, G. Hu, Z. Sun, H.-M. Cheng, F. Li, *J. Energy Chem.* **2021**, *54*, 452.
[22] F. Wang, J. Li, J. Zhao, Y. Yang, C. Su, Y. L. Zhong, Q.-H. Yang, J. Lu, *ACS Mater. Lett.* **2020**, *2*, 1450.
[23] C. Zhou, Z. Li, X. Xu, L. Mai, *Natl. Sci. Rev.* **2021**, *8*, nwab055.
[24] R. Yan, T. Ma, M. Cheng, X. Tao, Z. Yang, F. Ran, S. Li, B. Yin, C. Cheng, W. Yang, *Adv. Mater.* **2021**, *33*, 2008784.
[25] G.-P. Hao, C. Tang, E. Zhang, P. Zhai, J. Yin, W. Zhu, Q. Zhang, S. Kaskel, *Adv. Mater.* **2017**, *29*, 1702829.
[26] S. Bai, X. Liu, K. Zhu, S. Wu, H. Zhou, *Nat. Energy* **2016**, *1*, 16094.
[27] G. Kyriakou, B. Boucher Matthew, D. Jewell April, A. Lewis Emily, J. Lawton Timothy, E. Baber Ashleigh, L. Tierney Heather, M. Flytzani-Stephanopoulos, E. C. H. Sykes, *Science* **2012**, *335*, 1209.

[28] J. H. Warner, Y.-C. Lin, K. He, M. Koshino, K. Suenaga, *ACS Nano* **2014**, *8*, 11806.
[29] J. H. Kwak, J. Hu, D. Mei, C.-W. Yi, D. H. Kim, C. H. F. Peden, L. F. Allard, J. Szanyi, *Science* **2009**, *325*, 1670.
[30] J. Liu, *ACS Catal.* **2017**, *7*, 34.
[31] Y. Yan, T. Lei, Y. Jiao, C. Wu, J. Xiong, *Electrochim. Acta* **2018**, *264*, 20.
[32] X. Tao, J. Wang, C. Liu, H. Wang, H. Yao, G. Zheng, Z. W. Seh, Q. Cai, W. Li, G. Zhou, C. Zu, Y. Cui, *Nat. Commun.* **2016**, *7*, 11203.
[33] T. Chen, L. Ma, B. Cheng, R. Chen, Y. Hu, G. Zhu, Y. Wang, J. Liang, Z. Tie, J. Liu, Z. Jin, *Nano Energy* **2017**, *38*, 239.
[34] Z. Yuan, H.-J. Peng, T.-Z. Hou, J.-Q. Huang, C.-M. Chen, D.-W. Wang, X.-B. Cheng, F. Wei, Q. Zhang, *Nano Lett.* **2016**, *16*, 519.
[35] J. He, G. Hartmann, M. Lee, G. S. Hwang, Y. Chen, A. Manthiram, *Energy Environ. Sci.* **2019**, *12*, 344.
[36] H. Wong, X. Ou, M. Zhuang, Z. Liu, M. D. Hossain, Y. Cai, H. Liu, H. Lee, C.-Z. Wang, Z. Luo, *ACS Appl. Mater. Interfaces* **2019**, *11*, 19986.
[37] D. Cai, B. Liu, D. Zhu, D. Chen, M. Lu, J. Cao, Y. Wang, W. Huang, Y. Shao, H. Tu, W. Han, *Adv. Energy Mater.* **2020**, *10*, 1904273.
[38] C. Zhang, B. Fei, D. Yang, H. Zhan, J. Wang, J. Diao, J. Li, G. Henkelman, D. Cai, J. J. Biendicho, J. R. Morante, A. Cabot, *Adv. Funct. Mater.* **2022**, *32*, 2201322.
[39] F. Zhou, Z. Li, X. Luo, T. Wu, B. Jiang, L.-L. Lu, H.-B. Yao, M. Antonietti, S.-H. Yu, *Nano Lett.* **2018**, *18*, 1035.
[40] J. Qian, Y. Xing, Y. Yang, Y. Li, K. Yu, W. Li, T. Zhao, Y. Ye, L. Li, F. Wu, R. Chen, *Adv. Mater.* **2021**, *33*, 2100810.
[41] C. Zha, X. Zhu, J. Deng, Y. Zhou, Y. Li, J. Chen, P. Ding, Y. Hu, Y. Li, H. Chen, *Energy Storage Mater.* **2020**, *26*, 40.
[42] P. Wang, N. Li, Z. Zhang, B. Hong, J. Li, K. Zhang, K. Xie, Y. Lai, *J. Mater. Chem. A* **2019**, *7*, 21934.
[43] C. Li, X. Liu, L. Zhu, R. Huang, M. Zhao, L. Xu, Y. Qian, *Chem. Mater.* **2018**, *30*, 6969.
[44] Z. Li, P. Li, X. Meng, Z. Lin, R. Wang, *Adv. Mater.* **2021**, *33*, 2102338.
[45] Z. Ye, Y. Jiang, J. Qian, W. Li, T. Feng, L. Li, F. Wu, R. Chen, *Nano Energy* **2019**, *64*, 103965.
[46] S. Huang, Y. V. Lim, X. Zhang, Y. Wang, Y. Zheng, D. Kong, M. Ding, S. A. Yang, H. Y. Yang, *Nano Energy* **2018**, *51*, 340.
[47] G. Zhou, S. Zhao, T. Wang, S.-Z. Yang, B. Johannessen, H. Chen, C. Liu, Y. Ye, Y. Wu, Y. Peng, C. Liu, S. P. Jiang, Q. Zhang, Y. Cui, *Nano Lett.* **2020**, *20*, 1252.
[48] J. Wang, W. Qiu, G. Li, J. Liu, D. Luo, Y. Zhang, Y. Zhao, G. Zhou, L. Shui, X. Wang, Z. Chen, *Energy Storage Mater.* **2022**, *46*, 269.
[49] Y. Yang, Z. Wang, T. Jiang, C. Dong, Z. Mao, C. Lu, W. Sun, K. Sun, *J. Mater. Chem. A* **2018**, *6*, 13593.
[50] X.-J. Hong, C.-L. Song, Y. Yang, H.-C. Tan, G.-H. Li, Y.-P. Cai, H. Wang, *ACS Nano* **2019**, *13*, 1923.
[51] J. Shen, X. Xu, J. Liu, Z. Liu, F. Li, R. Hu, J. Liu, X. Hou, Y. Feng, Y. Yu, M. Zhu, *ACS Nano* **2019**, *13*, 8986.
[52] J. K. Nørskov, T. Bligaard, J. Rossmeisl, C. H. Christensen, *Nat. Chem.* **2009**, *1*, 37.
[53] J. Zhou, X. Liu, L. Zhu, J. Zhou, Y. Guan, L. Chen, S. Niu, J. Cai, D. Sun, Y. Zhu, J. Du, G. Wang, Y. Qian, *Joule* **2018**, *2*, 2681.
[54] C. Ye, Y. Jiao, D. Chao, T. Ling, J. Shan, B. Zhang, Q. Gu, K. Davey, H. Wang, S.-Z. Qiao, *Adv. Mater.* **2020**, *32*, 1907557.
[55] J. Shen, X. Xu, J. Liu, Z. Wang, S. Zuo, Z. Liu, D. Zhang, J. Liu, M. Zhu, *Adv. Energy Mater.* **2021**, *11*, 2100673.
[56] W. Xue, Z. Shi, L. Suo, C. Wang, Z. Wang, H. Wang, K. P. So, A. Maurano, D. Yu, Y. Chen, L. Qie, Z. Zhu, G. Xu, J. Kong, J. Li, *Nat. Energy* **2019**, *4*, 374.
[57] J. Wang, S. Yang, Z. Xu, G. Ai, T. Zhang, W. Mao, *Adv. Mater. Interfaces* **2022**, *9*, 2101699.
[58] F. Liu, G. Sun, H. B. Wu, G. Chen, D. Xu, R. Mo, L. Shen, X. Li, S. Ma, R. Tao, X. Li, X. Tan, B. Xu, G. Wang, B. S. Dunn, P. Sautet, Y. Lu, *Nat. Commun.* **2020**, *11*, 5215.
[59] X. Yang, X. Gao, Q. Sun, S. P. Jand, Y. Yu, Y. Zhao, X. Li, K. Adair, L.-Y. Kuo, J. Rohrer, J. Liang, X. Lin, M. N. Banis, Y. Hu, H. Zhang, X. Li, R. Li, H. Zhang, P. Kaghazchi, T.-K. Sham, X. Sun, *Adv. Mater.* **2019**, *31*, 1901220.
[60] F. Y. Fan, W. C. Carter, Y.-M. Chiang, *Adv. Mater.* **2015**, *27*, 5203.
[61] H. Yuan, H.-J. Peng, B.-Q. Li, J. Xie, L. Kong, M. Zhao, X. Chen, J.-Q. Huang, Q. Zhang, *Adv. Energy Mater.* **2019**, *9*, 1802768.
[62] J.-L. Yang, D.-Q. Cai, X.-G. Hao, L. Huang, Q. Lin, X.-T. Zeng, S.-X. Zhao, W. Lv, *ACS Nano* **2021**, *15*, 11491.
[63] G. Zhou, H. Tian, Y. Jin, X. Tao, B. Liu, R. Zhang, W. Seh Zhi, D. Zhuo, Y. Liu, J. Sun, J. Zhao, C. Zu, S. Wu David, Q. Zhang, Y. Cui, *Proc. Natl. Acad. Sci. USA* **2017**, *114*, 840.
[64] S. Risse, C. J. Jafta, Y. Yang, N. Kardjilov, A. Hilger, I. Manke, M. Ballauff, *Phys. Chem. Chem. Phys.* **2016**, *18*, 10630.
[65] M. Liu, W. Bai, H. Guo, J. Sun, Y. Liu, M. Fang, T. Guo, S. Yang, A. L. Vasiliev, P. J. Kulesza, Y. Hu, X. Ouyang, X. Wang, J. Zhu, Y. Fu, *Electrochim. Acta* **2022**, *421*, 140430.
[66] S. Rehman, M. Pope, S. Tao, E. McCalla, *Energy Environ. Sci.* **2022**, *15*, 1423.
[67] J. He, A. Bhargav, A. Manthiram, *Adv. Mater.* **2020**, *32*, 2004741.
[68] M. Liu, P. Chen, X. Pan, S. Pan, X. Zhang, Y. Zhou, M. Bi, J. Sun, S. Yang, A. L. Vasiliev, P. J. Kulesza, X. Ouyang, J. Xu, X. Wang, J. Zhu, Y. Fu, *Adv. Funct. Mater.* **2022**, *32*, 2205031.
[69] S. Yu, Y. Sun, L. Song, X. Cao, L. Chen, X. An, X. Liu, W. Cai, T. Yao, Y. Song, W. Zhang, *Nano Energy* **2021**, *89*, 106414.
[70] H. Ci, J. Cai, H. Ma, Z. Shi, G. Cui, M. Wang, J. Jin, N. Wei, C. Lu, W. Zhao, J. Sun, Z. Liu, *ACS Nano* **2020**, *14*, 11929.
[71] X. Gao, X. Zheng, Y. Tsao, P. Zhang, X. Xiao, Y. Ye, J. Li, Y. Yang, R. Xu, Z. Bao, Y. Cui, *J. Am. Chem. Soc.* **2021**, *143*, 18188.
[72] Y. Zuo, Y. Zhu, R. Wan, W. Su, Y. Fan, R. Liu, Y. Tang, Y. Chen, *Chem. Eng. J.* **2021**, *415*, 129053.
[73] L. Luo, J. Li, H. Yaghoobnejad Asl, A. Manthiram, *ACS Energy Lett.* **2020**, *5*, 1177.
[74] Z. Shi, Z. Sun, J. Cai, Z. Fan, J. Jin, M. Wang, J. Sun, *Adv. Funct. Mater.* **2021**, *31*, 2006798.
[75] J. Wang, L. Jia, J. Zhong, Q. Xiao, C. Wang, K. Zang, H. Liu, H. Zheng, J. Luo, J. Yang, H. Fan, W. Duan, Y. Wu, H. Lin, Y. Zhang, *Energy Storage Mater.* **2019**, *18*, 246.
[76] L. Zhang, M. Ling, J. Feng, G. Liu, J. Guo, *Nano Energy* **2017**, *40*, 559.
[77] X. Zhou, T. Liu, G. Zhao, X. Yang, H. Guo, *Energy Storage Mater.* **2021**, *40*, 139.
[78] C. Dillard, A. Singh, V. Kalra, *J. Phys. Chem. C* **2018**, *122*, 18195.
[79] X. Wang, Y. Tan, G. Shen, S. Zhang, *J. Energy Chem.* **2020**, *41*, 149.
[80] C. Zhao, G.-L. Xu, Z. Yu, L. Zhang, I. Hwang, Y.-X. Mo, Y. Ren, L. Cheng, C.-J. Sun, Y. Ren, X. Zuo, J.-T. Li, S.-G. Sun, K. Amine, T. Zhao, *Nat. Nanotechnol.* **2021**, *16*, 166.
[81] K. A. See, M. Leskes, J. M. Griffin, S. Britto, P. D. Matthews, A. Emly, A. Van der Ven, D. S. Wright, A. J. Morris, C. P. Grey, R. Seshadri, *J. Am. Chem. Soc.* **2014**, *136*, 16368.
[82] M. U. M. Patel, I. Arčon, G. Aquilanti, L. Stievano, G. Mali, R. Dominko, *ChemPhysChem* **2014**, *15*, 894.
[83] Y. Qiu, G. Rong, J. Yang, G. Li, S. Ma, X. Wang, Z. Pan, Y. Hou, M. Liu, F. Ye, W. Li, Z. W. Seh, X. Tao, H. Yao, N. Liu, R. Zhang, G. Zhou, J. Wang, S. Fan, Y. Cui, Y. Zhang, *Adv. Energy Mater.* **2015**, *5*, 1501369.
[84] H. Marceau, C.-S. Kim, A. Paolella, S. Ladouceur, M. Lagacé, M. Chaker, A. Vijh, A. Guerfi, C. M. Julien, A. Mauger, M. Armand, P. Hovington, K. Zaghib, *J. Power Sources* **2016**, *319*, 247.
[85] G. Tan, R. Xu, Z. Xing, Y. Yuan, J. Lu, J. Wen, C. Liu, L. Ma, C. Zhan, Q. Liu, T. Wu, Z. Jian, R. Shahbazian-Yassar, Y. Ren, D. J. Miller, L. A. Curtiss, X. Ji, K. Amine, *Nat. Energy* **2017**, *2*, 17090.
[86] Z.-L. Xu, J.-Q. Huang, W. G. Chong, X. Qin, X. Wang, L. Zhou, J.-K. Kim, *Adv. Energy Mater.* **2017**, *7*, 1602078.

[87] K. Mahankali, N. K. Thangavel, L. M. Reddy Arava, *Nano Lett.* **2019**, *19*, 5229.
[88] S.-Y. Lang, Y. Shi, Y.-G. Guo, D. Wang, R. Wen, L.-J. Wan, *Angew. Chem., Int. Ed.* **2016**, *55*, 15835.
[89] W. Chen, T. Lei, T. Qian, W. Lv, W. He, C. Wu, X. Liu, J. Liu, B. Chen, C. Yan, J. Xiong, *Adv. Energy Mater.* **2018**, *8*, 1702889.
[90] L. Jia, J. Wang, S. Ren, G. Ren, X. Jin, L. Kao, X. Feng, F. Yang, Q. Wang, L. Pan, Q. Li, Y.-s. Liu, Y. Wu, G. Liu, J. Feng, S. Fan, Y. Ye, J. Guo, Y. Zhang, *Energy Environ. Mater.* **2021**, *4*, 222.
[91] S.-H. Yu, X. Huang, K. Schwarz, R. Huang, T. A. Arias, J. D. Brock, H. D. Abruña, *Energy Environ. Sci.* **2018**, *11*, 202.
[92] J. Xiao, J. Z. Hu, H. Chen, M. Vijayakumar, J. Zheng, H. Pan, E. D. Walter, M. Hu, X. Deng, J. Feng, B. Y. Liaw, M. Gu, Z. D. Deng, D. Lu, S. Xu, C. Wang, J. Liu, *Nano Lett.* **2015**, *15*, 3309.
[93] N. Xu, T. Qian, X. Liu, J. Liu, Y. Chen, C. Yan, *Nano Lett.* **2017**, *17*, 538.
[94] H. Kim, J. T. Lee, A. Magasinski, K. Zhao, Y. Liu, G. Yushin, *Adv. Energy Mater.* **2015**, *5*, 1501306.
[95] M. A. Al-Tahan, Y. Dong, A. E. Shrshr, X. Liu, R. Zhang, H. Guan, X. Kang, R. Wei, J. Zhang, *J. Colloid Interface Sci.* **2022**, *609*, 235.
[96] Q. Li, Y. Song, R. Xu, L. Zhang, J. Gao, Z. Xia, Z. Tian, N. Wei, M. H. Rümmeli, X. Zou, J. Sun, Z. Liu, *ACS Nano* **2018**, *12*, 10240.
[97] M. Wang, L. Fan, X. Sun, B. Guan, B. Jiang, X. Wu, D. Tian, K. Sun, Y. Qiu, X. Yin, Y. Zhang, N. Zhang, *ACS Energy Lett.* **2020**, *5*, 3041.
[98] Z. Shi, M. Li, J. Sun, Z. Chen, *Adv. Energy Mater.* **2021**, *11*, 2100332.
[99] R. Wang, C. Luo, T. Wang, G. Zhou, Y. Deng, Y. He, Q. Zhang, F. Kang, W. Lv, Q.-H. Yang, *Adv. Mater.* **2020**, *32*, 2000315.
[100] S. Zhang, Y. Yao, X. Jiao, M. Ma, H. Huang, X. Zhou, L. Wang, J. Bai, Y. Yu, *Adv. Mater.* **2021**, *33*, 2103846.
[101] Y. Zhang, J. Liu, J. Wang, Y. Zhao, D. Luo, A. Yu, X. Wang, Z. Chen, *Angew. Chem., Int. Ed.* **2021**, *60*, 26622.
[102] S. Zhang, X. Ao, J. Huang, B. Wei, Y. Zhai, D. Zhai, W. Deng, C. Su, D. Wang, Y. Li, *Nano Lett.* **2021**, *21*, 9691.
[103] Y. Xiao, W. Gong, S. Guo, Y. Ouyang, D. Li, X. Li, Q. Zeng, W. He, H. Deng, C. Tan, Q. Zhang, S. Huang, *ACS Mater. Lett.* **2021**, *3*, 1684.
[104] B. Jiang, Y. Qiu, D. Tian, Y. Zhang, X. Song, C. Zhao, M. Wang, X. Sun, H. Huang, C. Zhao, H. Zhou, A. Chen, L. Fan, N. Zhang, *Adv. Energy Mater.* **2021**, *11*, 2102995.
[105] H. Zhao, D. Zhang, H. Li, W. Qi, X. Wu, Y. Han, W. Cai, Z. Wang, J. Lai, L. Wang, *Adv. Energy Mater.* **2020**, *10*, 2002131.
[106] S. Bai, L. Wang, Z. Li, Y. Xiong, *Adv. Sci.* **2017**, *4*, 1600216.
[107] Z.-Y. Wang, B. Zhang, S. Liu, G.-R. Li, T. Yan, X.-P. Gao, *Adv. Funct. Mater.* **2022**, *32*, 2200893.
[108] L. Peng, Z. Wei, C. Wan, J. Li, Z. Chen, D. Zhu, D. Baumann, H. Liu, C. S. Allen, X. Xu, A. I. Kirkland, I. Shakir, Z. Almutairi, S. Tolbert, B. Dunn, Y. Huang, P. Sautet, X. Duan, *Nat. Catal.* **2020**, *3*, 762.
[109] Z. Shen, M. Cao, Z. Zhang, J. Pu, C. Zhong, J. Li, H. Ma, F. Li, J. Zhu, F. Pan, H. Zhang, *Adv. Funct. Mater.* **2020**, *30*, 1906661.
[110] W. Yang, J. Xiao, Y. Ma, S. Cui, P. Zhang, P. Zhai, L. Meng, X. Wang, Y. Wei, Z. Du, B. Li, Z. Sun, S. Yang, Q. Zhang, Y. Gong, *Adv. Energy Mater.* **2019**, *9*, 1803137.
[111] D. Tian, X. Song, Y. Qiu, X. Sun, B. Jiang, C. Zhao, Y. Zhang, X. Xu, L. Fan, N. Zhang, *ACS Nano* **2021**, *15*, 16515.
[112] L. Guan, H. Hu, L. Li, Y. Pan, Y. Zhu, Q. Li, H. Guo, K. Wang, Y. Huang, M. Zhang, Y. Yan, Z. Li, X. Teng, J. Yang, J. Xiao, Y. Zhang, X. Wang, M. Wu, *ACS Nano* **2020**, *14*, 6222.
[113] Z. Shen, Z. Zhang, M. Li, Y. Yuan, Y. Zhao, S. Zhang, C. Zhong, J. Zhu, J. Lu, H. Zhang, *ACS Nano* **2020**, *14*, 6673.
[114] D. Luo, Z. Zhang, G. Li, S. Cheng, S. Li, J. Li, R. Gao, M. Li, S. Sy, Y.-P. Deng, Y. Jiang, Y. Zhu, H. Dou, Y. Hu, A. Yu, Z. Chen, *ACS Nano* **2020**, *14*, 4849.
[115] Y. Li, J. Wu, B. Zhang, W. Wang, G. Zhang, Z. W. Seh, N. Zhang, J. Sun, L. Huang, J. Jiang, J. Zhou, Y. Sun, *Energy Storage Mater.* **2020**, *30*, 250.
[116] Y. Zhang, G. Li, J. Wang, G. Cui, X. Wei, L. Shui, K. Kempa, G. Zhou, X. Wang, Z. Chen, *Adv. Funct. Mater.* **2020**, *30*, 2001165.
[117] W. Yao, W. Zheng, J. Xu, C. Tian, K. Han, W. Sun, S. Xiao, *ACS Nano* **2021**, *15*, 7114.
[118] Y. Song, W. Zhao, L. Kong, L. Zhang, X. Zhu, Y. Shao, F. Ding, Q. Zhang, J. Sun, Z. Liu, *Energy Environ. Sci.* **2018**, *11*, 2620.
[119] J.-L. Yang, S.-X. Zhao, Y.-M. Lu, X.-T. Zeng, W. Lv, G.-Z. Cao, *Nano Energy* **2020**, *68*, 104356.
[120] P. Wang, B. Xi, Z. Zhang, M. Huang, J. Feng, S. Xiong, *Angew. Chem., Int. Ed.* **2021**, *60*, 15563.
[121] Z. Yu, W. Lv, Q. Lin, X. Huang, Y. Yang, *ACS Nano* **2021**, *15*, 16878.
[122] B. Jiang, D. Tian, Y. Qiu, X. Song, Y. Zhang, X. Sun, H. Huang, C. Zhao, Z. Guo, L. Fan, N. Zhang, *Nano-Micro Lett.* **2021**, *14*, 40.
[123] R. Li, D. Rao, J. Zhou, G. Wu, G. Wang, Z. Zhu, X. Han, R. Sun, H. Li, C. Wang, W. Yan, X. Zheng, P. Cui, Y. Wu, G. Wang, X. Hong, *Nat. Commun.* **2021**, *12*, 3102.
[124] Y. Liu, S. Ma, L. Liu, J. Koch, M. Rosebrock, T. Li, F. Bettels, T. He, H. Pfnür, N. C. Bigall, A. Feldhoff, F. Ding, L. Zhang, *Adv. Funct. Mater.* **2020**, *30*, 2002462.
[125] X. Zhao, Y. Guan, X. Du, G. Liu, J. Li, G. Li, *Chem. Eng. J.* **2022**, *431*, 134242.
[126] A. P. Vijaya Kumar Saroja, Y. Xu, *Matter* **2022**, *5*, 808.
[127] J. Wang, W.-Q. Han, *Adv. Funct. Mater.* **2022**, *32*, 2107166.
[128] A. Shen, Y. Zou, Q. Wang, R. A. W. Dryfe, X. Huang, S. Dou, L. Dai, S. Wang, *Angew. Chem., Int. Ed.* **2014**, *53*, 10804.
[129] C. Ye, H. Jin, J. Shan, Y. Jiao, H. Li, Q. Gu, K. Davey, H. Wang, S.-Z. Qiao, *Nat. Commun.* **2021**, *12*, 7195.
[130] Z. Shi, Z. Sun, J. Cai, X. Yang, C. Wei, M. Wang, Y. Ding, J. Sun, *Adv. Mater.* **2021**, *33*, 2103050.
[131] M. Zhao, H.-J. Peng, Z.-W. Zhang, B.-Q. Li, X. Chen, J. Xie, X. Chen, J.-Y. Wei, Q. Zhang, J.-Q. Huang, *Angew. Chem., Int. Ed.* **2019**, *58*, 3779.
[132] H.-J. Li, K. Xi, W. Wang, S. Liu, G.-R. Li, X.-P. Gao, *Energy Storage Mater.* **2022**, *45*, 1229.
[133] S. Huang, Z. Wang, Y. Von Lim, Y. Wang, Y. Li, D. Zhang, H. Y. Yang, *Adv. Energy Mater.* **2021**, *11*, 2003689.
[134] P. Chen, T. Wang, F. Tang, G. Chen, C. Wang, *Chem. Eng. J.* **2022**, *446*, 136990.
[135] W. Yan, S. Chen, M. Wen, Q. Wu, S. Yu, *J. Mater. Chem. A* **2021**, *9*, 2276.
[136] R. Chu, T. T. Nguyen, Y. Bai, N. H. Kim, J. H. Lee, *Adv. Energy Mater.* **2022**, *12*, 2102805.
[137] S.-G. Han, D.-D. Ma, Q.-L. Zhu, *Small Methods* **2021**, *5*, 2100102.
[138] B. Lu, Q. Liu, S. Chen, *ACS Catal.* **2020**, *10*, 7584.
[139] D. Fang, P. Sun, S. Huang, Y. Shang, X. Li, D. Yan, Y. V. Lim, C.-Y. Su, B.-J. Su, J.-Y. Juang, H. Y. Yang, *ACS Mater. Lett.* **2022**, *4*, 1.
[140] R. Meng, Q. Du, N. Zhong, X. Zhou, S. Liu, S. Yin, X. Liang, *Adv. Energy Mater.* **2021**, *11*, 2102819.
[141] R. Lin, J. Wan, Y. Xiong, K. Wu, W.-c. Cheong, G. Zhou, D. Wang, Q. Peng, C. Chen, Y. Li, *J. Am. Chem. Soc.* **2018**, *140*, 9078.
[142] X. Zhang, Z. Luo, P. Yu, Y. Cai, Y. Du, D. Wu, S. Gao, C. Tan, Z. Li, M. Ren, T. Osipowicz, S. Chen, Z. Jiang, J. Li, Y. Huang, J. Yang, Y. Chen, C. Y. Ang, Y. Zhao, P. Wang, L. Song, X. Wu, Z. Liu, A. Borgna, H. Zhang, *Nat. Catal.* **2018**, *1*, 460.
[143] G. Xia, L. Zhang, J. Ye, Z. Fu, X. Li, X. Yang, Z. Zheng, C. Chen, C. Hu, *Chem. Eng. J.* **2022**, *431*, 133705.
[144] S. Dutta, A. Bhaumik, K. C. W. Wu, *Energy Environ. Sci.* **2014**, *7*, 3574.
[145] J. Guo, Y. Xu, C. Wang, *Nano Lett.* **2011**, *11*, 4288.
[146] H. Wang, Y. Yang, Y. Liang, J. T. Robinson, Y. Li, A. Jackson, Y. Cui, H. Dai, *Nano Lett.* **2011**, *11*, 2644.

[147] D. Liu, C. Zhang, G. Zhou, W. Lv, G. Ling, L. Zhi, Q.-H. Yang, *Adv. Sci.* **2018**, *5*, 1700270.
[148] M. Cheng, R. Yan, Z. Yang, X. Tao, T. Ma, S. Cao, F. Ran, S. Li, W. Yang, C. Cheng, *Adv. Sci.* **2022**, *9*, 2102217.
[149] J.-Y. Hwang, H. M. Kim, S.-K. Lee, J.-H. Lee, A. Abouimrane, M. A. Khaleel, I. Belharouak, A. Manthiram, Y.-K. Sun, *Adv. Energy Mater.* **2016**, *6*, 1501480.
[150] Z. Zhang, Q. Li, K. Zhang, W. Chen, Y. Lai, J. Li, *J. Power Sources* **2015**, *290*, 159.
[151] C. Dong, W. Gao, B. Jin, Q. Jiang, *iScience* **2018**, *6*, 151.
[152] W. Du, Y. Wu, T. Yang, B. Guo, D. Liu, S.-J. Bao, M. Xu, *Chem. Eng. J.* **2020**, *379*, 122359.
[153] Z. Li, J. Zhang, X. W. Lou, *Angew. Chem., Int. Ed.* **2015**, *54*, 12886.
[154] C. Zhao, C. Shen, F. Xin, Z. Sun, W. Han, *Mater. Lett.* **2014**, *137*, 52.
[155] N. Zhang, B. D. A. Levin, Y. Yang, D. A. Muller, H. D. Abruña, *J. Electrochem. Soc.* **2018**, *165*, A1656.
[156] J. Lee, Y. Jeon, J. Oh, M. Kim, L. Y. S. Lee, Y. Piao, *J. Electroanal. Chem.* **2020**, *858*, 113806.
[157] Y. Lu, J.-L. Qin, T. Shen, Y.-F. Yu, K. Chen, Y.-Z. Hu, J.-N. Liang, M.-X. Gong, J.-J. Zhang, D.-L. Wang, *Adv. Energy Mater.* **2021**, *11*, 2101780.
[158] M. Yu, J. Ma, H. Song, A. Wang, F. Tian, Y. Wang, H. Qiu, R. Wang, *Energy Environ. Sci.* **2016**, *9*, 1495.
[159] J. Song, J. Zheng, S. Feng, C. Zhu, S. Fu, W. Zhao, D. Du, Y. Lin, *Carbon* **2018**, *128*, 63.
[160] M. Fang, Z. Chen, Y. Liu, J. Quan, C. Yang, L. Zhu, Q. Xu, Q. Xu, *J. Mater. Chem. A* **2018**, *6*, 1630.
[161] Q. Pang, D. Kundu, M. Cuisinier, L. F. Nazar, *Nat. Commun.* **2014**, *5*, 4759.
[162] H. Wei, E. F. Rodriguez, A. S. Best, A. F. Hollenkamp, D. Chen, R. A. Caruso, *Adv. Energy Mater.* **2017**, *7*, 1601616.
[163] M. Liu, S. Jhulki, Z. Sun, A. Magasinski, C. Hendrix, G. Yushin, *Nano Energy* **2021**, *79*, 105428.
[164] F. Wang, X. Ding, R. Shi, M. Li, Y. Lei, Z. Lei, G. Jiang, F. Xu, H. Wang, L. Jia, R. Jiang, Z. Liu, J. Sun, *J. Mater. Chem. A* **2019**, *7*, 10494.
[165] X. Liang, C. Hart, Q. Pang, A. Garsuch, T. Weiss, L. F. Nazar, *Nat. Commun.* **2015**, *6*, 5682.
[166] X. Liang, C. Y. Kwok, F. Lodi-Marzano, Q. Pang, M. Cuisinier, H. Huang, C. J. Hart, D. Houtarde, K. Kaup, H. Sommer, T. Brezesinski, J. Janek, L. F. Nazar, *Adv. Energy Mater.* **2016**, *6*, 1501636.
[167] S. Luo, J. Ruan, Y. Wang, J. Hu, Y. Song, M. Chen, L. Wu, *Small* **2021**, *17*, 2101879.
[168] J. Xu, L. Xu, Z. Zhang, B. Sun, Y. Jin, Q. Jin, H. Liu, G. Wang, *Energy Storage Mater.* **2022**, *47*, 223.
[169] W. Yao, C. Tian, C. Yang, J. Xu, Y. Meng, I. Manke, N. Chen, Z. Wu, L. Zhan, Y. Wang, R. Chen, *Adv. Mater.* **2022**, *34*, 2106370.
[170] Q. Zhang, L. Mei, X. Cao, Y. Tang, Z. Zeng, *J. Mater. Chem. A* **2020**, *8*, 15417.
[171] X. Chen, H.-J. Peng, R. Zhang, T.-Z. Hou, J.-Q. Huang, B. Li, Q. Zhang, *ACS Energy Lett.* **2017**, *2*, 795.
[172] Y. Wang, Y. Lai, J. Chu, Z. Yan, Y.-X. Wang, S.-L. Chou, H.-K. Liu, S. X. Dou, X. Ai, H. Yang, Y. Cao, *Adv. Mater.* **2021**, *33*, 2100229.
[173] L. Hu, C. Dai, J.-M. Lim, Y. Chen, X. Lian, M. Wang, Y. Li, P. Xiao, G. Henkelman, M. Xu, *Chem. Sci.* **2018**, *9*, 666.
[174] F. Xiao, H. Wang, T. Yao, X. Zhao, X. Yang, D. Y. W. Yu, A. L. Rogach, *ACS Appl. Mater. Interfaces* **2021**, *13*, 18010.
[175] M. K. Aslam, I. D. Seymour, N. Katyal, S. Li, T. Yang, S.-j. Bao, G. Henkelman, M. Xu, *Nat. Commun.* **2020**, *11*, 5242.
[176] Z. Yang, Z. Zhao, H. Zhou, M. Cheng, R. Yan, X. Tao, S. Li, X. Liu, C. Cheng, F. Ran, *ACS Appl. Mater. Interfaces* **2021**, *13*, 51174.
[177] Z. Yan, Y. Liang, J. Xiao, W. Lai, W. Wang, Q. Xia, Y. Wang, Q. Gu, H. Lu, S.-L. Chou, Y. Liu, H. Liu, S.-X. Dou, *Adv. Mater.* **2020**, *32*, 1906700.
[178] S. S. Zhang, D. T. Tran, *J. Mater. Chem. A* **2016**, *4*, 4371.
[179] H.-J. Peng, J.-Q. Huang, Q. Zhang, *Chem. Soc. Rev.* **2017**, *46*, 5237.
[180] L. Mei, X. Gao, Z. Gao, Q. Zhang, X. Yu, A. L. Rogach, Z. Zeng, *Chem. Commun.* **2021**, *57*, 2879.
[181] H. Wang, Q. Zhang, H. Yao, Z. Liang, H.-W. Lee, P.-C. Hsu, G. Zheng, Y. Cui, *Nano Lett.* **2014**, *14*, 7138.
[182] X. Geng, Y. Zhang, Y. Han, J. Li, L. Yang, M. Benamara, L. Chen, H. Zhu, *Nano Lett.* **2017**, *17*, 1825.
[183] W. Sun, Y. Li, S. Liu, Q. Guo, Y. Zhu, X. Hong, C. Zheng, K. Xie, *Nano Res.* **2020**, *13*, 2143.
[184] Q. Pang, D. Kundu, L. F. Nazar, *Mater. Horiz.* **2016**, *3*, 130.
[185] W. Tian, B. Xi, Z. Feng, H. Li, J. Feng, S. Xiong, *Adv. Energy Mater.* **2019**, *9*, 1901896.
[186] J. Guo, Q. Wang, C. Qi, J. Jin, Y. Zhu, Z. Wen, *Chem. Commun.* **2016**, *52*, 5613.
[187] G. Babu, N. Masurkar, A. H. Salem, L. M. R. Arava, *J. Am. Chem. Soc.* **2017**, *139*, 171.
[188] C. -Y. Fan, Y.-P. Zheng, X.-H. Zhang, Y.-H. Shi, S.-Y. Liu, H.-C. Wang, X.-L. Wu, H.-Z. Sun, J.-P. Zhang, *Adv. Energy Mater.* **2018**, *8*, 1703638.
[189] Z. Wang, X. Xu, Z. Liu, S. Ji, S. O. Ahmed Idris, J. Liu, *Electrochim. Acta* **2020**, *332*, 135482.
[190] X. Zhou, Z. Yu, Y. Yao, Y. Jiang, X. Rui, J. Liu, Y. Yu, *Adv. Mater.* **2022**, *34*, 2200479.
[191] N. Shi, B. Xi, J. Liu, Z. Zhang, N. Song, W. Chen, J. Feng, S. Xiong, *Adv. Funct. Mater.* **2022**, *32*, 2111586.
[192] C. Qi, Z. Li, C. Sun, C. Chen, J. Jin, Z. Wen, *ACS Appl. Mater. Interfaces* **2020**, *12*, 49626.
[193] S. Li, B. Chen, Y. Wang, M.-Y. Ye, P. A. van Aken, C. Cheng, A. Thomas, *Nat. Mater.* **2021**, *20*, 1240.
[194] Y. Song, Z. Sun, Z. Fan, W. Cai, Y. Shao, G. Sheng, M. Wang, L. Song, Z. Liu, Q. Zhang, J. Sun, *Nano Energy* **2020**, *70*, 104555.
[195] X. Zhang, M. Zhang, Y. Deng, M. Xu, L. Artiglia, W. Wen, R. Gao, B. Chen, S. Yao, X. Zhang, M. Peng, J. Yan, A. Li, Z. Jiang, X. Gao, S. Cao, C. Yang, A. J. Kropf, J. Shi, J. Xie, M. Bi, J. A. van Bokhoven, Y.-W. Li, X. Wen, M. Flytzani-Stephanopoulos, C. Shi, W. Zhou, D. Ma, *Nature* **2021**, *589*, 396.
[196] P. Zeng, C. Yuan, J. An, X. Yang, C. Cheng, T. Yan, G. Liu, T.-S. Chan, J. Kang, L. Zhang, X. Sun, *Energy Storage Mater.* **2022**, *44*, 425.
[197] Z. Cui, C. Zu, W. Zhou, A. Manthiram, J. B. Goodenough, *Adv. Mater.* **2016**, *28*, 6926.
[198] W. Chen, H. Jin, S. Xie, H. Xie, J. Zhu, H. Ji, L.-J. Wan, *J. Energy Chem.* **2021**, *54*, 16.
[199] J. He, A. Manthiram, *Adv. Energy Mater.* **2020**, *10*, 1903241.
[200] Z. Sun, J. Zhang, L. Yin, G. Hu, R. Fang, H.-M. Cheng, F. Li, *Nat. Commun.* **2017**, *8*, 14627.
[201] X. Ai, X. Zou, H. Chen, Y. Su, X. Feng, Q. Li, Y. Liu, Y. Zhang, X. Zou, *Angew. Chem., Int. Ed.* **2020**, *59*, 3961.
[202] Z. Li, H. Jiang, N.-C. Lai, T. Zhao, Y.-C. Lu, *Chem. Mater.* **2019**, *31*, 10186.
[203] G. Xia, Z. Zheng, J. Ye, X. Li, M. J. Biggs, C. Hu, *Chem. Eng. J.* **2021**, *406*, 126823.
[204] S. Yu, W. Cai, L. Chen, L. Song, Y. Song, *J. Energy Chem.* **2021**, *55*, 533.
[205] Y. Zhong, L. Yin, P. He, W. Liu, Z. Wu, H. Wang, *J. Am. Chem. Soc.* **2018**, *140*, 1455.
[206] J. He, A. Bhargav, A. Manthiram, *ACS Nano* **2021**, *15*, 8583.
[207] H. Xu, R. Hu, Y. Zhang, H. Yan, Q. Zhu, J. Shang, S. Yang, B. Li, *Energy Storage Mater.* **2021**, *43*, 212.
[208] Y. Wang, H. Su, Y. He, L. Li, S. Zhu, H. Shen, P. Xie, X. Fu, G. Zhou, C. Feng, D. Zhao, F. Xiao, X. Zhu, Y. Zeng, M. Shao, S. Chen, G. Wu, J. Zeng, C. Wang, *Chem. Rev.* **2020**, *120*, 12217.
[209] Z. Liu, L. Zhou, Q. Ge, R. Chen, M. Ni, W. Utetiwabo, X. Zhang, W. Yang, *ACS Appl. Mater. Interfaces* **2018**, *10*, 19311.

[210] Z. Du, X. Chen, W. Hu, C. Chuang, S. Xie, A. Hu, W. Yan, X. Kong, X. Wu, H. Ji, L.-J. Wan, *J. Am. Chem. Soc.* **2019**, *141*, 3977.
[211] L. Zhang, D. Liu, Z. Muhammad, F. Wan, W. Xie, Y. Wang, L. Song, Z. Niu, J. Chen, *Adv. Mater.* **2019**, *31*, 1903955.
[212] F. Ma, Y. Wan, X. Wang, X. Wang, J. Liang, Z. Miao, T. Wang, C. Ma, G. Lu, J. Han, Y. Huang, Q. Li, *ACS Nano* **2020**, *14*, 10115.
[213] J. Yang, D. W. Kang, H. Kim, J. H. Park, W. Y. Choi, J. W. Lee, *J. Mater. Chem. A* **2021**, *9*, 23660.
[214] T. Huang, Y. Sun, J. Wu, J. Jin, C. Wei, Z. Shi, M. Wang, J. Cai, X.-T. An, P. Wang, C. Su, Y.-y. Li, J. Sun, *ACS Nano* **2021**, *15*, 14105.
[215] Z. Han, S. Zhao, J. Xiao, X. Zhong, J. Sheng, W. Lv, Q. Zhang, G. Zhou, H.-M. Cheng, *Adv. Mater.* **2021**, *33*, 2105947.
[216] C. Lu, Y. Chen, Y. Yang, X. Chen, *Nano Lett.* **2020**, *20*, 5522.
[217] M. O. Cichocka, Z. Liang, D. Feng, S. Back, S. Siahrostami, X. Wang, L. Samperisi, Y. Sun, H. Xu, N. Hedin, H. Zheng, X. Zou, H.-C. Zhou, Z. Huang, *J. Am. Chem. Soc.* **2020**, *142*, 15386.
[218] J. Zhou, Z. Han, X. Wang, H. Gai, Z. Chen, T. Guo, X. Hou, L. Xu, X. Hu, M. Huang, S. V. Levchenko, H. Jiang, *Adv. Funct. Mater.* **2021**, *31*, 2102066.
[219] J. Zheng, J. Tian, D. Wu, M. Gu, W. Xu, C. Wang, F. Gao, M. H. Engelhard, J.-G. Zhang, J. Liu, J. Xiao, *Nano Lett.* **2014**, *14*, 2345.
[220] S. Li, J. Lin, Y. Ding, P. Xu, X. Guo, W. Xiong, D.-Y. Wu, Q. Dong, J. Chen, L. Zhang, *ACS Nano* **2021**, *15*, 13803.
[221] Z. Wang, H. Tao, Y. Yue, *ChemElectroChem* **2019**, *6*, 5358.
[222] W. Li, X. Guo, P. Geng, M. Du, Q. Jing, X. Chen, G. Zhang, H. Li, Q. Xu, P. Braunstein, H. Pang, *Adv. Mater.* **2021**, *33*, 2105163.
[223] D. Cai, M. Lu, L. Li, J. Cao, D. Chen, H. Tu, J. Li, W. Han, *Small* **2019**, *15*, 1902605.
[224] D. Yang, Z. Liang, P. Tang, C. Zhang, M. Tang, Q. Li, J. J. Biendicho, J. Li, M. Heggen, R. E. Dunin-Borkowski, M. Xu, J. Llorca, J. Arbiol, J. R. Morante, S.-L. Chou, A. Cabot, *Adv. Mater.* **2022**, *34*, 2108835.
[225] Q. Pang, X. Liang, C. Y. Kwok, L. F. Nazar, *Nat. Energy* **2016**, *1*, 16132.
[226] G. Cui, G. Li, D. Luo, Y. Zhang, Y. Zhao, D. Wang, J. Wang, Z. Zhang, X. Wang, Z. Chen, *Nano Energy* **2020**, *72*, 104685.
[227] B. Z. Yang, P. Xie, Q. Luo, Z. W. Li, C. Y. Zhou, Y. H. Yin, X. B. Liu, Y. S. Li, Z. P. Wu, *Adv. Funct. Mater.* **2022**, *32*, 2110665.
[228] J. Kang, X. Tian, C. Yan, L. Wei, L. Gao, J. Ju, Y. Zhao, N. Deng, B. Cheng, W. Kang, *Small* **2022**, *18*, 2104469.
[229] N. Jayaprakash, J. Shen, S. S. Moganty, A. Corona, L. A. Archer, *Angew. Chem., Int. Ed.* **2011**, *50*, 5904.
[230] S. Chen, X. Huang, B. Sun, J. Zhang, H. Liu, G. Wang, *J. Mater. Chem. A* **2014**, *2*, 16199.
[231] Z. Yu, M. Liu, D. Guo, J. Wang, X. Chen, J. Li, H. Jin, Z. Yang, X. a. Chen, S. Wang, *Angew. Chem., Int. Ed.* **2020**, *59*, 6406.
[232] Z. Wei Seh, W. Li, J. J. Cha, G. Zheng, Y. Yang, M. T. McDowell, P.-C. Hsu, Y. Cui, *Nat. Commun.* **2013**, *4*, 1331.
[233] D. Li, B. Gong, X. Cheng, F. Ling, L. Zhao, Y. Yao, M. Ma, Y. Jiang, Y. Shao, X. Rui, W. Zhang, H. Zheng, J. Wang, C. Ma, Q. Zhang, Y. Yu, *ACS Nano* **2021**, *15*, 20607.
[234] Y. Zhang, Y. Si, W. Guo, X. Li, S. Tang, Z. Zhang, X. Wang, Y. Fu, *ACS Appl. Energy Mater.* **2021**, *4*, 10104.
[235] W. Sun, C. Liu, Y. Li, S. Luo, S. Liu, X. Hong, K. Xie, Y. Liu, X. Tan, C. Zheng, *ACS Nano* **2019**, *13*, 12137.
[236] J. Zhang, H. Hu, Z. Li, X. W. Lou, *Angew. Chem., Int. Ed.* **2016**, *55*, 3982.
[237] E. H. M. Salhabi, J. Zhao, J. Wang, M. Yang, B. Wang, D. Wang, *Angew. Chem., Int. Ed.* **2019**, *58*, 9078.
[238] X. Wu, Q. Zhang, G. Tang, Y. Cao, H. Yang, H. Li, X. Ai, *Small* **2022**, *18*, 2106144.
[239] Z. Liu, R. Lian, Z. Wu, Y. Li, X. Lai, S. Yang, X. Ma, Y. Wei, X. Yan, *Chem. Eng. J.* **2022**, *431*, 134163.
[240] S. Evers, T. Yim, L. F. Nazar, *J. Phys. Chem. C* **2012**, *116*, 19653.
[241] S. Xin, L. Gu, N.-H. Zhao, Y.-X. Yin, L.-J. Zhou, Y.-G. Guo, L.-J. Wan, *J. Am. Chem. Soc.* **2012**, *134*, 18510.
[242] Z. Li, L. Yuan, Z. Yi, Y. Sun, Y. Liu, Y. Jiang, Y. Shen, Y. Xin, Z. Zhang, Y. Huang, *Adv. Energy Mater.* **2014**, *4*, 1301473.
[243] W. -G. Lim, C. Jo, A. Cho, J. Hwang, S. Kim, J. W. Han, J. Lee, *Adv. Mater.* **2019**, *31*, 1806547.
[244] M. Chen, Z. Su, K. Jiang, Y. Pan, Y. Zhang, D. Long, *J. Mater. Chem. A* **2019**, *7*, 6250.
[245] G. Zhou, E. Paek, G. S. Hwang, A. Manthiram, *Nat. Commun.* **2015**, *6*, 7760.
[246] S. Lu, Y. Chen, X. Wu, Z. Wang, Y. Li, *Sci. Rep.* **2014**, *4*, 4629.
[247] S. Lin, Y. Wang, Y. Chen, Z. Cai, J. Xiao, T. Muhmood, X. Hu, *Small* **2022**, *18*, 2104224.
[248] Y. Li, K. K. Fu, C. Chen, W. Luo, T. Gao, S. Xu, J. Dai, G. Pastel, Y. Wang, B. Liu, J. Song, Y. Chen, C. Yang, L. Hu, *ACS Nano* **2017**, *11*, 4801.
[249] K. Zou, T. Zhou, Y. Chen, X. Xiong, W. Jing, X. Dai, M. Shi, N. Li, J. Sun, S. Zhang, C. Zhang, Y. Liu, Z. Guo, *Adv. Energy Mater.* **2022**, *12*, 2103981.
[250] N. Wang, X. Zhang, Z. Ju, X. Yu, Y. Wang, Y. Du, Z. Bai, S. Dou, G. Yu, *Nat. Commun.* **2021**, *12*, 4519.
[251] W. Wu, X. Li, L. Liu, X. Zhu, Z. Guo, W. Guo, Q. Han, J. He, Y. Zhao, *J. Mater. Chem. A* **2022**, *10*, 1433.
[252] B. Zhang, C. Luo, G. Zhou, Z.-Z. Pan, J. Ma, H. Nishihara, Y.-B. He, F. Kang, W. Lv, Q.-H. Yang, *Adv. Funct. Mater.* **2021**, *31*, 2100793.

Ran Zhu is currently a master's student at the College of Polymer Science and Engineering, Sichuan University. His research interest is synthesizing micro-/nanocatalytic systems for metal–sulfur batteries.

Weiqiong Zheng is currently a master's student at the College of Polymer Science and Engineering, Sichuan University. Her research interest is synthesizing single-atom catalysts and other functional nanomaterials for energy conversion applications.

Chong Cheng is currently a full professor in the department of polymer science at Sichuan University. He obtained his B.Sc. and Ph.D. from Sichuan University. After a research stay at the University of Michigan, Ann Arbor, USA, he joined the Freie Universität Berlin as an AvH research fellow. His current scientific interests include fabricating advanced low-dimensional materials for nanomedicines, antibacterial materials, stem cell scaffolds, energy storage devices, and electro-catalysts, especially the cutting-edge catalytic applications of metal–organic frameworks.

Shuang Li received her bachelor's degree from Sichuan University, master's degree from Shanghai Jiao Tong University and Ph.D. degree from Technische Universität Berlin. She has been doing independent researches funded by Technische Universität Berlin, UniSysCat, and Deutsche Forschungsgemeinschaft (DFG) from 2019 to 2021. Currently, she is appointed as a full professor in the College of Polymer Science and Engineering at Sichuan University. Her current research focuses on designing metal–organic hybrid catalysts with atomic-scale controlled structures, and their applications in catalysis, including water splitting, fuel cells, CO_2 reductions, and metal–sulfur batteries.

Changsheng Zhao obtained the Ph.D. degree in Biomedical Engineering from Sichuan University, China, in 1998. From 2001 to 2003, he was doing the research work in Hokkaido University (Japan) as a postdoctoral research fellow. Currently, he is the Chair and Leading Professor at Department of Polymer Science and Engineering in Sichuan University. His research interests focused on the development of nanomaterials, polymer–nanomaterial composites, environmental sensitive, blood compatible and biological active polymers, and the regarding functional membranes, and biocatalytic nanosystems.